SURFACE ENERGY BALANCE IN ARID LANDS AGRICULTURE 1960-61

Production Research Report No. 76

Agricultural Research Service

U.S. DEPARTMENT OF AGRICULTURE

USAEPG SUMMARY

DA Task: 3A99–27–005–08, Micrometeorology
Title: Surface Energy Balance in Arid Lands Agriculture
Originator: U.S. Water Conservation Laboratory, Agricultural Research Service, U.S. Department of Agriculture, Tempe, Arizona

The broad objective of this research is to measure and evaluate the energy balance components at the earth's surface and to devise and test theories on the energy disposition at the vegetated surface under typically prevailing outdoor conditions. More specific objectives for fiscal year 1961 were to install and verify an accurate and sensitive lysimeter system, to procure and test a multichannel data handling system, to select or devise appropriate instruments for the measurement of net radiation, soil heat flow, windspeed, air temperature, and vapor content. Furthermore, a specific objective was to arrange for and program machine calculation of data and to complete one or more energy balance studies over bare soil. The report contains a discussion of the experimental site, the instrumentation design and operation, and the preliminary results of four experiments.

These experiments included investigations of the energy balance over: (1) a small wetted soil surface, (2) a small ponded surface area, (3) a large ponded surface, and (4) a large wetted soil surface. From the results of these experiments it may be concluded that:

(1) There is little difference in the energy used for evaporation over a wetted or ponded surface. In both cases the air blowing over the plot was heated, considering the day as a whole. However, during a part of the day energy was extracted from the air.

(2) Progressive drying of the soil had a marked effect on the partition of energy due to increased surface reflection and increased surface temperature. Even though surface temperature increased, heat entering the soil did not increase appreciably. Net radiation and evaporation decreased and the balance was achieved by increased heating of the air.

(3) Although radiation and soil heating progressed smoothly during the tests, the amount of energy used for evaporation was not regular, particularly during the afternoon. In addition, the amount used to heat the air varied in sign and magnitude, seemingly depending on surface conditions and character of the wind.

No recommendations are made by the investigator.

Meteorology Department
USAEPG

SURFACE ENERGY BALANCE IN ARID LANDS AGRICULTURE 1960-61

Prepared by

C. H. M. VAN BAVEL, Project Leader

L. J. FRITSCHEN

R. J. REGINATO

U.S. Water Conservation Laboratory

Agricultural Research Service

U.S. DEPARTMENT OF AGRICULTURE

For

Meteorology Department

U.S. ARMY ELECTRONIC PROVING GROUND

Production Research Report No. 76

Washington, D.C.

Issued December 1963

CONTENTS

SURFACE ENERGY BALANCE IN ARID LANDS AGRICULTURE: 1960–61

By C. H. M. van Bavel, *project leader,* L. J. Fritschen and R. J. Reginato, *soil scientists, U.S. Water Conservation Laboratory, Agricultural Research Service*

SUMMARY

Instrumentation and an appropriate experimental site have been completed at the U.S. Water Conservation Laboratory for the detailed study of the surface energy balance in an arid climate.

Outstanding features of the installation are a precision weighing lysimeter system for the measurement of evaporative flux, greatly improved and accurate net radiometry, and a completely automatic and trouble-free data handling system with a total capacity of 46 channels, including lysimeter weight, windspeed and direction, heat flux, radiation, temperature, and humidity.

Four major experiments were carried out during the late spring of 1961. In the first a small wetted surface was observed, in the second a small ponded surface, in the third a large ponded area, and in the fourth a large wetted area. The soil was bare in all cases.

In each experiment pertinent data were collected every 15 minutes for several days under near-perfect and identical weather conditions, which were typified by clear skies, light winds, and low humidity.

The complete body of data is now being processed by automatic computing, the original data having been copied from punched tape onto punched cards. The final calculations will consist in computing surface energy balances from periods varying from 15 minutes to 24 hours.

A preliminary, gross analysis of the data is presented in this report in addition to selected examples of more detailed information. Tentative conclusions at this time are the following.

When the entire observation area (about 100×100 m.) is uniformly treated, the evaporative flux from a shallow layer of water and from a wet, bare soil surface show little difference despite greater net radiative flux over the shallow layer of water. In neither case was heat extracted from the air on a daily basis, but the opposite took place, particularly over shallow water.

Over an isolated (1×1 m.) ponded surface considerable downward flux of sensible heat was found over a 24-hour period and also over an isolated wet surface (1×1 m.) The progressive drying of the soil surface affects the energy balance profoundly by increasing the albedo and surface temperature, and by decreasing the transport of soil moisture to the surface. In consequence, net radiation decreased, evaporation decreased, and heat flux from the surface into the air increased. No great influence on soil heat flux was found.

Even though net radiation and soil heat flux varied smoothly with time of day, as one would expect under the prevailing weather conditions, evaporative flux was not regular, particularly during the middle and latter part of the day. Also, sensible heat flux into the air varied in sign and magnitude, seemingly dependent upon surface conditions and wind character. Additional study of the data may throw more light on this aspect of the surface energy balance.

OBJECTIVES

The long-term objectives of the cooperative studies in micrometeorology at the United States Water Conservation Laboratory are (1) to understand the energy balance of the surface of irrigated lands in an arid, warm climate and (2) to devise practical means whereby the irrigation requirements of such lands may be adequately predicted and whereby the effect of irrigation upon the properties of the environment close to the surface both in and above the ground can be characterized.

Specifically, the effect of the nature of the soil surface and its management upon the magnitude

and dispositon of net radiative flux is one object of study. A second major goal is to determine the amount of energy in the form of sensible heat that is utilized in evaporation and derived from other areas by horizontal advection. Also, an attempt will be made to single out the factors that determine the magnitude of horizontal advection.

More specific objectives for the 1960–61 year were to install and verify an accurate and sensitive lysimeter system, to procure and test a multichannel data handling system, to select or devise appropriate instruments for the measurement of net radiation, soil heat flow, windspeed, air temperature, and vapor content. Furthermore, a specific objective was to arrange for and program machine calculation of data and to complete one or more energy balance studies over bare soil.

DESCRIPTION OF GENERAL AREA AND EXPERIMENTAL SITE

The U.S. Water Conservation Laboratory (33°24′24″ N., 111°58′11″ W., elevation, 1,130 feet) is located in south-central Arizona in the Salt River Valley. It stands 1 mile south of the Salt River, which is dry except for brief periods after local heavy rainfall. The valley extends from east to west.

Almost due north of the Laboratory, at a distance of 8 miles, is Camelback Mountain with an elevation of 2,710 feet. At a distance of 3.5 miles in a north-northeasterly direction the Papago Buttes rise to 1,413 feet. To the east-northeast 3 miles lies the city of Tempe. Due east 1.2 miles from the Laboratory are the Bell Buttes with an elevation of 1,369 feet. South of the site, at a distance of 2 miles, the Salt River Mountains extend to the southwest for 12 miles, rising to a maximum height of 2,600 feet. Northwest of the Laboratory, at a distance of 2 to 3 miles, is the city of Phoenix.

Within a radius of 1 mile from the Laboratory the land slopes from southeast to northwest toward the Salt River with the elevation ranging from 1,118 to 1,155 feet. The area is all farmland, the predominant crops being cotton, alfalfa, and sorghum.

The lysimeter field is 300 by 240 feet, and is enclosed on the east, south, and west by an 8-foot chain link fence and on the north by a 4-foot chain link fence. The three lysimeters lie in an east-west direction 40 feet apart in the center of the field. Due north of the center lysimeter at a distance of 27 feet is an 18-foot mast for micrometeorological observations. As seen in figure 1, the Laboratory buildings are 135 feet north of the lysimeters. To the east, south, and west is the University of Arizona Cotton Research Center with the crops mentioned above planted in the area.

The soil in the lysimeter field is classified as Adelanto loam and grades into a clay loam at a depth of 5 feet. From 6 to 8 feet is a well-cemented caliche layer. The amount of organic matter in the first 3 feet is 0.5 percent by weight. At −100 mb. pressure potential the moisture content of the soil is about 0.30 by volume and at the −15 bar pressure potential it is 0.11 by volume. The bulk density of the soil is approximately 1.4 g. cm.$^{-3}$.

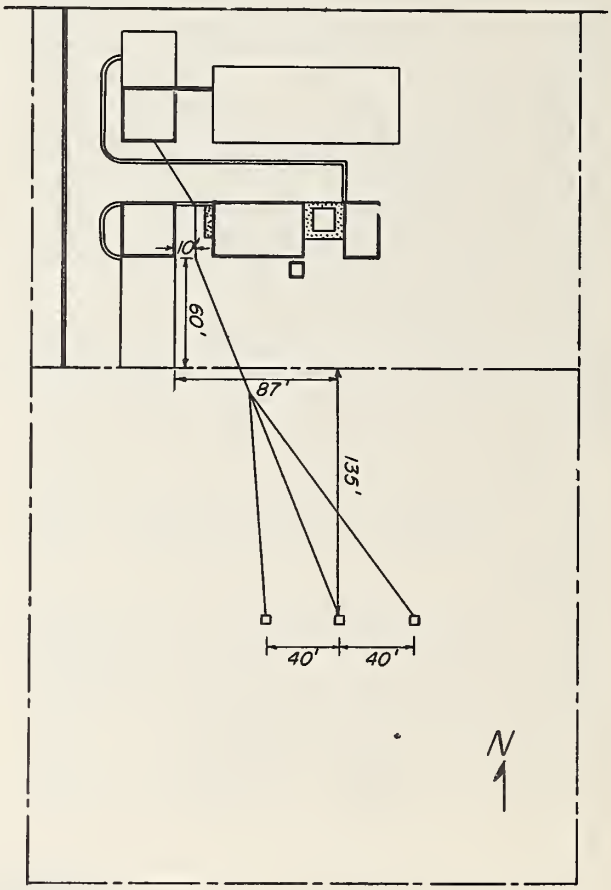

FIGURE 1.—Location of lysimeters on the Laboratory grounds.

The general area and the exact dimensions of the experimental area may be studied from maps and photographs in figures 2, 3, and 4.

Since 1957 the lysimeter field has been fallow, and was disked twice just prior to the installation of the lysimeters in December 1960.

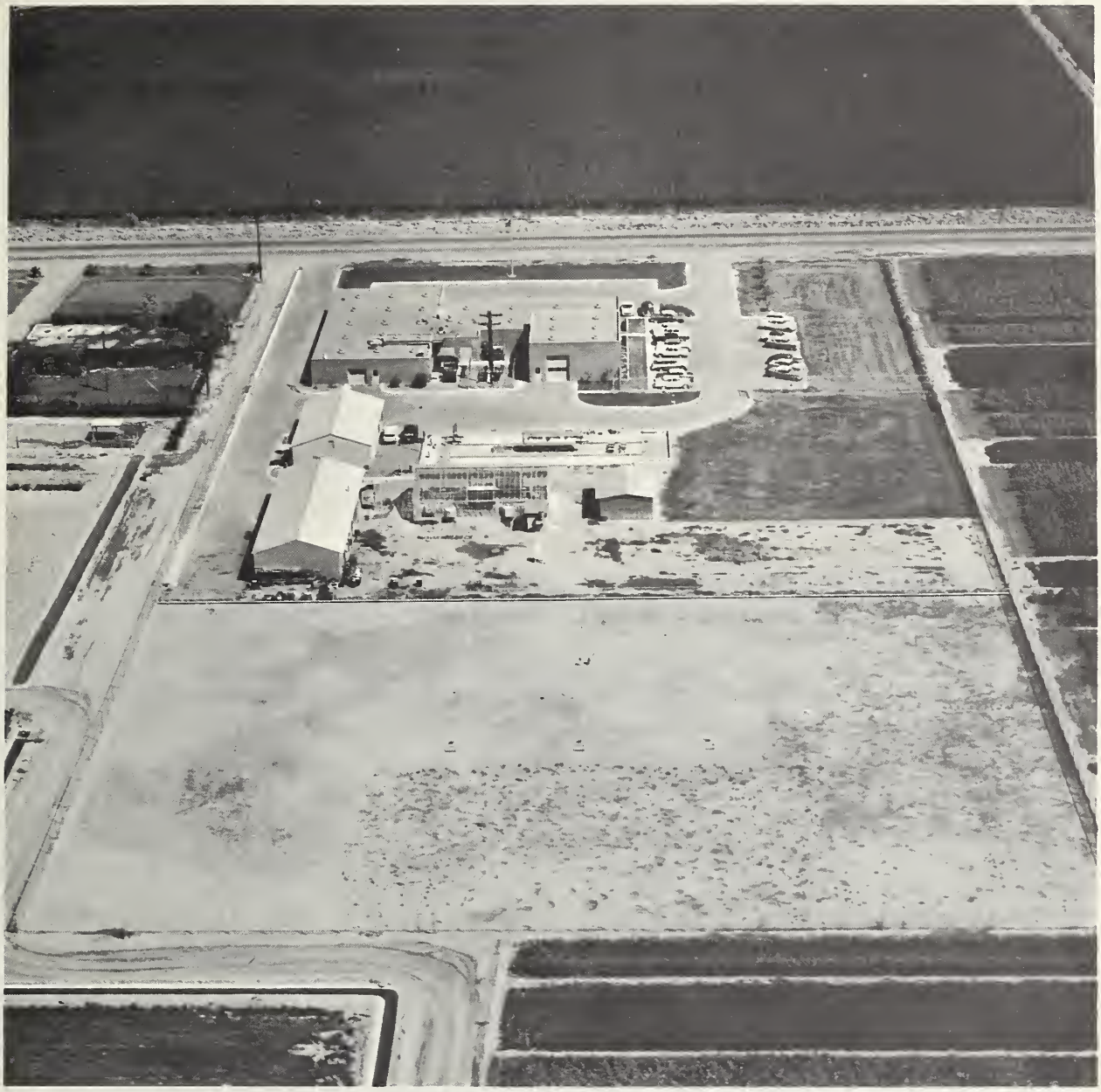

FIGURE 2.—Lysimeter field and Laboratory, looking north.

SYMBOLS

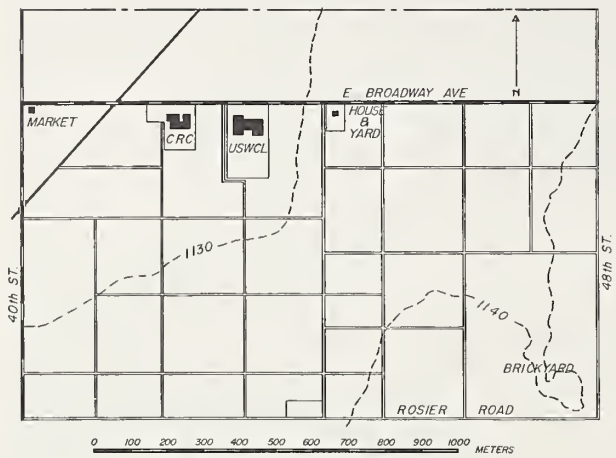

FIGURE 3.—Map of Laboratory and surrounding area: CRC is the Cotton Research Center and USWCL is the U.S. Water Conservation Laboratory.

FOR ENERGY-BALANCE AND AERODYNAMIC STUDIES AND WINDSPEED DATA

The following nomenclature was adopted for use in the energy-balance and aerodynamic methods and for the windspeed data. The units used are those of the centimeter-gram-second (c.g.s.) system.

Legend	*Unit measurement*	*Definition*
A	Cal. cm.$^{-2}$ min.$^{-1}$	Sensible heat flux to the air.
A	----------	Austausch, or exchange coefficient [windspeed].
C	Cal. g.$^{-1}$ ° C.$^{-1}$	Specific heat.
C_D	----------	Drag coefficient.
D	Cm.^{2} sec.$^{-1}$	Diffusivity of water vapor in air.
E	G. cm.$^{-2}$ min.$^{-1}$	Evaporation rate.
G	G. x 10	Weight of lysimeter.
K_A	Cm.^{2} sec.$^{-1}$	Eddy diffusivity for sensible heat.

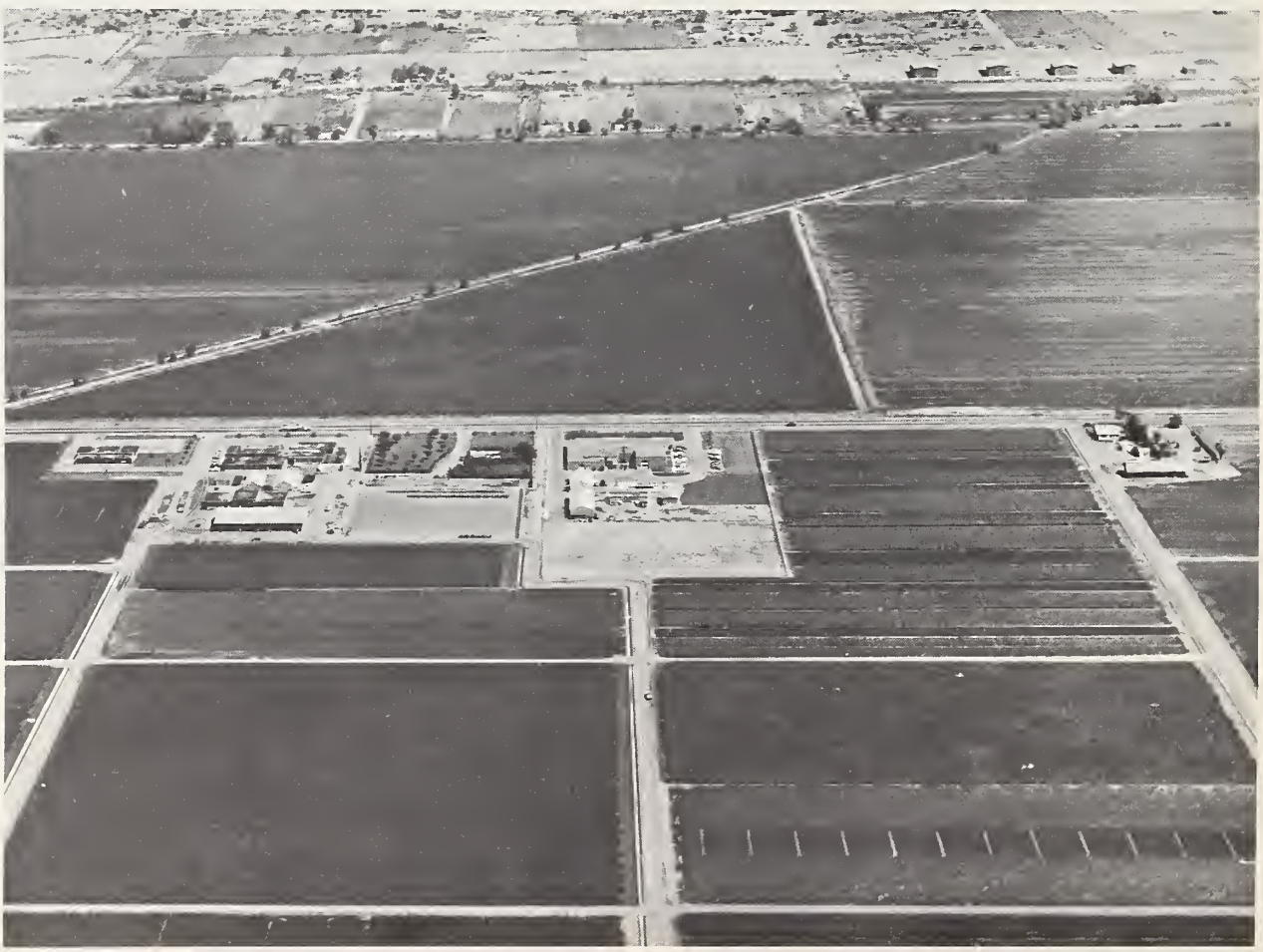

FIGURE 4.—Laboratory and surrounding area, looking north.

Legend	Unit measurement	Definition
K_E	Cm.^{2} sec.$^{-1}$	Eddy diffusivity for atmospheric moisture.
K_M	Cm.^{2} sec.$^{-1}$	Eddy diffusivity for horizontal momentum.
K_m	Cm.^{2} sec.$^{-1}$	Eddy viscosity.
L	Cal. g.$^{-1}$	Latent heat of vaporization.
P	Mb.	Pressure.
R	Cal. cm.$^{-2}$ min.$^{-1}$	Radiative heat flux.
S	Cal. cm.$^{-2}$ min.$^{-1}$	Heat flux in the soil at the heat-flow plate level.
S'	Cal. cm.$^{-2}$ min.$^{-1}$	Heat flux into the soil above the heat-flow plate.
T	° C.	Temperature.
U	Cm. sec.$^{-1}$	Windspeed.
U_*	Cm. sec.$^{-1}$	Friction velocity, equal to $\sqrt{\tau/\rho}$ or $Uk/\left(\ln\frac{Z}{Z_0}\right)$.
W	Cal. cm.$^{-2}$ min.$^{-1}$	Heat flux through the layer of water.
Z	Cm.	Height above the ground.
c_p	Cal. g.$^{-1}$ °C.$^{-1}$	Specific heat at constant pressure of dry air.
d	Cm.	Depth.
e	Mb.	Vapor pressure.
g	Cm. sec.$^{-2}$	Acceleration of gravity.
k	0.4	Von Karman's constant.
ly	1 cal. cm.^{2}	Langley.
q	G. kg.$^{-1}$	Specific humidity.
t	Min.	Time.
δ	Cm.	Thickness of the laminar layer.
θ	° A.	Potential temperature.
μ		Dynamic viscosity.
ν	Cm.^{2} sec.$^{-1}$	Kinetic viscosity.
ρ	G. cm.$^{-3}$	Density of air.
τ	Dynes cm.$^{-2}$	Eddy stress.

Subscript legend	Unit measurement	Definition
I		Lysimeter 1.
II		Lysimeter 2.
III		Lysimeter 3.
0		Ground reference level.
1	40 cm.[1]	Height of level 1.
2	80 cm.[1]	Height of level 2.
3	160 cm.[1]	Height of level 3.
4	320 cm.[1]	Height of level 4.
5	640 cm.[1]	Height of level 5.

[1] The mast zero reference was originally the soil surface. With cultivation and addition of water, the height of the level above the surface where the atmospheric properties were measured was changed; therefore, the following heights apply:

Height	Little Splash, Little Mud, and Big Mud tests	Big Splash test
	Cm.	Cm.
Z_1	35	30
Z_2	75	70
Z_3	155	150
Z_4	315	310
Z_5	635	630

A	Air.
b	Beginning of period (i.e., 04140100).
c	Calculated.
D	Drag.
E	Water vapor.
e	End of period (i.e., 04140115), water vapor.
h	Horizontal.
hf	Heat-flow plate.
i	Initial weight of lysimeter before water was added in "Splash" experiments.
l	Mixing length.
m	Measured.
M	Momentum.
n	Net.
s	Soil.
sf	Soil surface.
su	Solar.
v	Vertical.
w	Water.

FOR NET RADIATION STUDIES

Legend	Unit measurement	Definition
A	Cm.^{2}	Area.
B	μv.	Thermoelectric power.
C_p	Cal. g.$^{-1}$ ° C.$^{-1}$	Heat capacity at constant pressure.
E	Cal. cm.$^{-2}$ min.$^{-1}$	Total emissive power where $E=\sigma T^4$ for a blackbody.
G	μv. ° C.$^{-1}$	Thermoelectric potential.
H	Cal. cm.$^{-2}$ min.$^{-1}$	Heat-flow.
Q	Cal. ° C.$^{-1}$	Quantity of heat.
R	Ly. min.$^{-1}$	Radiation.
T	° C. or A.	Temperature.
c		Proportionality constant.
f		Fraction of energy leaving one surface and falling on the other.
g	Mv. ly.$^{-1}$ min.	Calibration constant.
h	Cal. cm.$^{-1}$ min.$^{-1}$ ° C.$^{-1}$.	Thermal convection coefficient.
k	Cal. cm.$^{-1}$ min.$^{-1}$ ° C.$^{-1}$.	Thermal conductivity.
l	Cm.	Length.
ly	1 cal. cm.^{2}	Langley.
q	Cal. min.$^{-1}$	Flux of energy.
r		Reflectivity where $r=1-\epsilon$.
α		Absorptivity.
ϵ		Emissivity.
μ	Microns	Wavelength.
σ	8.132 x 10^{-11} cal. cm.$^{-2}$ A.$^{-4}$ min.$^{-1}$	Stefan-Boltzmann constant.

Subscript legend	
a	Air and to identify equation.
b	Bottom and to identify equation.
ea	Earth.
n	Net.
sk	Sky.
su	Solar.
t	Top and time.
w	Wall.
1	Surface 1.
2	Surface 2.

EXPERIMENTAL DATA AND PROCEDURES

DESCRIPTION OF PRINCIPAL STUDIES

In addition to a number of exploratory studies the following major experiments dealing with evaporation from a bare surface were carried out.

Little Mud 1 (LM1)

The lysimeter field was bare and had been irrigated last on March 1, 1961. About 5.5 mm. of rain fell on March 28–30, 1961. Tap water was added to the lysimeters only on the afternoon of

April 13 in the amount of 30 mm. The official observation period started at 0000 April 14 and ended at 0000 April 17, a total of three 24-hour periods.

The objective of the LM1 experiment was to study evaporation and the energy balance of a recently wetted soil surface of small extent, surrounded by a dry area. Since the surface of the lysimeters became progressively drier as time went on, the contrast between lysimeters and surroundings diminished.

Records of lysimeter weight were obtained every 30 minutes, and of all other variables every 15 minutes. The meteorological variables recorded were: (1) net radiation over each lysimeter at the 10-cm. height, (2) soil heat flux in each lysimeter and temperature of heat flow plate at the 1.5-cm. depth, (3) soil temperature immediately below the surface (1–2 mm.), (4) air temperature at 40, 80, 160, 320, and 640 cm. and windspeed at 40, 80, 160, 320, and 640 cm., (5) difference in air temperature between heights of 40 and 80 cm. and wind direction at 8 m., (6) incoming short-wave radiation, and (7) relative humidity at 160 cm.

A total of 29 channels was used in the data handling system, including three zeros for referral of the three ranges.

No particular difficulties were experienced with the instrumentation or the data recording. The overall weather conditions during the 3 days of recording are given in table 1. Data are from the U.S. Weather Bureau located at Sky Harbor Airport 3 miles northwest of the Laboratory.

Little Splash 2 (LS2)

After the previous experiment, two sheets of black polyethylene were placed on the surface of each lysimeter so that a thin layer of water could be maintained. Water was then added for the first time on the afternoon of April 17, 1961. The experimental period began at 0000 April 18 and ended 0000 April 23, a total of five 24-hour periods. During this period water was added around 0815, to make up water lost the previous day. The amount added each time was about 10 mm. so that the water layer each morning was about 20 mm. after the addition.

TABLE 1.—*Weather conditions for Little Mud 1 for test days, April 14–16, 1961*

Date	Sky cover	Solar radiation	Maximum temperature	Minimum temperature	Average wind
	Tenths	*Ly.*	*°C.*	*°C.*	*Cm. sec.⁻¹*
Apr. 14__	0	680	30	9	400
Apr. 15__	0	700	29	11	290
Apr. 16__	0	686	33	10	240

The objective of LS2 was similar to that of LM1, except that in this case the surface condition would be the same throughout and drying of the surface would not be a factor in the results. Thus, a 5-day study was obtained of the evaporation and energy balance of an isolated surface covered with a thin layer of water.

Records of lysimeter weight were obtained every 30 minutes at first and, beginning with 0800 April 20, every 15 minutes. The meteorological variables were recorded every 15 minutes and were identical to those listed for LM1 with the following exception: The heat-flow plates were placed immediately under the plastic film, and the temperature of the water, rather than of the soil surface, was recorded. The data handling system used 29 channels to record information.

Wind data were lost for a 10-hour period (19042200–20040800), owing to a blown fuse in the wind recording system. Otherwise, no significant instrumental difficulties were experienced.

Generally prevailing weather conditions are summarized in table 2.

TABLE 2.—*Weather conditions for Little Splash 2 for test days, April 18–22, 1961*

Date	Sky cover	Solar radiation	Maximum temperature	Minimum temperature	Average wind
	Tenths	*Ly.*	*°C.*	*°C.*	*Cm. sec.⁻¹*
Apr. 18__	3	655	36	15	450
Apr. 19__	4	591	32	19	450
Apr. 20__	1	672	29	13	350
Apr. 21__	2	724	30	9	310
Apr. 22__	2	712	30	11	360

Big Splash 1 (BS1)

In the BS1 experiment the entire field, including the lysimeters, was flooded for 2 days. The plastic film mentioned in the LS2 study remained on the lysimeters. Thus it cannot be stated that the surface conditions inside and outside the lysimeters were wholly identical. Also, the depth of water inside and out differed appreciably at times. These factors may have caused some dissimilarity in net radiation, soil heat flow, and evaporation between field and lysimeters.

Nevertheless, it is felt that BS1 is a representative picture obtained of evaporation and energy balance over an extended shallow water surface.

Water was admitted to the field and added to the lysimeters beginning in the morning of April 24, 1961. The field and lysimeters were maintained flooded through the morning of April 27. The official period of record was from 0000 April 25 through 0000 April 27, or two 24-hour periods.

Records of lysimeter weight were obtained every 15 minutes, as were micrometeorological data in

a manner identical to the previous experiment, LS2. Instrument behavior was normal with the exception of the following. Beginning at about 1700 April 26, lysimeter No. 2 showed an abnormal drift. This was attributed in a general way to the continuous excessive irrigation that resulted in positive pressure potentials at 1.5-m. depth in the soil outside the lysimeter, the exact cause not being known.

General weather conditions are given in table 3.

TABLE 3.—*Weather conditions for Big Splash 1 for test days, April 25 and 26, 1961*

Date	Sky cover	Solar radiation	Maximum temperature	Minimum temperature	Average wind
	Tenths	*Ly.*	*°C.*	*°C.*	*Cm. sec.⁻¹*
Apr. 25	0	734	28	8	260
Apr. 26	0	730	31	8	260

Big Mud 1 (BM1)

The BM1 experiment followed the BS1 experiment immediately. The water disappeared from the surface of the field on April 27 and on the same day the plastic covers were removed from the lysimeters and the lysimeters were irrigated with about 65 mm. of tap water. Official recording started at 0000 April 28 and was continued through 0000 May 3, a total of five 24-hour periods. As time progressed the lysimeters and field became progressively drier until the last day, the entire area had changed to a light color and the surface had become firm. Prior to the experiment, the heat-flow plates were again buried in the soil and thermocouples placed near the surface in a manner identical to experiment LM1.

Records were obtained every 15 minutes of lysimeter weight and other variables in the same way as in previous experiments. All equipment operated without any difficulty.

General weather conditions during the experiment appear in table 4.

TABLE 4.—*Weather conditions for Big Mud 1 for test days, April 28–May 2, 1961*

Date	Sky cover	Solar radiation	Maximum temperature	Minimum temperature	Average wind
	Tenths	*Ly.*	*°C.*	*°C.*	*Cm. sec.⁻¹*
Apr. 28	1	715	34	8	240
Apr. 29	0	748	36	9	320
Apr. 30	0	731	36	13	300
May 1	2	730	37	14	270
May 2	1	730	36	14	340

LYSIMETERS

Design

The following items were considered as the basis for the lysimeter design:

1. The lysimeter should provide a normal rooting profile. This was interpreted as being a normally drained soil column of approximately 150 cm. in depth.
2. The lysimeters should be large enough to minimize the effect of the rims. It was felt that a 100- by 100-cm. square lysimeter with thin steel rims, separated by no more than approximately 8 mm. would come close to meeting this requirement.
3. The installation should be in triplicate to provide at all times an estimate of the error of measurement.
4. The overall weight and construction of the installation should be such that it could be moved if so desired.
5. The weighing mechanism itself should be electronic and extremely compact so that the weight signal could be taken out by underground cable to an appropriate location for registration.
6. The registration of the weight should be automatic, continuous, and in a form immediately usable for automatic data processing.
7. The sensitivity of the installation should be at least 0.05 mm. (0.002 of an inch).

Weighing Mechanism

The weighing mechanism can be considered to be composed of the following parts (figs. 5, 6, and 7): (1) The soil container, or lysimeter proper; (2) the platform carrying the soil container; (3) the counterweights; (4) the counterweight platform; (5) the beam; (6) the flexures which suspend the beam from the foundation and which suspend the soil container platform and the counterweight platform from the beam; (7) the load cell; and (8) the metal enclosure protecting the above parts from the soil and from the atmosphere.

These items are described in further detail as follows:

1. The soil container has an area 100 by 100 cm. and is 161 cm. deep. It is made from 3.1-mm. (11 gage) steel and reinforced with horizontal ribs on the inside at approximately 30-cm. distances. The empty weight of the container is about 380 kg.; when filled with soil at a moisture content of approximately 30 percent by volume, the total weight is approximately 3,110 kg. When the soil is at the 15-bar percentage, the weight decreases to about 2,800 kg. The soil container is completely closed. In order to permit drainage of excess water, five stainless steel filters were laid on the bottom and connected by copper tubing to an outlet at the surface of the

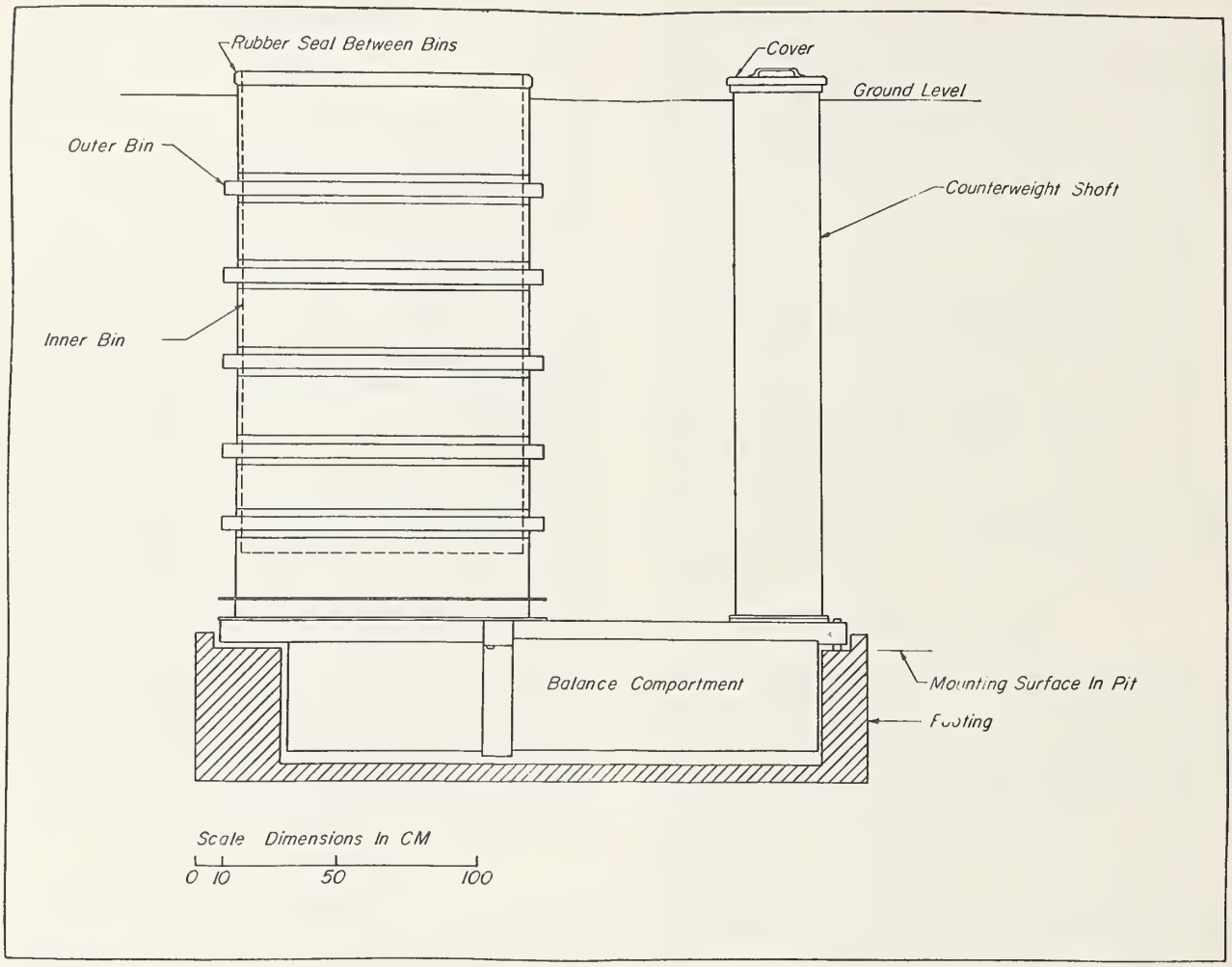

FIGURE 5.—External view of lysimeters.

soil container to permit the application of a vacuum for establishing negative pressure potentials at the bottom of the soil column (see figs. 8, 9, and 10). The stainless steel filters are embedded in fine sand, and the entire arrangement is covered with a 1-cm. layer of 50-micron glass beads. This provides for the establishment of pressure potentials to a maximum of —200 mb. at the bottom of the soil column.

2. The soil container platform consists of four heavy steel columns that support the soil container at the four corners. The steel columns are joined by heavy members, transferring all the weight to a centrally located column, which in turn is hung from the short end of the balance beam. Sideways movement of the platform is prevented by the installation of horizontal flexures, which would be tensioned if any sideway forces would be applied to the platform.

3. The counterweights consist of cylindrical steel weights with a diameter of approximately 30 cm. A number of these are permanently installed and their weight is known only approximately. The rest of the weight is counterbalanced by counterweights that are 12½ kg. ± a few grams in weight. The number of these counterweights changes in accordance with the changes in weight of the soil.

4. The counterweight support platform consists of a single column broadened at the top, which is in turn hung from the end of the beam in a manner similar to the soil container platform. Stops are provided at the counterweight end of the beam to prevent excessive movement.

5. The beam is made of a 20-cm. steel I-beam that is suspended from a yoke, which in turn rests on the foundation by means of cross flexures.

6. The flexures are strips of spring steel about 0.040 inch thick that have considerable strength in tension but resist bending only slightly. Thus, an almost frictionless suspension is achieved in which there is no possibility of change of mechani-

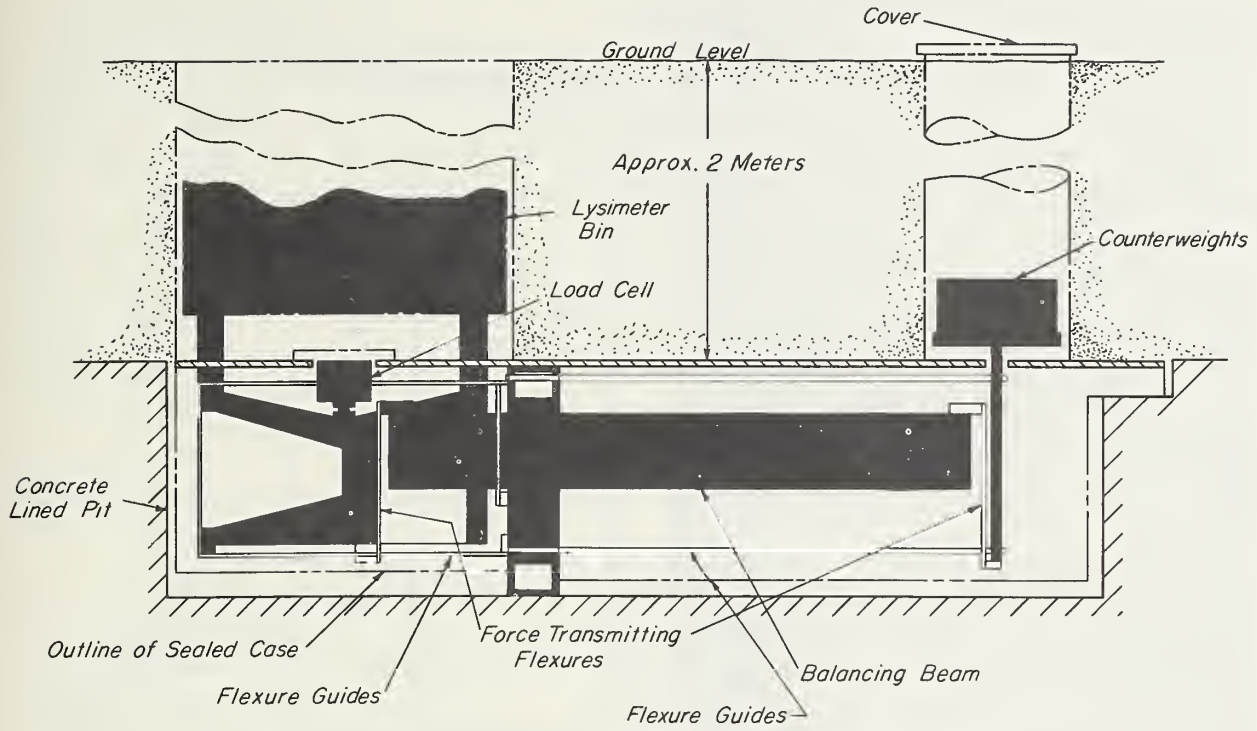

FIGURE 6.—Schematic drawing of the weighing mechanism of lysimeters.

cal advantage. The flexures are bolted to the beam and the platform or supporting yoke, as the case may be.

7. The load cell is a strain gage pressure measuring device that is placed between the soil support platform and a plate, which in turn is secured to the foundation. Thus, the load cell will be compressed whenever the counterweights exceed the weight of the soil container. The mechanical advantage of the beam is four, and therefore the load cell senses four times the weight change, if any, that is created at the counterweight side. When soil container and counterweights are in perfect balance, the load cell is free and the circuitry is adjusted so as to give a slightly negative output. This insures that the load cell is in good contact with the platform when a zero indication is given. The capacity of the load cell is approximately 50 kg. and its indication is adjusted in the circuitry to give exactly this readout when a 50-kg. weight is taken from the soil container after the above-mentioned zero adjustment has been made. By adjusting the number of 12½-kg. counterweights, therefore, the output of the load cell will always be between an indication of zero and 50 kg.

8. The enclosure consists of a hermetically sealed steel container that is sealed either by welding or by gasketing. Actually, this container consists of three parts as follows. (1) A "coffin," which encases the weighing mechanism and through which the four soil platform support pins and the counterweight support pin protrude. (2) A casing for the soil container that, close to the surface, conforms so closely to the soil container as to create an average clearance of less than 8 mm. A very flexible rubber seal bridges the gap between container and casing, to exclude water and moisture, with the area of the rim 5 percent of the total area of the lysimeter. (3) A similar casing surrounds the counterweights and extends to the surface of the soil also and is provided with an access door for the purpose of changing counterweights.

Recording System

The recording panel of the system consists of the following main parts (fig. 11): (1) Input panels; (2) strip chart recorder; (3) digital clock and date input panel; (4) controller; (5) digitizer; and (6) power supply.

1. The input panels are provided with controls to regulate the power to the load cells in such a way as to give an output calibrated in units of weight or of digits. Furthermore, the input panel contains the information on the equivalent weight of the counterweights for each lysimeter. This information is to be dialed in by hand. Finally, the input panel connects the load cells to the measuring components of the digitizer when so instructed by the controller.

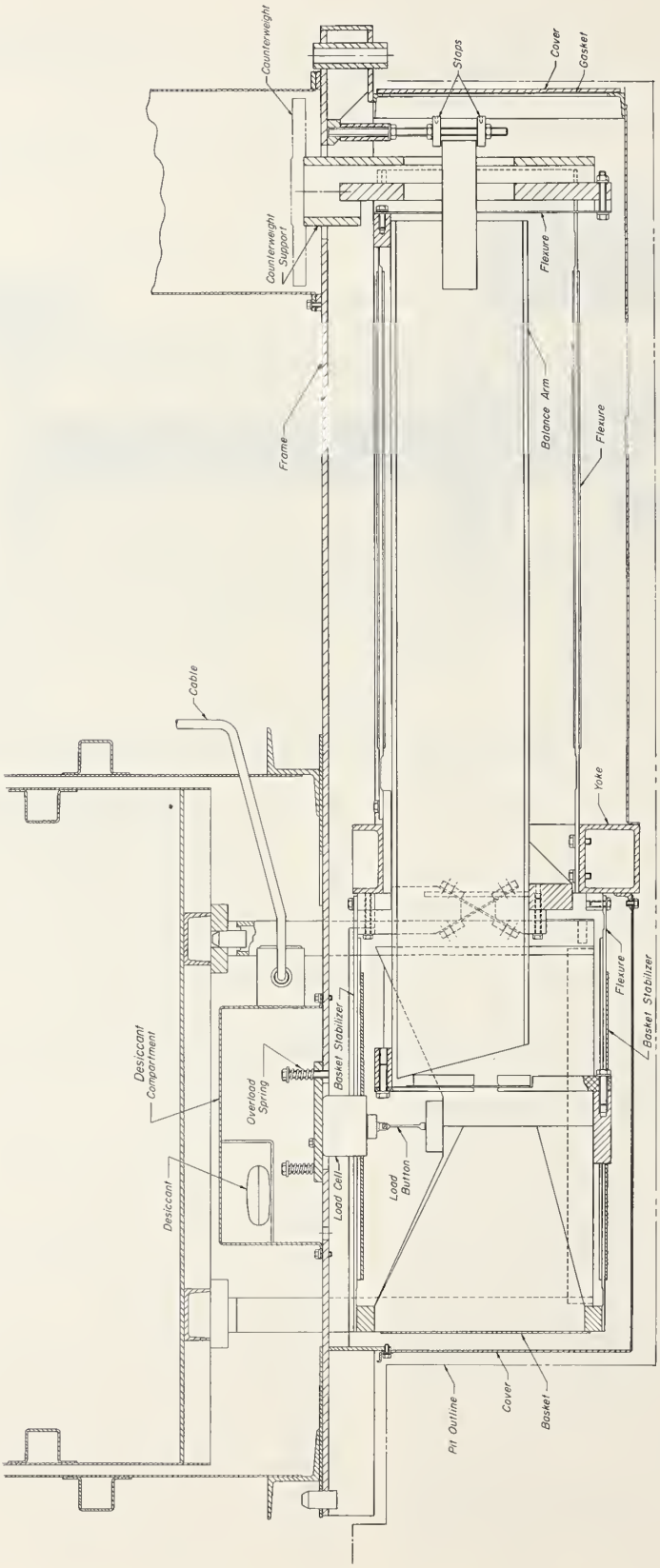

FIGURE 7.—Detailed drawing of the weighing mechanism of lysimeters.

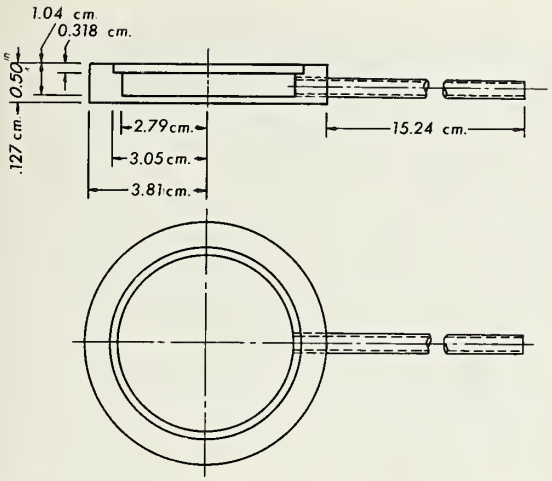

FIGURE 8.—Water extraction cell for lysimeter drainage.

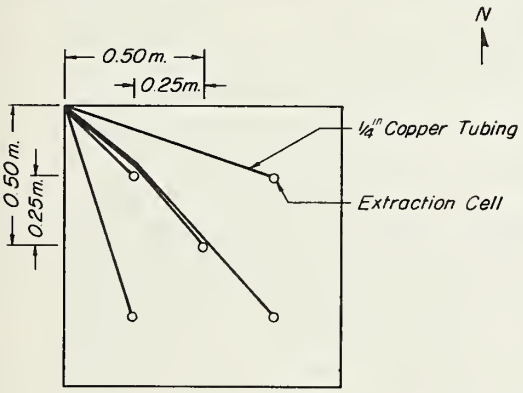

FIGURE 9.—Location of water extraction cells on bottom of lysimeters.

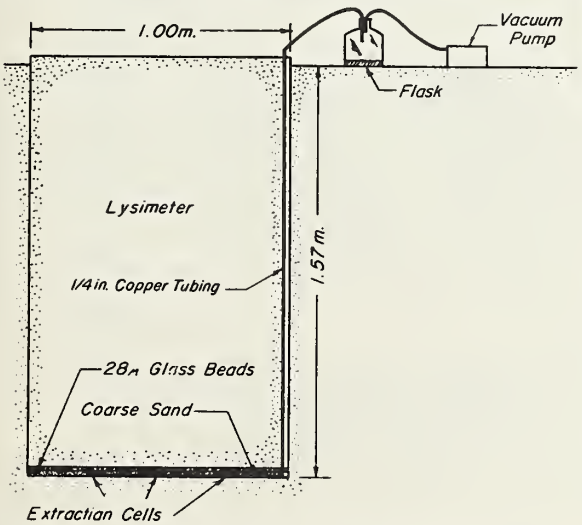

FIGURE 10.—Method of using water extraction cells to provide regulated pressure potentials of bottom of lysimeters.

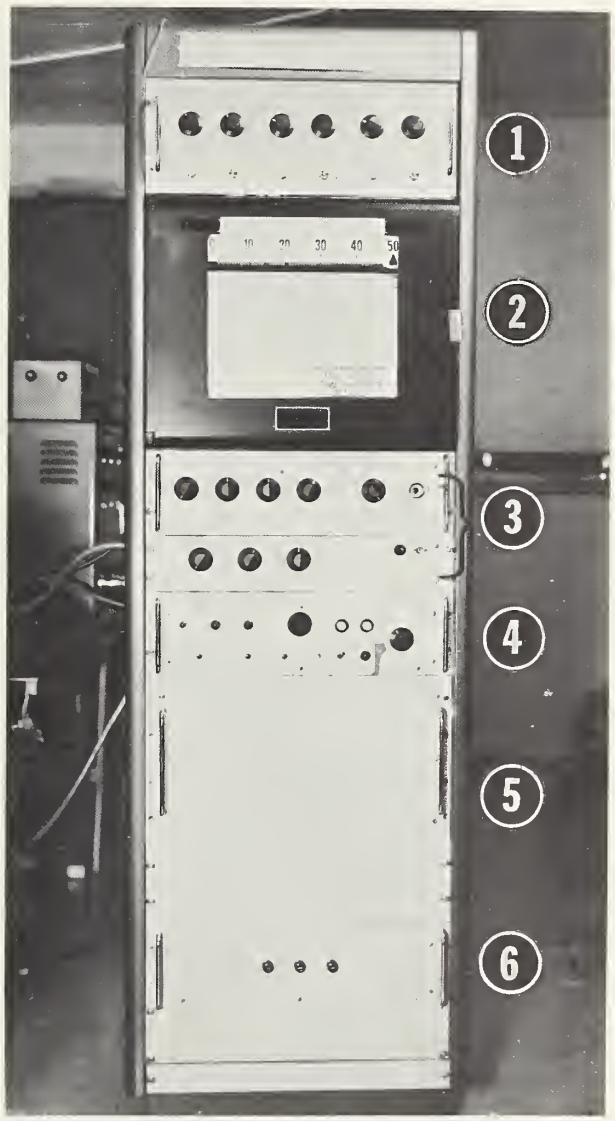

FIGURE 11.—Recording console for weighing lysimeters.

2. The strip chart recorder receives its information from a transmitting potentiometer that is mounted on the digitizer. This signal is then translated into a position of the recorder slide wire contact and mechanically coupled there to a print wheel mechanism. The recorder causes the weight to be printed out on the strip chart, which moves a definite length each time a switch is made from one channel to the next. The switching of lysimeter channels is done by the recorder. The information on the chart of the recorder serves primarily as a visual indication to see if all is well. Accurate evaluation of the weight must be done by resorting to the information stored on the tape. This information may

be listed by means of an automatic typewriter or it can be directly converted to IBM cards with appropriate equipment.

3. The digital clock and date input panel provides running information on the time of day and on the date. Furthermore, by appropriate dial setting the clock will give the signal for an automatic measuring cycle to start. This can be done at every multiple of 5, 10, 15, 20, 30, or 60 minutes.

4. The controller causes the various phases of information retrieval and storage to proceed in the desired manner once a start signal has been given either manually or from the clock mentioned above. Once started, the controller interrogates the clock for the time information and then proceeds to interrogate the three lysimeters as to their number, the weight of the counterweights, and the live weight. As each bit of information is obtained, it is stored in a tape by means of an automatic tape punch. All the information having been obtained, the controller shuts itself and the rest of the system down after everything has been readied for the next cycle.

5. The digitizer receives the signal from the load cell after the proper connections have been created by a command from the controller through the lysimeter input panel. The signal from the load cell is, first, amplified by the digitizer and then a balancing signal is produced that corresponds to a particular angular position of a ten-turn potentiometer. The balance position of the shaft is read out by means of 4 contact wheels for the 4 digits of the number that represents the load cell output. This number may range from zero to 5,000, each digit corresponding to 10 g.

6. The power supply provides stabilized voltages to the various components and in particular a constant 9-volt DC supply to the load cells. This power is applied to the load cells at all times.

DATA HANDLING SYSTEM

To study efficiently the fluxes of sensible and latent heat by the aerodynamic and energy budget methods, a data handling system is required that is capable of rapidly recording micrometeorological elements at specified intervals and presenting the data in a form suitable for machine calculations. To accomplish this, a data system was designed and purchased from the Datex Corp.[1] of Monrovia, Calif., that is capable of recording and translating into tape form forty different EMF, or thermocouple inputs at a maximum rate of one input per second. This system was modified to record 4-unit digital inputs from six Veeder-Root counters.

[1] The use of this or other patented equipment in this report does not imply approval of the product to the exclusion of others that may also be suitable.

Description

The data handling system consists of a self-balancing potentiometer (SBP) with shaft encoder, a storage translator, programmer, digital clock, light-bank unit, four input selector modules, six electromagnetic counters, a Friden Flexowriter and a Friden tape punch. The data handling system is shown in figure 12.

The SBP (fig. 12, A) is a Leeds & Northrup "Speedomax" G millivolt (mv.) recorder. The potentiometer has three ranges: -1 to $+1$ mv., -0.2 to $+2.5$ mv. with cold junction compensation for copper-constantan thermocouples, and -2 to $+18$ mv. The potentiometer has an accuracy rating of ± 0.3 percent of span or 5 microvolts (μv.), whichever is the larger. The sensitivity of the potentiometer is ± 0.15 percent of full scale or ± 2.5 μv., whichever is larger. The full traverse and balance time is less than one second.

The shaft encoder converts the analog shaft position of the SBP to a digital-coded contact closure output. The output is 0000 to 1999 for 324° of shaft rotation. The accuracy of the shaft encoder is plus or minus one-half digit.

The overall accuracy of the SBP and encoder amounts to 6 μv. on a ± 1 mv. range. The accuracy of the system in terms of temperature measured with a single copper-constantan thermocouple is $\pm 0.14°$ C. The accuracy in terms of solar radiation measured with an Eppley pyrheliometer is ± 0.007 ly. min.$^{-1}$ and the accuracy in terms of net radiation measured with a single miniature net radiometer is ± 0.03 ly. min.$^{-1}$.

The control chassis translates and stores the coded decimal representation in a form of contact closures. A serial and parallel output are provided. The parallel output is used for visual display of the encoder data on the light-bank (fig. 12, C) and the serial output for transmission of the data to the programmer (fig. 12, D).

Each of the four input scanner modules (fig. 12, E, F, G, H) provides facilities to select automatically or manually any of its ten input channels. The module contains a dial indicator to display the point that has been selected. In addition, each module contains a bypass switch so that the module may be bypassed from the data recording cycle. With the bypass switch, the number of input variables to be recorded may be selected in groups of ten. The input selector modules are designed to switch sequentially low EMF or thermocouple signals. Two gold-plated levels of a stepping switch within the scanner accomplish this switching.

The programmer (fig. 12, D) controls the advancing of the input selector modules, storage, and clearing of the encoder data and will sequentially present the digital data in a specified format necessary to operate the Friden Flexowriter and/or tape punch. Any of the 40 channels may be

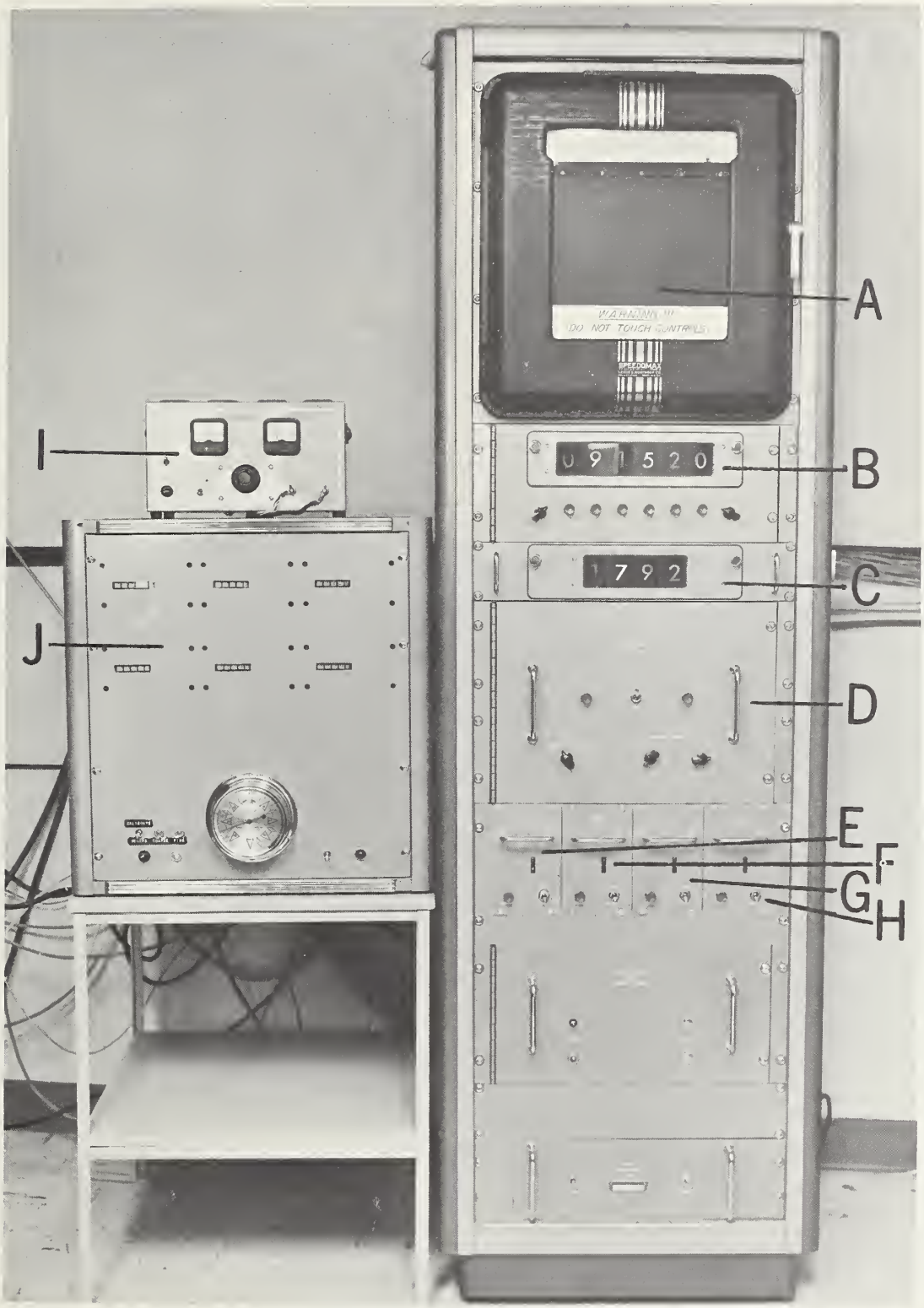

FIGURE 12.—Data handling system.

programmed to any of the 3 ranges by a plugboard arrangement within the programmer.

The data handling system contains a digital clock (fig. 12, B) arranged to present visual and contact closure outputs representing the days of the month 0 to 31, hours 0 to 23, and minutes 0 to 59. The digital clock contains switches for month input and recording cycle. The digital clock automatically initiates a data recording cycle at 5-, 15-, 30-, or 60-minute intervals as selected.

An addition (fig. 12, J) was made to the Datex system to facilitate the recording of windspeed. This addition is discussed in the next section (wind system).

The output from the data handling system is fed into a Friden motorized tape punch, a Friden Flexowriter, or both simultaneously as selected. The tape punch and Flexowriter operate on an 8-channel systems code that can be used on an IBM 046 and 047 tape-to-card converter.

The recording cycle can be initiated automatically or manually as selected, and any single channel may be displayed manually or recorded. When the record cycle is initiated, the data handling system will first record the date-time group (month, day, hours, and minutes); then, will sequentially record the point identification and magnitude of each of the 40 channels in groups of 10 as selected, and will record the contact closures of the 6 electromagnetic counters. The channels are interrogated at the rate of one per second, while the complete recording cycle is completed in one minute.

A sample of the print-out of 40 channels and 5 counters is shown in figure 13. The 40 channels are printed in terms of 2,000 counts full scale and must be referred to the proper range for EMF or temperature value; i.e., channels 02 and 09, 01261600, indicate zero EMF on the ±1 mv. range and the −2 to +18 mv. ranges, respectively, while channel 06 is indicating the system temperature of 84.1° F. In the present form, each line of the data listing contains 88 spaces. The IBM punch card contains only 80 available spaces; therefore, to punch one line of data for 10 channels with data identifier in an IBM card, the system will have to be re-programmed to eliminate the spaces between the channel identifier and the digital readout. When this is accomplished, all 46 channels can be punched into 5 cards, one card per line.

Input Cable Arrangement

The micrometeorological observations are made in the experimental field approximately 250 feet from the building in which the data system is installed. Four cables, buried at a depth of 4 feet, are used to conduct the signal to the system. The cables consist of one 15-pair shielded thermocouple cable, two 16-pair copper wire cables with each pair individually shielded, and one 26-pair shielded copper wire cable. The cables, with the exception of the thermocouple cable, are terminated in junction boxes utilizing Cinch-Jones terminal strips. The thermocouple cable is terminated in a junction box in the experimental field and uses three 5-thermocouple panels. The other end of the thermocouple cable is attached directly to the input selector modules.

Capability

The data handling system is a system that (1) can efficiently transform various inputs into punch tape or data sheets, (2) is very flexible with regard to the number and magnitude of inputs to be recorded, and (3) on the basis of experience ac-

```
04210900 01 1004 02 0154 03 0201 04 1105 05 1110 06 1102 07 0328 08 0278 09 0340 10 0728
04210900 11 0720 12 0724 13 0700 14 0685 15 0665 16 0643 17 0635 18 0658 19 1078 20 0850
04210900 21 1829 22 1967 23 1974 24 0726 25 0697 26 0734 27 0723 28 1586 29 1597 30 1604
04210900 41 0848 42 0969 43 1043 44 1233 45 1079

04210915 01 1004 02 0153 03 0201 04 1120 05 1123 06 1115 07 0366 08 0283 09 0348 10 0652
04210915 11 0739 12 0732 13 0717 14 0708 15 0678 16 0681 17 0674 18 0693 19 1079 20 0904
04210915 21 1906 22 1999 23 1999 24 0756 25 0732 26 0769 27 0706 28 1592 29 1604 30 1615
04210915 41 0997 42 1144 43 1227 44 1444 45 1298

04210930 01 1004 02 0152 03 0201 04 1129 05 1132 06 1125 07 0387 08 0293 09 0366 10 0739
04210930 11 0755 12 0751 13 0734 14 0710 15 0707 16 0722 17 0707 18 0729 19 1046 20 0943
04210930 21 1999 22 1999 23 1977 24 0801 25 0769 26 0805 27 0723 28 1545 29 1552 30 1563
04210930 41 0903 42 1017 43 1087 44 1221 45 1116

04210945 01 1005 02 0152 03 0201 04 1137 05 1142 06 1134 07 0390 08 0307 09 0368 10 0764
04210945 11 0772 12 0719 13 0715 14 0712 15 0723 16 0753 17 0744 18 0772 19 1060 20 0985
04210945 21 1999 22 1999 23 1999 24 0833 25 0803 26 0833 27 0673 28 1494 29 1507 30 1519
04210945 41 0918 42 1037 43 1114 44 1305 45 1194
```

FIGURE 13.—Example of data handling system printout of 30 analog channels (1–30) and five windspeed registers (41–45).

cumulated to date, seems to require very little maintenance to maintain an operational status.

WIND SYSTEM

Estimation of the fluxes of heat and water vapor by the aerodynamic methods requires the automatic recording of windspeeds indicated by sensitive anemometers. The wind system utilized in these studies consists of anemometers (fig. 14)[2] having electrical contacts that actuate remote counters.

Anemometers

The sensitivity of the anemometers is determined by their construction. The three small aluminum cups, approximately 2⅛ inches in diameter and of conical shape with beaded edges, are attached by faired light alloy arms onto a cup boss (assembly weighs 39 g.). This assembly is fitted to a vertical spindle into whose bottom end is fixed a steel pivot that runs in a spherical spring-loaded jewel. At the center of the pressure of the cup assembly, the spindle runs in a special form of ring-type jewel bearing. The combination of jewels is such that the spindle rotates with a minimum starting speed and running torque. The minimum running speeds are less than 0.2 meter per second.

The recording of the windspeed is accomplished by remote electromagnetic counters. A very light contact assembly (rated at 6VDC) is geared into the spindle assembly, which closes contact twice for every three revolutions of the cups. The two contacts are connected to terminals which protrude through the outer case.

Recording System

The recording system (fig. 12, J) consists of six electromagnetic counters[3] having electrical read-

[2] Catalog No. 684A, C. F. Casella & Co., Ltd., Regent House, Fitzroy Square, London, W. 1., England.

[3] Veeder-Root data readout counter, Series B–1538, electrical reset.

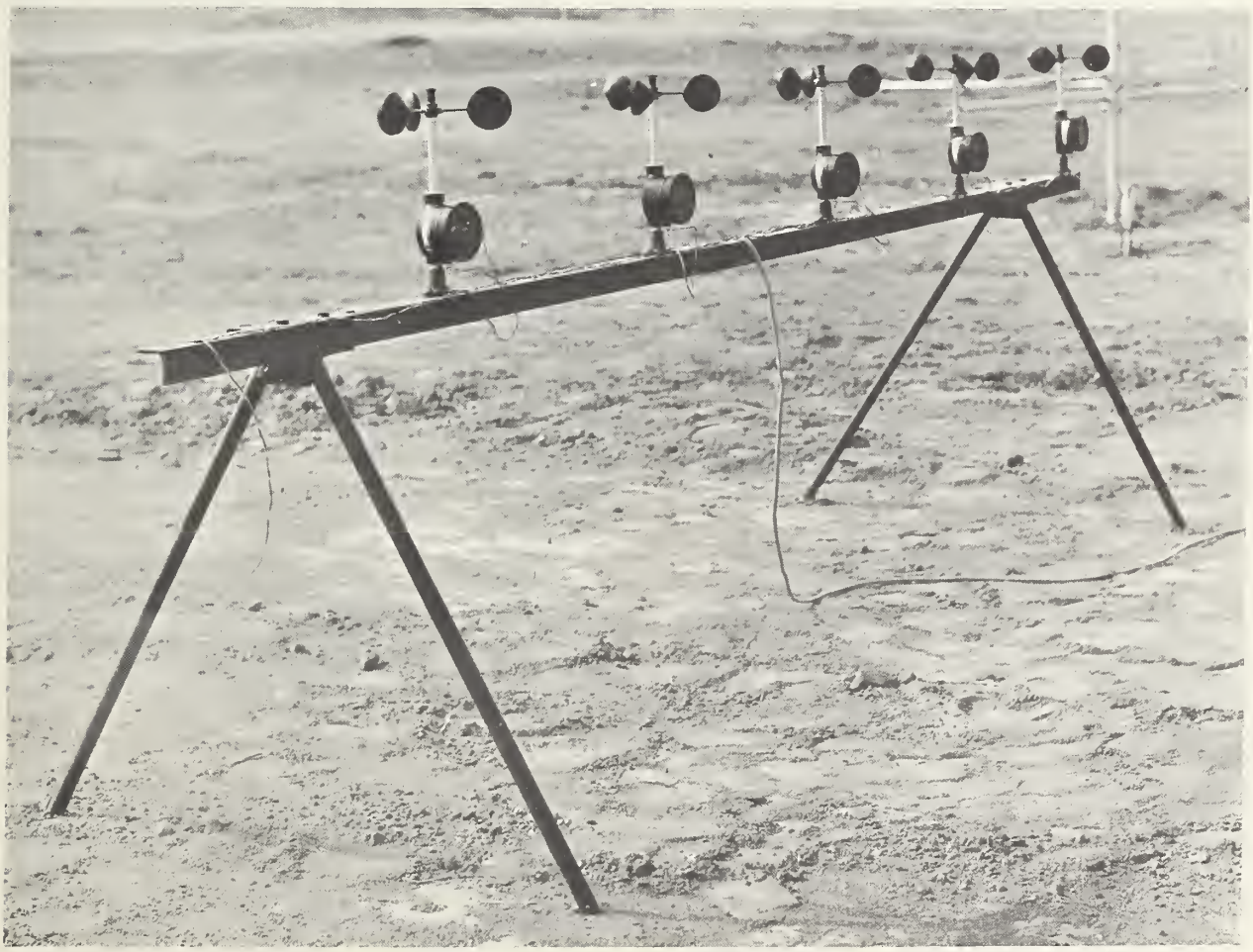

FIGURE 14.—Anemometers mounted on test bar in field.

out and reset features. The counters are mounted in a relay rack and interconnected to the data handling in such a way that the counting action, readout cycle, and reset are controlled by the data handling system. The counter readout utilizes a 10-line code that is translated by the control chassis into the proper signal for the Friden motorized tape punch or Flexowriter. The counters are capable of 1,000 counts $min.^{-1}$, approximately 78 m.p.h., which far exceeds the rating of the anemometers being used.

The recording sequence is arranged so that a signal from the data handling system stops the counting action after the last EMF or thermocouple input is printed out. The counters are then sequentially interrogated, reset to zero, and allowed to start counting again. The noncount time is 8 seconds, which can be neglected when the print-out cycles are 5 minutes or more.

Since the anemometer contacts are rated for 6VDC and the counters are 110VAC, an intermediate relay is required. The relays used (6VDC, 300 ohms) were specially selected because of their low power requirement (0.12 watt). The anemometer contacts became pitted when relays requiring more power (1.2 watts) were used.

The 6VDC is supplied by a filtered power supply [4] having a capacity of 10 amperes (fig. 12, I).

Field Location of the Anemometers

The anemometers were mounted on horizontal pipes that extended 1.3 m. from a triple-guyed, 8-m. mast with pivot base. The mast is located in the middle of the 240- by 300-foot lysimeter field 27 feet due north of lysimeter No. 2. The fetch is adequate in the east, south, and west quadrants, with the Laboratory building obstructing the fetch in the north quadrant.

AIR, WATER, AND SOIL TEMPERATURE MEASUREMENTS

Air Temperature

Air temperatures were measured at five heights: 40, 80, 160, 320, and 640 cm. The air temperature sensing elements (figs. 15 and 16) were constructed similar in principle to those described by Portman (*8*).[5] The air temperature sensing element was constructed by stacking chrome-plated circular brass disks at ¼-inch intervals. The brass disks (20-gage) were 2, 3.75, 5.50, and 7.25 inches in diameter and were spaced ¼ inch apart with plexiglass and Tygon tubing spacers. A 7/16-inch hexagon nut was soldered onto the lower surface

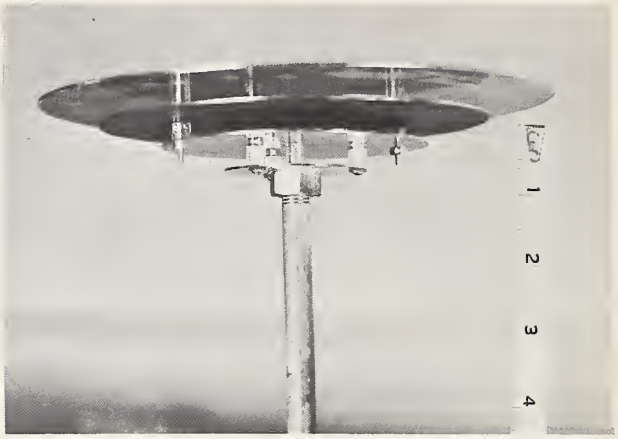

FIGURE 15.—Air-temperature sensing element.

of the bottom brass disk. A ⅛-inch galvanized pipe was threaded and screwed into the hexagon nut. This ⅛-inch pipe served as a support for the air temperature sensing element.

A 24-gage copper-constantan thermocouple junction was clamped between the two center brass disks with the plexiglass spacers. The inner surfaces of the black disks were painted black with Glidden flatblack paint No. 1208.

Quarter-inch holes drilled in the center of the lower two brass disks permitted the passage of a 3/16-inch O.D. plexiglass tubing, which was inserted through the ⅛-inch pipe. The end of the plexiglass tubing was located immediately below the thermocouple junction. The tubing was held in place by an O-ring which was inserted between the ⅛-inch pipe and the lower brass disk. The purpose of this plexiglass tubing was to provide means whereby an air sample may be taken at the same height and location as the air temperature sensing element. This air sample would then be analyzed for moisture content. The second reason for the tubing was to provide a means for aspiration of the thermocouple if necessary.

The overall construction of the air temperature element provided a means whereby the thermocouple was shielded from both thermal and terrestrial radiation. The spaces between the brass disks allowed for free air passage between them. The size and spacing of the circular brass disks were such that internal reflections were not permitted below sun angles less than 20°.

Water and Soil Temperatures

The water temperature was measured with three parallel 30-gage copper-constantan thermocouples. About 20 inches of the thermocouple wire was placed in the water. A small coil of wire was made near the end of the thermocouple wire to support the thermocouple junction above the plastic film and below the water surface. The parallel thermocouples were used to obtain

[4] Electro, Model D–612T.

[5] Italics figures in parentheses refer to Literature cited, p. 44.

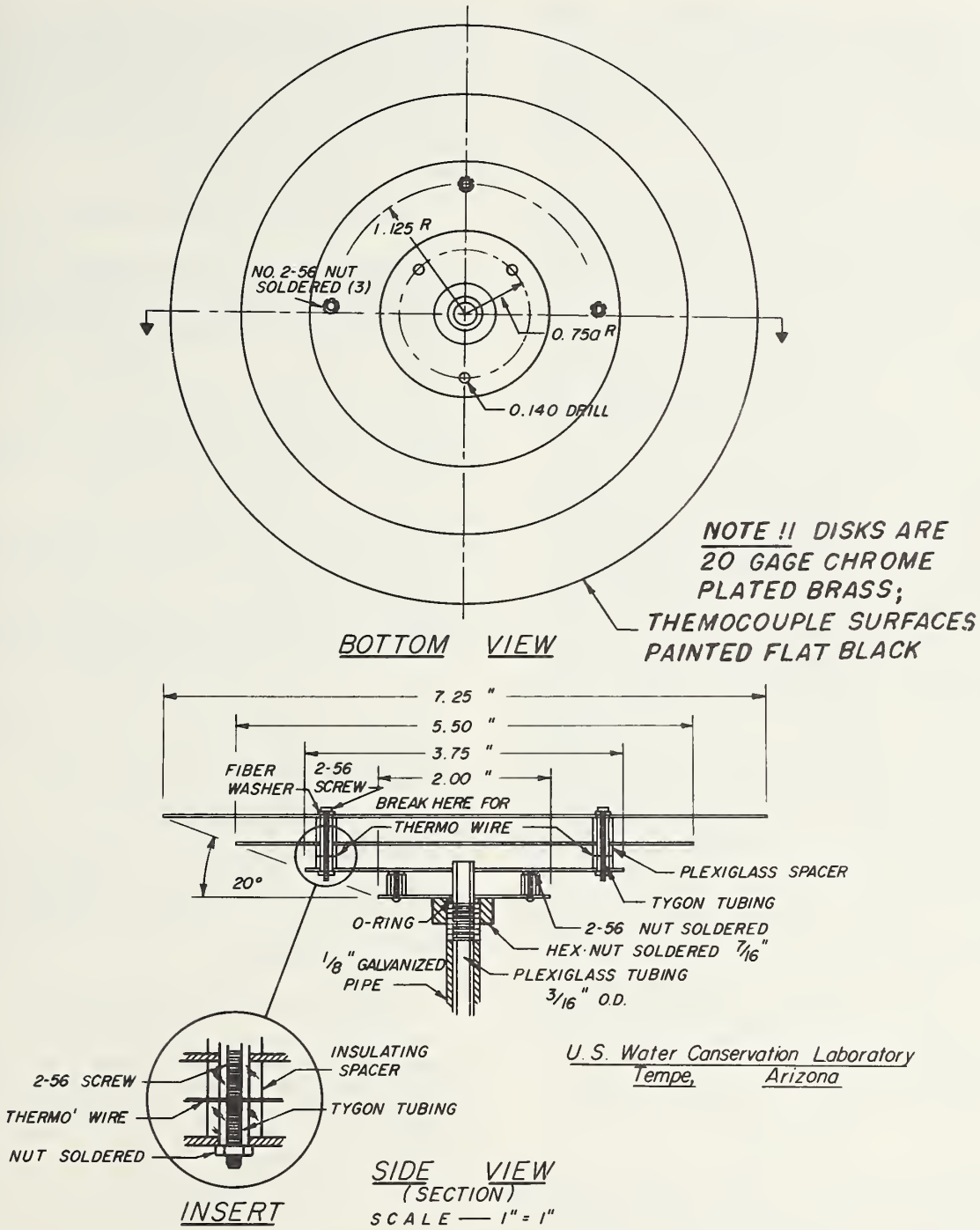

FIGURE 16.—Specifications of air-temperature sensing element.

an average of the water temperature at three locations within the lysimeter.

Soil temperatures were measured with the same arrangement described above, the thermocouples, however, being buried at a depth of 1 to 2 mm. below the soil surface (no plastic cover was used).

Soil Heat-Flow

The soil heat-flow was measured with Beckman and Whitley flow transducers, Model No. ST201–1. These heat-flow transducers are 3⅜ inches long, 1⅛ inches wide, and 3/64 inch thick. The heat-flow transducers were placed at a 2-cm. depth below the soil surface in the experiments of Big Mud 1 and Little Mud 1. In the experiments Big Splash 1 and Little Splash 2, the heat-flow transducers were located on the soil surface immediately below the plastic film that was covering the lysimeter.

These heat-flow transducers have been previously used by other personnel before being used in these experiments. Some separation of the outer surfaces of the heat-flow transducers were noted. These were again clamped together and resealed. A comparative check indicated that the calibration factors of some of the heat-flow transducers had changed.

The heat-flow transducers were considered unsuitable for future research because of the separation of the outer surfaces of the transducer and, also, discontinuity in some of the thermocouple circuits. Therefore, five additional thermal transducers were purchased from the National Instrument Laboratory, Washington 18, D.C., Model No. HF–2. These transducers are approximately 50 mm. in diameter and 3.3 mm. thick. They are constructed of polyvinyl chloride, which has a thermal conductivity of 0.033 cal. $min.^{-1}$ $cm.^{-1}$ $°C.^{-1}$. They have internal electrical resistance of 100 ohms and have a calibration constant of approximately 50 mv. per cal. $cm.^{-2}$ $min.^{-1}$. These heat-flow transducers were calibrated at 20° C. and have a temperature coefficient of approximately 1 percent decrease per increase of 10° C.

ATMOSPHERIC WATER VAPOR CONTENT

Under the existing climatic conditions present instrumentation was not considered adequate for precise profile measurement of water vapor. The climatic conditions referred to all those of high temperatures, low humidities, and dusty conditions.

To obtain the atmospheric water vapor content at one point, a sensing element manufactured by the American Instrument Co., Silver Spring, Md., called the Amino-Dunmore Electric Hygrometer, was utilized. The element is an electrical resistor consisting of a polystyrene cylinder, a dual winding of precious metal wire, and a coating of lithium chloride. The operation of the element is based on the ability of a hygroscopic film to change its electrical resistance instantly with micro-changes in relative humidity. Specifications indicate reproducibility within tenths of a percent of relative humidity and calibration accuracy of ±1½ percent relative humidity.

ENERGY-BALANCE METHODS

The primary emphasis in these studies is on the energy-balance method because of the lack of adequate instrumentation for precise measurement of water vapor profiles under local climatic conditions. However, some aerodynamic formulas are utilized.

The energy-balance method is based on the principle of conservation of energy. The basic equation for an evaporating bare soil surface is

$$R_n+A_m+S+LE_m=0 \quad (1)$$

where all fluxes toward the surface are considered positive and fluxes away from the surface are considered negative.

When S is measured with a heat-flow transducer at some depth below the soil surface, we have:

$$R_n+A_m+S+S'+LE_m=0. \quad (2)$$

When the energy-balance method is applied to a shallow water layer, as in the case of Little and Big Splash experiments, the formula is:

$$R_n+A_m+S+W+LE_m=0. \quad (3)$$

Since all of the terms but A_m in these equations can be measured directly, A_m may be obtained by solving the equations. The values thus obtained can be compared to values of A calculated by the aerodynamic methods.

AERODYNAMIC METHODS

The vertical flux of sensible heat is to be computed from wind and temperature gradients by the formula cited by Sheppard (*9*). In terms of our notation, we have

$$A=\frac{\rho cpk^2(U_3-U_1)(T_1-T_3)}{(1nZ_3/Z_1)^2}. \quad (4)$$

Heights Z_1 and Z_2 will also be used to compute the sensible heat flux. In view of the fact that equation 4 was developed for a large homogeneous area, some doubts exist concerning the data for heights and even to the use of this equation at our experimental site.

Since adequate instrumentation was considered lacking for gradient measurements of water vapor,

the normal aerodynamic formulas could not be used to determine the local rate of evaporation. The method proposed by Sverdrup (*12*) was used. This method gave promising results in the Lake Hefner studies (*13*).

In terms of our notation

$$Ec=\frac{0.622\rho k\overline{U}_*(\overline{e}_0-\overline{e}_3)}{P\left\{\ln\frac{Z_3+Z_0}{\delta+Z_0}+\frac{k\delta\overline{U}_*}{D}\right\}}.$$

Again the height used for the measurement of water vapor may be questionable; however, the formula should be applicable in Big Splash and Big Mud experiments.

NET RADIATION

The net radiometer is an instrument designed to measure the net flux of radiation through a horizontal plane. The measurement of net radiation, in principle, is quite simple. One has to place a blackened plate in the radiational field and measure the temperature difference that develops between its two surfaces (see appendix, p. 45, for derivation).

Measurement of net radiation for meteorological purposes is more difficult because of the different wavelengths involved. Net radiation for meteorological use may be defined as

$$R_n=R_{su}-rR_{su}+R_{sk}-rR_{sk}-R_{ea}.$$

The symbols are defined on page 5. The wavelengths of the sun range from 0.2μ to 3μ and are approximated by blackbody radiation at $6{,}000A$, while the wavelengths of sky and terrestrial radiation range from 3μ to 60μ and are approximated by blackbody radiation at $300A$. In other words, the net radiometer must be equally sensitive to radiation ranging from 0.2μ to 60μ.

The terms involving thermal convection (appendix, p. 45, equation 14) may be eliminated or reduced by shielding the thermal transducer or by equalizing its effects on both surfaces of the sensor. Until recently, there has been no material that is weatherproof and has acceptable transmission characteristics, so enclosing the thermal transducer to eliminate the effects of thermal convection terms has not been feasible. Gier and Dunkle (*5*) have artificially reduced the thermal convection term by directing a constant windstream across the thermal transducer. To eliminate completely the effect of thermal convection, the windstream must have equal velocities over both surfaces and T_t must equal T_b. The thermal convection terms may be eliminated by enclosing the thermal transducer. The use of mica and vinylidene chloride for this purpose has been discussed (*3*, *4*).

Gier and Dunkle (*5*) have listed the following criteria for evaluation of net radiometers:

1. *Spectral characteristics.*—The response of the instrument should be independent of the wavelength of the incident energy. The instrument should have no windows, filters, or mirrors that would absorb radiation selectivity. The blackening material on the radiation-absorbing surface should be nonselective; that is, the absorptivity should be independent of the wavelength of the incident energy.
2. *Cosine law.*—The blackening material should obey the cosine law. The absorptivity should be independent of the angle of incidence of the radiation.
3. *Shape factor.*—The absorbing surface should be a plane surface and should be able to view the whole hemisphere.
4. *Transient response.*—The instrument should respond rapidly to changes in irradiation or net interchange and should come to a steady state rapidly.
5. *Stability.*—The instrument should give a stable, reproducible reading.
6. *Sensitivity.*—The output of the instrument should be sufficient so that it can be fed into a conventional recording instrument or read upon a standard portable potentiometer.
7. *Weathering.*—As the instrument is exposed to the weather, it should be constructed of materials that are subject to a minimum of deterioration.
8. *Portability.*—The instrument should be rugged enough to withstand handling, and it should be readily portable.
9. *Effect of surroundings.*—The value obtained for the irradiation with the radiometer should be independent of the temperature difference between the radiometer and the ambient conditions, and of the irradiation falling upon the back side of the radiometer.

The effect of surroundings should be expanded to include such factors as rainfall, wind velocity, dust, hail, and stability with time.

It is the purpose of this report to describe the construction of a shielded-type net radiometer and the methods of calibration, and to evaluate its use.

Construction of the Miniature Net Radiometer

The miniature net radiometer (MNR)[6] is constructed of the parts and materials shown in figures 17 and 18. The assembly of the MNR is accomplished by sandwiching a thermal transducer [7] between two sheets of polystyrene,[8] which

[6] Commercially available from C. W. Thornthwaite Associates, Route 1, Centerton, Elmer, N.J.

[7] National Instruments Laboratories, Inc., 828 Evarts Street, N.E., Washington, D.C., Cat. No. HF–1–U.

[8] Sold under the trademark "Polyflex," Plax Corp., P.O. Box 1019, Hartford, Conn.

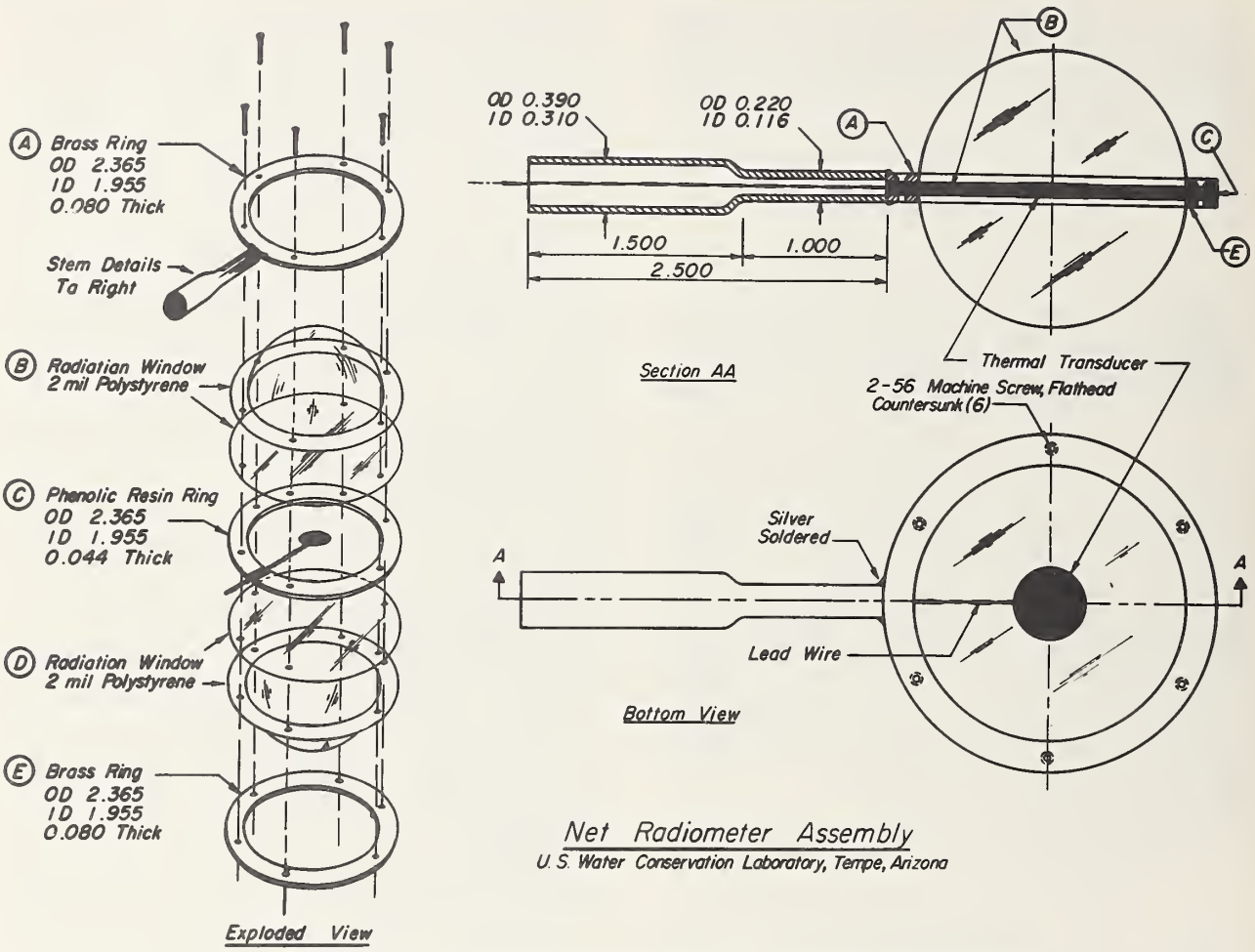

FIGURE 17.—Exploded and assembled views of the miniature net radiometer.

are spaced by means of a phenolic resin ring. (The surfaces of the thermal transducer had previously been painted with a lampblack-type paint.) Then, the two outer radiational windows, which were hemispherically shaped, were placed on either side. The polystyrene sheets and the hemispherical radiational windows, after shaping, were about 2 mil thick. This unit is then clamped together with two chrome-plated brass rings, one on either side. The thermal transducer wire was led through the stem to a 2-conductor cable-type connector.[9] The shell of the connector had previously been soldered onto the stem. This assembled unit can be plugged into a receptacle in the field or in the calibration chamber.

Condensation within the MNR and collapse of the hemispherically shaped radiational window due to sudden changes of ambient pressure were prevented and provided a continuum of air within each of the three sections of the MNR through a reservoir of desiccant in the connector to the atmosphere. This was accomplished by punching a small hole in each of the two polystyrene sheets and connector. A small quantity of finely ground silica gel was located within the void of the connector assembly as the desiccant.

The assembly of this unit is quite similar to those previously described (*3*, *4*). The major differences are that the outer radiational windows have been hemispherically shaped so that the response of the MNR to varying angles of incidence follows the cosine law and the unit as assembled facilitates runoff of precipitation. The radiational windows were constructed of polystyrene rather than vinylidene chloride or mica. The polystyrene has more acceptable transmission through the wavelengths of terrestrial radiation, namely, 3μ to 60μ.

The transmission of wavelengths through plastic films less than 2μ is generally very acceptable. The transmission of polystyrene (fig. 19) from 4μ to 15μ is irregular, with two major absorption

[9] "Amphenol" 80MC2M and 80MC2F.

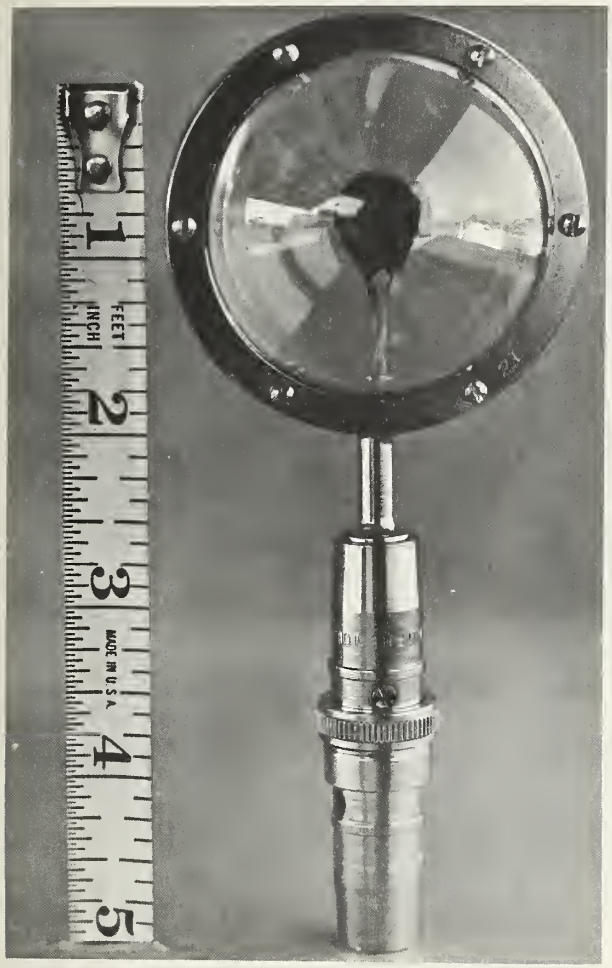

FIGURE 18.—Miniature net radiometer.

bands at 13μ and 14μ. The transmission through polystyrene through the wavelengths of 4μ to 13μ is about 80 percent and is very much better than that of vinylidene chloride and mica.

Methods of Calibration

The net radiometer was calibrated in a modified version of the calibration chamber described by Johnson.[10] The calibration chamber is capable of simulating solar- and terrestrial-type radiation.

Long-wave calibration.—The source of radiation is the walls of the calibration chamber that were lined with brass plates (painted black) having copper coils soldered onto the back of the plates (fig. 20). These plates were arranged so that each half of the calibration chamber contains five plates.

Water, of constant temperature, was pumped independently through each half of the calibration chamber. Valves, placed in the line to each plate, were used to regulate the amount of water flowing through the coils, and, consequently, to regulate the temperature of each plate. The temperature of the plates was controlled to $\pm$ 1° C.

Thermocouples were cemented to each plate to obtain (1) each plate temperature and (2) the temperature difference between the upper and lower half of the chamber.

A plastic divider was inserted between the upper and lower halves of the chamber (1) to support and center the MNR and (2) to prevent circulation between the two halves of the chamber.

The emissivity of the calibration chamber was obtained by the *nonequilibrium method* (appendix p. 46) and was found to be 0.95.

The heat transferred by radiation between the two halves of the calibration chamber was calculated by

$$q=\epsilon\sigma(T_1^4-T_2^4). \qquad (5)$$

The complete derivation of the equation is given in the appendix, page 45, as equation 19.

The radiational flux between the upper and lower half of the calibration chamber could be regulated by adjusting the water temperature. In practice, the water circulating through the lower half of the chamber is held at a temperature above the dewpoint (i.e., 20° C.) and the temperature of the water circulating through the upper half of the chamber is adjusted to obtain the desired radiational flux.

Short-wave calibration.—The short-wave calibration was accomplished in the chamber (see fig. 20, B), with an Eppley pyrheliometer, Model 50, as a standard. The source of radiation was a tungsten filament lamp. The peak emission of the tungsten filament is approximately 0.99μ.

Since the Eppley pyrheliometer is only sensitive to radiation of less than 4μ and the net radiometers are sensitive to radiation of much longer wavelengths, glass filters were used to filter the long-wave radiation from the surfaces of the lamp and calibration chamber. Two glass filters were placed on top and one glass filter was placed on the bottom of the calibration area in the chamber. Two filters were used on top because the uppermost filter would absorb enough radiation to become heated and would reradiate long-wave radiation. The second upper glass filter would absorb the majority of the long-wave radiation from the top filter. The difference in radiation between the glass filters adjacent to the calibration area was corrected for in calibration.

During short-wave calibration, the temperature of the brass plates was controlled at 20° C. and the output of the Eppley pyrheliometer was corrected for its temperature dependence.

[10] Johnson, D. S. Progress report on radiometer test. U.S. Weather Bureau unpublished mimeo. rpt. December 1956.

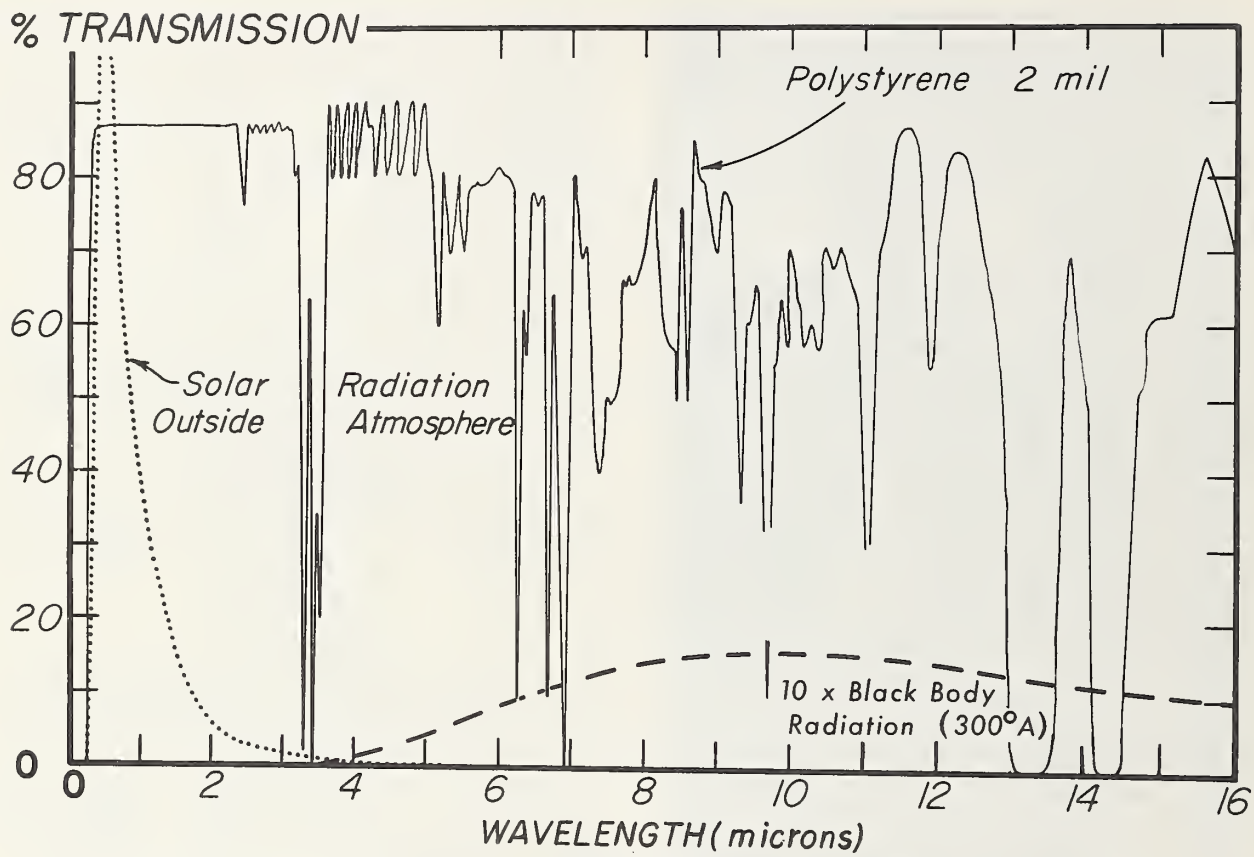

FIGURE 19.—Percentage of transmission of 2 mil polystyrene as a function of wavelength.

The radiational intensity of the tungsten lamp was controlled by a voltage stabilizer and was regulated by adjusting the line voltage.

WIND PROFILE METHODS IN THE NEUTRAL SURFACE LAYERS

The wind data obtained in these four experiments were rather unique in that the data were obtained consecutively over surfaces of different roughness, using the same instruments and under similar climatic conditions. The parameters derived therefrom are used in the aerodynamic equations to obtain estimates of the fluxes of sensible heat and water vapor, but are also of considerable interest in themselves.

The average wind data obtained under conditions of neutral stability ($dT/dZ<0.12C/280$ cm.) were plotted against $\ln Z$ and a linear regression was obtained for each profile. Using the following relation

$$\overline{U}=\frac{\overline{U}_*}{k}\ln\frac{Z}{Z_0}, \qquad Z\geq Z_0,\ k=0.4, \tag{6}$$

we obtained the values for the basic parameters, Z_0 and U_*, where Z_0 is the Y intercept and U_* is equal to k divided by the slope of the line. Other parameters derived from equation 6 were the eddy stress, drag coefficient, the eddy viscosity, and Nikuradse's test for smooth and fully rough flow.

The eddy stress was computed by

$$\tau=\rho\overline{U}_*^2. \tag{7}$$

According to Sutton (*11*) the mean flux of momentum per unit area or eddy stress also equals

$$\tau=(\mu+A)\frac{d\overline{U}}{d\overline{Z}}. \tag{8}$$

By writing $K_m=A/\rho$ and $\nu=\mu/\rho$, equation 8 becomes

$$\frac{\tau}{\rho}=(\nu+K_m)\frac{d\overline{U}}{dZ}\simeq K_m\frac{d\overline{U}}{dZ}\text{ if }\nu\ll K_m, \tag{9}$$

where K_m is called eddy viscosity, ν the kinematic viscosity, μ the dynamic viscosity, and A the Austausch or exchange coefficient.

If we neglect ν in equation 9 and utilize a mixing length hypothesis where l is the mixing length,

$$K_m=\frac{\overline{U}_*^2}{d\overline{U}/dZ}=\overline{U}_*l=k\overline{U}_*Z. \tag{10}$$

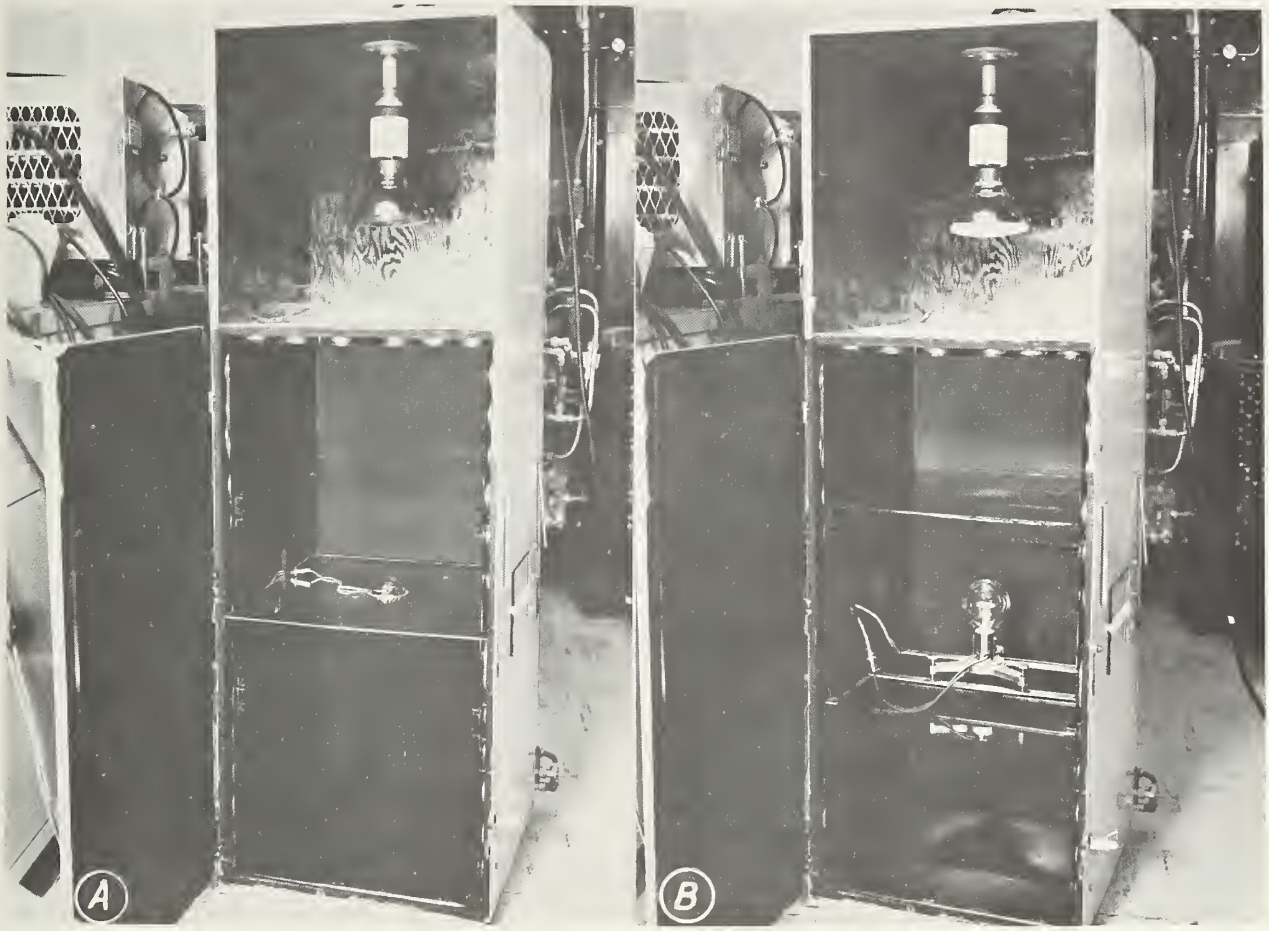

FIGURE 20.—Calibration chamber: *A*, With a miniature net radiometer in position for long-wave calibration; *B*, with the Eppley pyrheliometer in position for short-wave calibration.

This assumes that the mixing length is of the same order of magnitude as the height of the reference plane above the surface. Values of K_m were computed at Z_3.

The drag coefficient at Z_3 was calculated by

$$C_D=\frac{\tau 0}{1/2\rho\overline{U}^2}=2\left[\frac{U_*}{\overline{U}_3}\right]^2. \qquad (11)$$

Values of $(U_*Z_0)/\nu$ were computed for Nikuradse's test for smooth and rough surfaces (*2*) written as

$$\text{Smooth flow: } \frac{U_*Z_0}{\nu}<0.13$$

$$\text{Fully rough flow: } \frac{U_*Z_0}{\nu}>2.5$$

RESULTS

LYSIMETER PERFORMANCE

Lysimeter performance can be described under the following categories: (1) Sensitivity, referring to the least weight changes that may be detected; (2) accuracy or calibration, referring to the agreement between true and indicated weight changes; (3) the effect of load distribution; and (4) external effects on indicated weight, primarily wind effects,

1. The sensitivity of the system proved to be considerably in excess of the specifications, which called for a sensitivity of 5 digits, or 50 grams. This aspect was studied by means of adding or taking off small weights such as 20-, 50-, and 100-gram balance weights. It appears that the sensitivity of the system is somewhere between 1 and 2 digits, or 10 or 20 grams (fig. 21). This is equivalent to a sensitivity between 0.0004 and

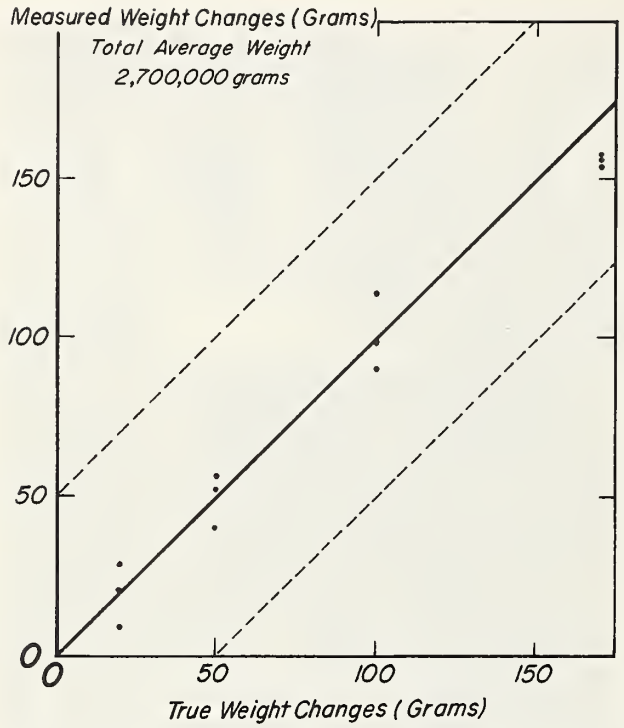

FIGURE 21.—Sensitivity of lysimeters (data not identified by lysimeter number).

0.0008 inch, or 0.01 to 0.02 mm. The weighing lysimeters appear to be more sensitive than any reported heretofore.

2. Since the end points of the calibration can be accurately set and maintained, the accuracy depends on the linearity over the range from 0 to 50 kg. This was examined by placing large weights on the lysimeter after it had been zeroed in at both end points. It was found that the largest deviation from the true weight was 60 g. and in most cases it was no more than 20 g. Thus, it appears that accurate changes of weight will be obtained over the entire range of the load cell. The movable counterweights having been made with considerable precision, the foregoing statement would apply to the entire range of measurement.

The true weight of the soil is less easily ascertained, owing to the fact that the permanent counterweights are not accurately weighed and also since the weight of the various components of the balance itself has not been precisely determined. Therefore, there is probably uncertainty of about 50 kg. in the total weight of the system. However, the total weight itself is of no particular interest for most purposes. Rather it is the change in weight as a result of evaporation or precipitation that one wishes to study.

The estimated total weights, however, were very close to the predicted total weights on the basis of the known properties of the soil, and the soil container is quite accurately known, probably to the nearest kilogram.

3. One of the problems in the lysimeter design was to eliminate any effect of changes in the load distribution as might result from unequal extraction of moisture with regard to the center of gravity of the lysimeter proper. Tests were carried out by moving a fairly large weight from one corner of the lysimeter to the other and to the center. The change in weight caused by such changes in distribution of weight were not larger than 2 digits, or 20 grams, and are therefore considered insignificant.

4. The effect of wind on the measured weight of the lysimeters has been studied. Data show that with windspeed below 4.0 to 5.0 m. sec.$^{-1}$ the fluctuations in weight of the lysimeters are less than the rated accuracy, i.e., less than 50 g. For periods of time where the windspeed is occasionally greater than 5.0 m. sec.$^{-1}$ the deviation from the true weight may exceed 50 g. The replication within lysimeters and the repetitive weighing still enable maintenance of the error below 50 g. in most instances. The wind effect is definitely the factor that limits the precision of the lysimeters.

MODIFICATIONS REQUIRED FOR WIND SYSTEM

During the first test of the wind system, a dust storm was encountered. The bearings of the anemometers became dirty, thus altering the calibration curves. The anemometers were cleaned in the laboratory, fitted for an air tap, and adjusted for minimum starting speed. The anemometers were then placed 1.5 feet apart on a test bar (fig. 14) oriented perpendicular to the wind and were pressurized (1 pound square inch^{-1}) with filtered, dry, compressed air. After cleaning and pressurization, the number of contact closures of the anemometers, when compared with a newly calibrated anemometer, agreed within 1 percent for 30-minute print-out cycles over a 24-hour period. This close agreement between anemometers and the fact that the calibration curves are a linear equation, over the range used, simplify the computation of the wind data in that a common linear calibration curve can be used for all anemometers.

After limited use of the Veeder-Root counters, an intermittant open circuit was noticed in the readout features. This is easily remedied by proper adjustment; however, the open circuit causes an incomplete print-out cycle of the data handling system and a loss of subsequent data until the trouble is noted. To prevent this unnecessary loss of data, the wind system is to be modified so that a space signal automatically closes an open circuit and a trouble light is lighted.

This modification will (1) prevent the unnecessary loss of data and (2) will indicate which counter is faulty.

EVALUATION OF MINIATURE NET RADIOMETER AND CALIBRATION METHODS

Comparison of Calibration Methods

To verify the similarity of the long-wave and short-wave methods of calibration, an unshielded thermal transducer was calibrated by both methods. The results obtained are shown in figure 22. The double-ringed circles represent the radiational intensity versus the output for long-wave calibration, whereas the single-ringed circles represent the output at various intensities for short-wave radiation. There is very little difference between the sets of data points; therefore, the methods of calibration were considered comparable.

Long- and Short-Wave Calibration of a Miniature Net Radiometer

The same thermal transducer was then assembled into a MNR, as previously described, and was recalibrated for both sources of radiation. The *X*'s (fig. 22) represent the calibration curve obtained for long-wave radiation, and the solid circles represent the curve obtained for short-wave radiation. Again, the data points obtained by the two methods fall essentially on the same line. Therefore, it was concluded that the MNR was equally sensitive to both long- and short-wave radiation.

Cosine Response

The MNR was further evaluated to determine if the response to varying angles of incidence followed the cosine law. This was accomplished in the calibration chamber, with the light used as the source of radiation and with the angle varied between the MNR and the light beam.

The results obtained are shown in figure 23. The points fall on the theoretical line at angles simulating larger sun angles. The deviation from the theoretical values at 30° and below was associated with the reflectivity of the surface of the thermal transducer. This conclusion was arrived at by calibrating an unshielded thermal transducer at various sun angles. Similar results were obtained with a Beckman and Whitley net radiometer.[11] The error of cosine response, in terms of net radiation for 12 hours of daylight, is less than 2 percent.

[11] Portman, D. J., and Dias, Fleming. Influence of Wind and Angle of Incident Radiation on the Performance of a Beckman & Whitley Total Hemispherical Radiometer. Final report to the U.S. Weather Bureau, Contract Number Cwb-9350. 1959. [Mimeographed.]

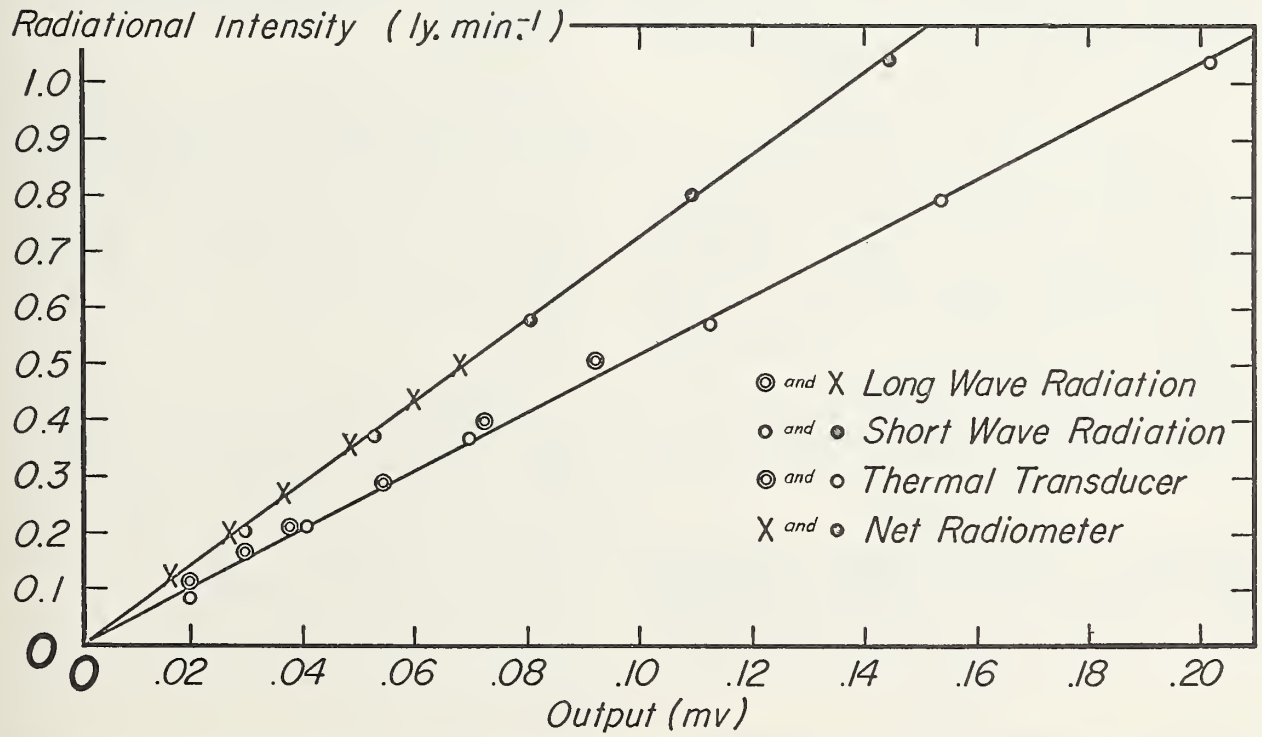

FIGURE 22.—Long- and short-wave calibration curves for an unshielded thermal transducer and a miniature net radiometer.

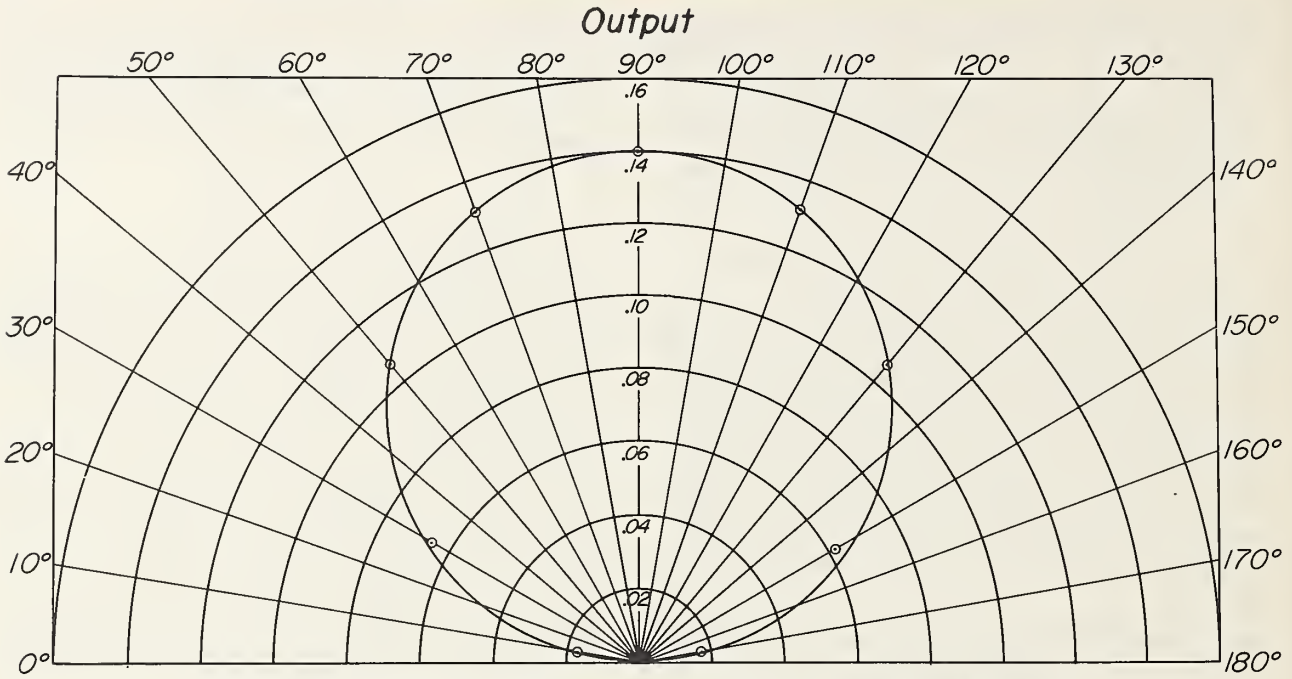

FIGURE 23.—Response of a miniature net radiometer to various angles of incidence.

Time Constant

The time constant of the MNR was determined on a recording potentiometer having a 2-second response time. Approximately 2 seconds were required for 80 percent of 1 g. cal. cm.$^{-2}$ min.$^{-1}$ change in net radiation to be recorded and 5 minutes for 100 percent of 1 g. cal. cm.$^{-2}$ min.$^{-1}$ change in net radiation to be recorded.

Effect of Ambient Temperature

The effect of ambient temperature on the output of the MNR was determined in the calibration chamber. A MNR was subjected to long-wave radiational fluxes when the ambient temperature (the average of the upper and lower plate temperatures) was varied between 20° and 60° C. The data points obtained appeared to fall on the same line when the radiational flux was plotted versus the output. The output was assumed to be independent of ambient temperatures from 20° to 60° C. Hatfield (*6*) reported no sensible change in the disk constant over the range 15° to 100° C.

Effect of Wind

The MNR was subjected to blasts of compressed air while in the calibration chamber and to very gusty winds in the field. The output of the MNR, under conditions of uniform radiation, appeared to be unaffected by either wind direction or speed.

Weathering

A MNR was placed in the field for 60 days. The instrument was then recalibrated. The calibration factor remained unchanged and there were no visible signs of deterioration of the radiational windows.

Comparison of the Miniature Net Radiometer and a Beckman & Whitley Model N188–01 Net Radiometer

A miniature net radiometer and a new Beckman & Whitley, Model N188–01, net radiometer were located in the middle of a 300-foot-square field of bare soil, 115 cm. above the soil surface, 3 m. apart on an east-west axis, and were oriented to the south. The field was then flooded and allowed to dry. Net radiation measurements were made at 30-minute intervals for four consecutive days after flooding and for one day, 12 days after flooding.

The results obtained for the first 3 days while the soil surface was moist were quite similar and are exemplified by figure 24. The net radiation measured by the two net radiometers is essentially the same during the daylight hours but differs by about 0.05 ly. min.$^{-1}$ during the nocturnal hours.

After the soil surface became dry, different radiational fluxes were indicated during the afternoon while similar nocturnal discrepancies existed as when the soil surface was moist (fig. 25).

The discrepancies may be partially explained with the aid of figure 26. The data for this figure were obtained when the Beckman & Whitley net radiometer was placed in the calibration chamber at zero radiational flux (20° ± 1° C.) and the output noted while the room temperature was varied between 6° C. and 40° C. The net radiation indi-

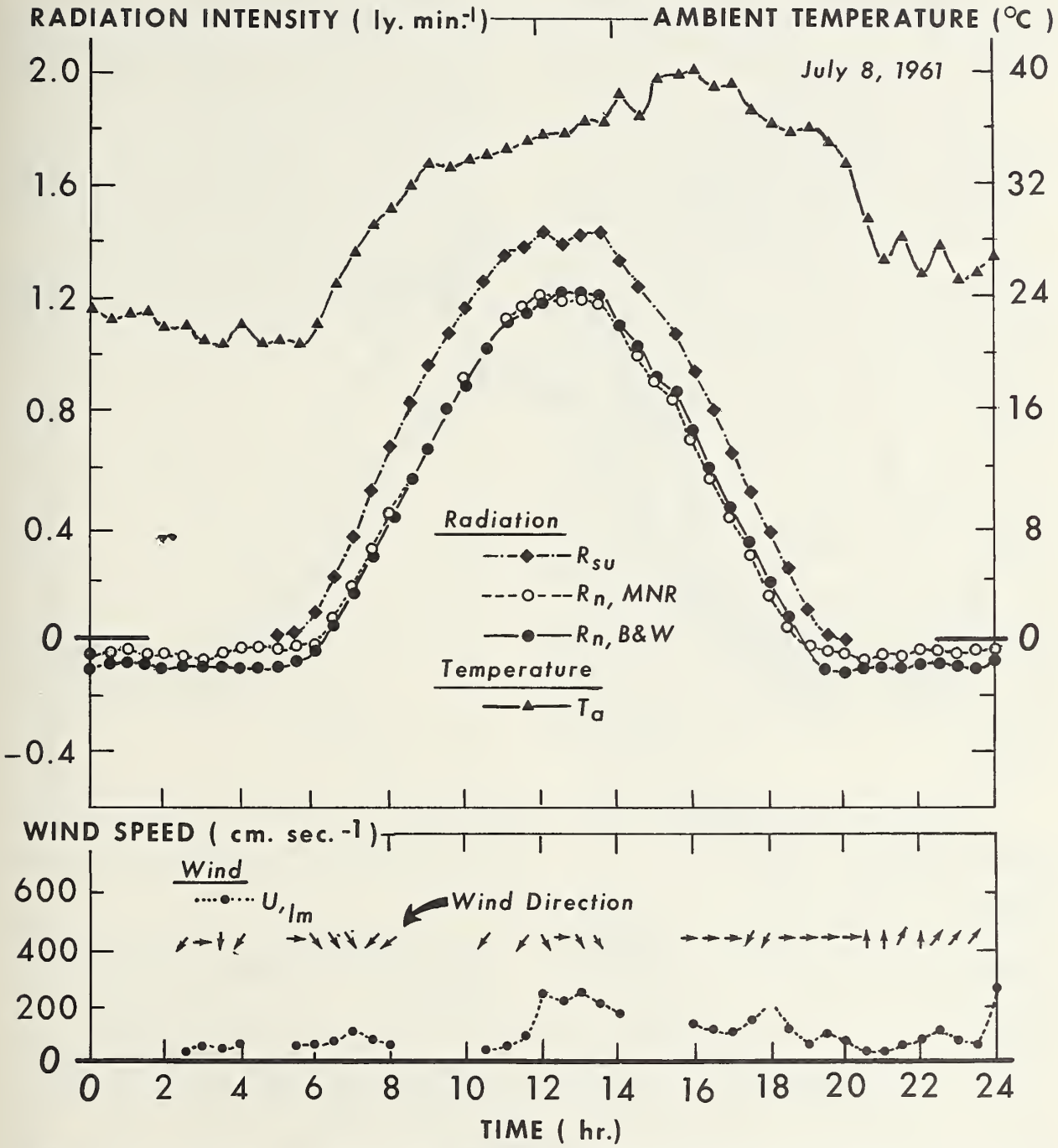

FIGURE 24.—Net radiation as measured by a miniature net radiometer and a Beckman and Whitley net radiometer, air temperature, windspeed and direction, and solar radiation over bare soil, July 8, 1961.

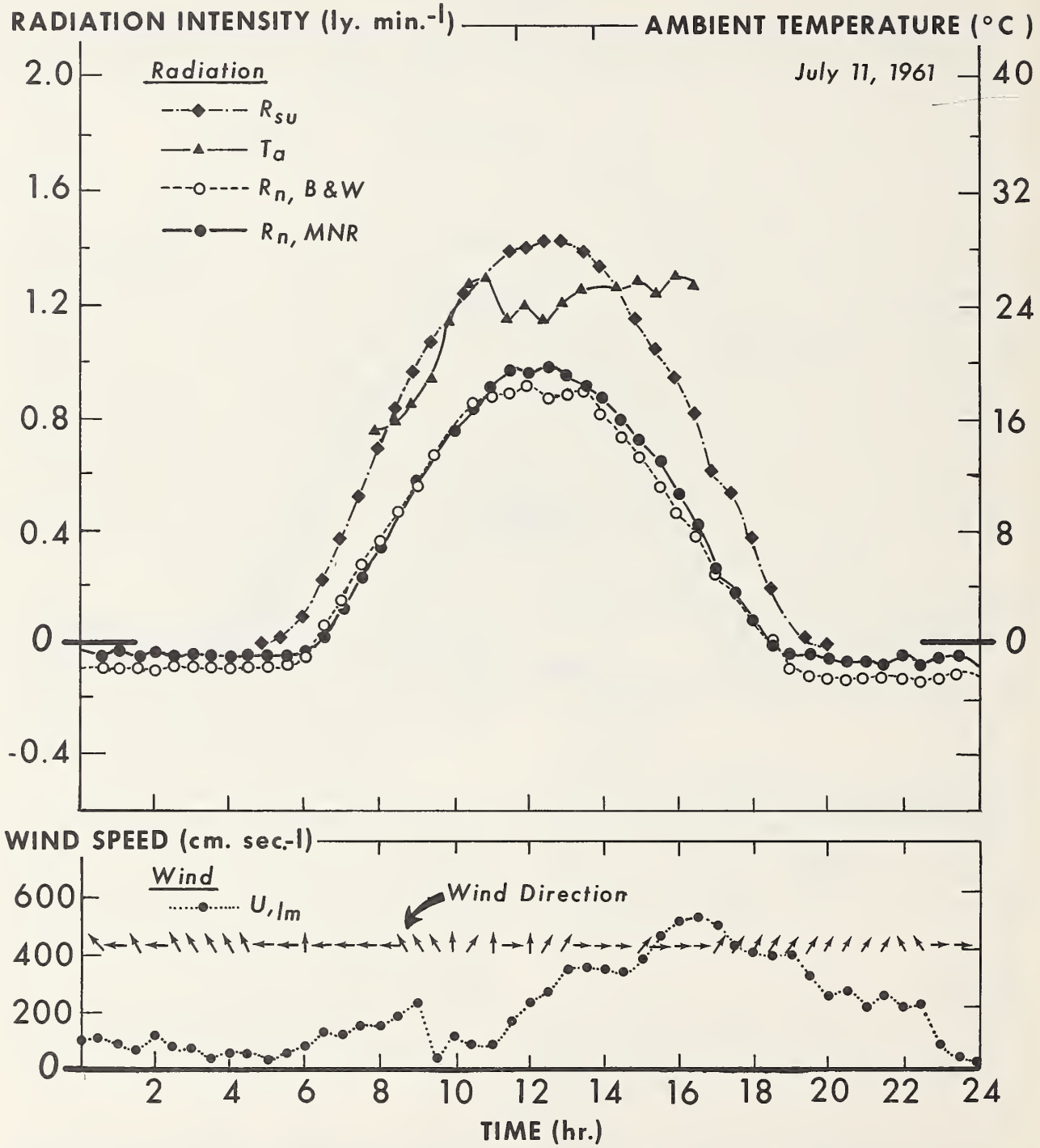

FIGURE 25.—Net radiation as measured by a miniature net radiometer and a Beckman and Whitley net radiometer, air temperature, windspeed and direction, and solar radiation over bare soil, July 11, 1961.

cated Beckman & Whitley net radiometer (normally positive when the radiative flux is down) is plotted as a function of the room temperature. It is evident from figure 26 that the net radiometer is more sensitive to ambient temperatures than the temperature coefficient of the transducer would indicate. This error appears to be associated with the design of the airstream. Similar results were reported by Portman.[12] Suomi and others (*10*) discussed the importance of equalizing the windstream on the top and bottom of the sensor.

The resulting errors could be a large percentage of the net radiation measured at low radiational fluxes (nocturnal hours, figs. 24 and 25); however, the errors appear to be somewhat masked during periods of strong radiational flux (fig. 24, daylight hours).

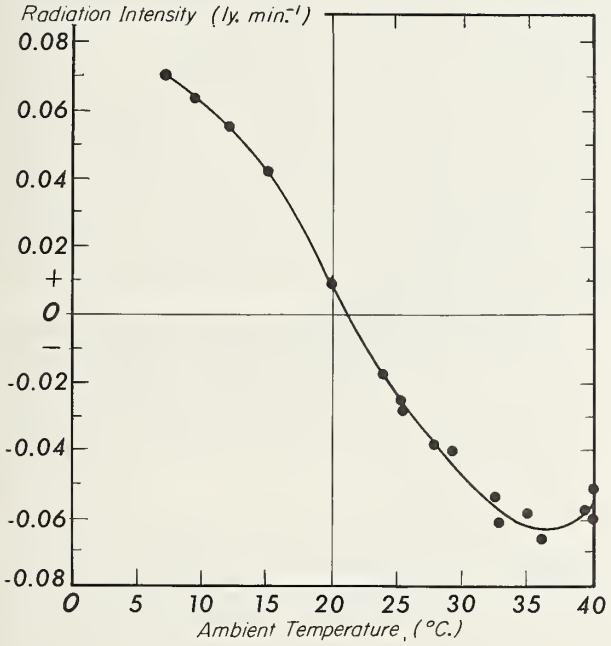

FIGURE 26.—The effect of ambient temperature upon a Beckman and Whitley, Model N188–01, net radiometer when subjected to zero radiational flux at 20° ± 1° C.

The difference in agreement of the net radiometers during the daylight hours appears to be associated with elevated temperatures and wind direction and speed; i.e., the Beckman & Whitley indicated less net radiation by comparison on July 11, 1961, when the ambient temperatures were warmer and the winds were moderate from the southerly direction.

Advantages of the MNR

(1) The MNR is a shielded-type net radiometer utilizing an economical thermal transducer as a sensor. The shields are shaped from polystyrene plastic.

[12] See footnote 11 on p. 25.

(2) It is small, approximately 2 inches in diameter, and can be used to measure net radiation close to a surface or within a plant canopy without appreciably altering the radiant balance by shading.

(3) Since the MNR is a shielded-type instrument, it does not require artificial ventilation.

(4) It was unaffected by ambient temperatures over the normal range; consequently, it does not require measurement of sensor temperature.

(5) The results of laboratory calibrations indicated that the MNR was equally sensitive to solar- and terrestrial-type radiation.

(6) The response to varying angles of incidence obeys the cosine law at the large sun angles. There is some deviation at the lower angles; however, these deviations were less than 2 percent in terms of net radiation for a day having 12 hours of daylight.

(7) The MNR was found to have a time constant of less than 2 seconds.

(8) The instrument was unaffected by windspeed or direction.

(9) The calibration constant was found to be unchanged after 2 months of field use. No visible signs of deterioration of the radiation windows were detected.

(10) Comparisons of radiation intensity indicated by a MNR and Beckman & Whitley net radiometer were made when the instruments were located over drastically different surfaces (wet and dry). Some consistent discrepancies were noted. These were explained as design errors of the Beckman and Whitley net radiometer's ventilation system.

NET RADIATION AND ENERGY-BALANCE STUDIES

At the time of preparation of this report a final analysis of the data obtained from the four major experiments is not in hand. The numerical analysis of the results will consist—in brief—of the computation of the surface energy balance and of the evaporative and sensible heat flux for every 15-minute period of observation and for the three lysimeters separately, where applicable. During the remainder of calendar year 1961 the numerical analysis of all data and appropriate summarization will be completed.

In the present report a preliminary analysis of the surface energy balance for each day is given, as well as an example of an hourly analysis for a single day selected at random from each of the four experiments. Further, an analysis and discussion of wind profile measurements are given.

Little Mud 1

In this experiment the soil inside the lysimeters was wetted, while the surrounding area was left

dry (see p. 6). The appropriate form of the energy balance equation (see p. 18) is

$$R_n+S+S'+A+LE=0.$$

For the preliminary analysis S' was assumed to be zero. All other measured values—R_n, S, and LE—were averaged for each day and for each hour on one day, April 14. The value for A was obtained by difference. Also, hourly and daily values were found for the windspeed at Z_3 ($\overline{U}_3$ in cm. sec.$^{-1}$) and for R_{su}, the incoming shortwave radiation.

A summary of the 24-hour data is given in table 5 for each lysimeter. It will be noted that solar radiation was practically identical on all 3 days, but that wind movement was greatest on the first day and least on the third day. Also, it appears that the three lysimeters behaved in much the same way. The small systematic differences may be due to minor differences in soil density or in soil moisture content.

TABLE 5.—*Energy balances (ly. day^{-1}), Little Mud 1, Tempe, Ariz., 1961* [1]

Day	Lysimeter No.	R_{su}	R_n	S	LE	A	U_3
							Cm. sec.$^{-1}$
Apr. 14	I		347	−28	−452	133	
	II		360	−32	−468	140	
	III		367	−22	−439	94	
Average		693	358	−27	−453	122	249
Apr. 15	I		288	−10	−174	−104	
	II		296	−26	−185	−85	
	III		281	−22	−186	−73	
Average		706	288	−19	−182	−87	175
Apr. 16	I		274	−29	−112	−133	
	II		288	−60	−112	−116	
	III		265	−52	−113	−100	
Average		692	276	−47	−112	−116	152

[1] See Symbols, p. 4.

On the first day we see that net radiation (R_n) is about 0.52 of solar radiation and is supplemented by a considerable amount of sensible heat (A) from the air. A small amount of energy (S) was used for heating the soil. Evaporation (E) was 7.7 mm. for the day.

On the second day, evaporation had declined to 3.1 mm. as the result of surface drying and reduced soil water transport to the surface. At the same time, net radiation decreased to 0.41 of solar radiation, attributable to increased albedo and increased surface temperature. Soil heat flow (S) was unchanged from the previous day, but on the second day sensible heat (A) was released to the air. The results on the third day were similar, with evaporation down to 1.9 mm., a perceptible increase in heating of the soil and an increase in the sensible heat flux into the air to an amount equal to the energy used for evaporation. Net radiation did not decline much further, being 39 percent of solar radiation.

Hourly values for the energy balance components on April 14 are shown in figure 27. The solar radiation curve indicates a clear day. Wind movement was typical for the Phoenix area. It shows a valley breeze with light easterly winds in the morning, changing from east to west-southwest between 1000 and 1200 with a temporary decrease in speed, and then increasing in speed and gustiness during the early afternoon, gradually dying down in the evening hours to become easterly again shortly after midnight.

The net radiation curve is regular and in phase with solar radiation, showing a constant nightly value of about −0.07 ly. min.$^{-1}$. Soil heat flux also shows a normal behavior, with heat flowing into the soil during the day and returning to the surface during the period of darkness. As stated, the storage of heat above the heat flux plate is here ignored, though it will be properly accounted for in the final analysis.

Evaporative energy flux was very low during the night, the required energy being supplied both by the air and the soil. During the period from 0800 to 1100 evaporation competes with soil heat flux and heating of the air for energy, but after 1100 energy is derived from the air and after 1630 also from the soil.

The evaporation curve and—in consequence—the sensible heat curve are not regular. It seems plausible to associate the irregularities with the changes in wind movement and the related exchange of air masses over the restricted lysimeter area. The lull at 1030 and the variable direction of the wind is unmistakably correlated with the decrease of A and the depression of LE. As the windspeed increases, the sign of A reverses and LE increases sharply. Similar correlations can be observed at 1730 and at 2230.

Little Splash 2

This experiment was similar to Little Mud 1 except that the lysimeters were covered with water supported by a black plastic sheet (see p. 6). The energy balance equation is

$$R_n+S+W+A+LE=0$$

Daily totals over five consecutive days are shown in table 6 with the exception of windspeed, which was not available for April 19 and 20.

Table 7 shows almost the same values for the 5 days for solar radiation and net radiation. Net

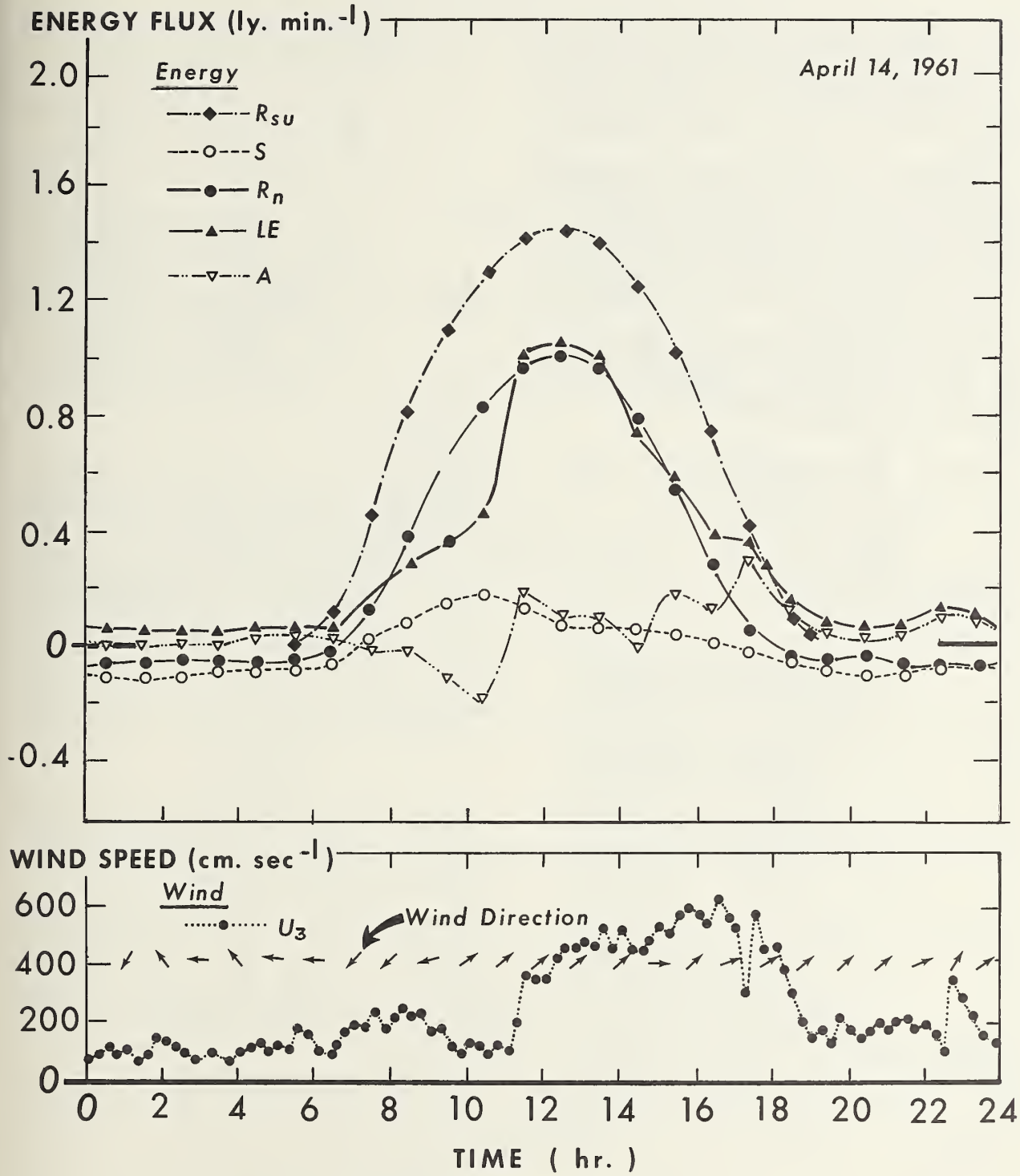

FIGURE 27.—Energy balance components for Little Mud 1 on April 14, 1961.

radiation was from 0.61 to 0.66 of the solar radiation. Similar amounts of heat were extracted from the soil on all 5 days, in contrast with the previous experiment (LM1). A small amount of heat was used on each day to warm the water, which was applied from a domestic supply each morning.

Evaporative flux varied considerably from day to day; this can be explained only on the basis of varying amounts of heat extracted from the air—a positive and significant quantity on all 5 days. Table 6 indicates a tendency for increased values of A with higher values of the windspeed at Z_3. A more detailed analysis must be completed to study this point further.

Figure 28 deals with hourly data on April 21, a clear day with variable light winds, which follows the valley breeze pattern. The curves for solar and net radiation are regular and are much the same as those in figure 27.

TABLE 6.—*Energy balances (ly. day^{-1}), Little Splash 2, Tempe, Ariz., 1961* [1]

Day	Lysimeter No.	R_{su}	R_n	S	$\overline{W}$	LE	A	U_3
								Cm. sec.$^{-1}$
Apr. 18	I	----	459	21	−7.4	−676	203	----
	II	----	453	26	−6.9	−675	203	----
	III	----	451	20	−10.3	−682	221	----
Average	------	694	454	22	−8.2	−678	209	341
Apr. 19	I	----	405	22	12.9	−611	171	----
	II	----	404	24	−1.1	−609	180	----
	III	----	409	15	−2.3	−602	176	----
Average	------	617	406	20	3.2	−607	176	----
Apr. 20	I	----	417	24	1.1	−503	61	----
	II	----	408	28	3.9	−473	33	----
	III	----	407	14	.6	−490	68	----
Average	------	669	411	22	1.8	−489	54	----
Apr. 21	I	----	451	18	−9.4	−521	62	----
	II	----	452	20	−9.7	−516	53	----
	III	----	443	8	−7.9	−515	72	----
Average	------	735	449	15	−9.0	−517	62	219
Apr. 22	I	----	443	16	−16	−574	132	----
	II	----	436	23	−11	−568	120	----
	III	----	431	11	−6	−559	122	----
Average	------	693	437	17	−11	−567	125	244

[1] See Symbols, p. 4.

For clarity, the sum of S and W is plotted, and it is seen that large amounts of energy go into this component from 0700 to 1500—mostly for heating of the water—to be released again predominantly between 1530 and 2100 but also continuously throughout the night. During this period the water is the chief source of heat for evaporation, which is low but not insignificant during the night.

During the period from 0700 to 1530 considerable energy is extracted from the air. Outside these hours the value for A is smaller and variable in sign. Inspection shows that the irregularities in the evaporation and sensible heat curves are correlated with changes in wind direction and speed, indicating that a change in direction of fetch, gustiness, or forced convection affects sensible heat flux and thereby evaporative flux, or possibly both simultaneously.

TABLE 7.—*Energy balances (ly. day^{-1}), Big Splash 1, Tempe, Ariz., 1961* [1]

Day	Lysimeter No.	R_{su}	R_n	S	$\overline{W}$	LE	A	U_3
								Cm. sec.$^{-1}$
Apr. 25	I	----	418	15	−9	−333	−91	----
	II	----	419	23	−10	−366	−67	----
	III	----	426	14	−10	−370	−60	----
Average	------	732	421	17	−10	−356	−73	206
Apr. 26	I	----	421	−6	−14	−298	−103	----
	II	----	418	−6	−17	−325	−71	----
	III	----	420	−13	−21	−334	−52	----
Average	------	727	420	−8	−17	−317	−75	151

[1] See Symbols, p. 4.

Big Splash 1

During the 2-day observation period the entire lysimeter area was flooded with water and the same energy balance equation was used for a preliminary analysis as for Little Splash 2.

Table 7 gives daily totals of the surface energy balance components. On both days clear weather prevailed with light winds. Net radiation was almost perfectly identical for the three lysimeters and the two periods. On the first day some sensible heat was derived from the soil, on the second one the situation was reversed. Some heat was utilized on both days to warm the water that was applied.

Evaporation averaged 6.2 mm. for the period, and the difference between the 2 days could be accounted for solely on the basis of the differences in soil heat flux.

On both days sensible heat was released to the air in equal amounts, though there was some variation between lysimeters. This, then, constitutes an obvious difference between Little Splash 2 and Big Splash 1. In LS2 the heat communicated by the dry surrounding surface to the air was available for evaporation within the

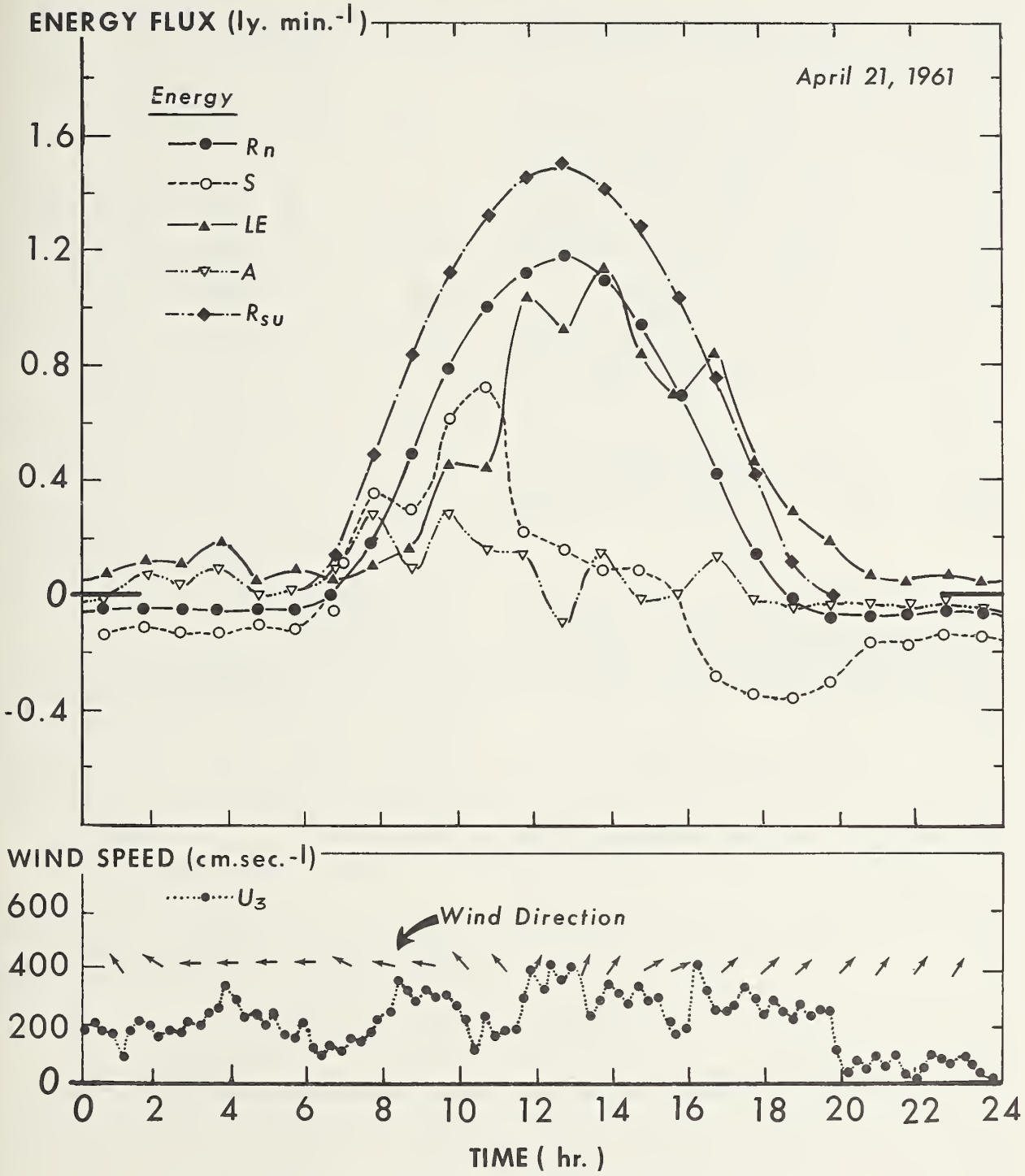

FIGURE 28.—Energy balance components for Little Splash 2, April 21, 1961.

lysimeter, owing to the lower temperature of the water surface. In BS1 the entire area was uniform and a more "normal" partition of energy on a daily basis was the result.

Hourly data for April 25 are given in figure 29 in which, again, S and W are combined. A regular pattern is found for solar and net radiation, identical to the previous experiment, LS2. During the period from 0630 to 1400 large amounts of heat are stored in the water layer to be released again, primarily during the late afternoon and, to a lesser extent, throughout the night. As a result evaporation is low during the morning and reaches maximum values during the afternoon.

The sensible heat curve is somewhat similar to the one showing, in figure 28, cooling of the air between 0600 and 1000 and heating during the rest of the day. However, in contrast with figure 28, the heat flux into the air greatly exceeds the outflow.

Wind direction was quite variable on April 25 and the usual pattern was not followed. This may account for the irregularity of the afternoon evaporation values, but the correlation is not clear upon inspection.

Big Mud 1

After the previous experiment the entire area was allowed to dry out and measurements were made over the first 5 days of drying. Only on the last 2 days, May 1 and 2, was the evaporation rate obviously affected by the progressive drying of the soil surface and the surface changed in color to a lighter hue.

In table 8 daily totals are shown, with data for lysimeter 2 omitted as this lysimeter did not behave normally. Clear to almost clear skies and light winds prevailed on all 5 days. Net radiation, constant at 0.55 of solar radiation over the first three periods, decreased to 0.45 of solar radiation on the last day.

On the first 2 days the soil heat flux term was positive, but, beginning with April 30, increasing amounts of sensible heat were taken up by the soil.

The evaporation declined over the entire period from a maximum of 7.0 to 3.9 mm. on the fifth day. In general, sensible heat went into the air, particularly so on the last day, when this term was about one-fifth of the total incoming energy.

An example of the energy balance by hours on April 29 is given in figure 30. Solar and net radiation behave regularly and cannot be distinguished from the counterpart curves on figures 27, 28, and 29. Also, soil heat flux shows a regular pattern and is a minor part of the total energy exchange.

The evaporative flux is not symmetrical with respect to true noon, because during the hours 0700 to 1400 a large amount of the radiative energy goes into heating of the air and of the soil.

TABLE 8.—*Energy balances (ly. day^{-1}), Big Mud 1, Tempe, Ariz., 1961* [1]

Day	Lysimeter No.	R_{su}	R_n	S	LE	A	U_3
							Cm. sec.$^{-1}$
Apr. 28	I	----	381	6	−345	−43	-----
	III	----	374	15	−351	−37	-----
Average	------	712	378	11	−348	−40	149
Apr. 29	I	----	412	9	−422	1	-----
	III	----	400	11	−407	−4	-----
Average	------	722	406	10	−415	−2	182
Apr. 30	I	----	386	−20	−380	14	-----
	III	----	367	−22	−337	−8	-----
Average	------	688	377	−21	−359	3	157
May 1	I	----	346	−31	−295	−20	-----
	III	----	319	−17	−245	−57	-----
Average	------	671	333	−24	−270	−39	154
May 2	I	----	337	−44	−254	−38	-----
	III	----	320	−22	−200	−98	-----
Average	------	728	329	−33	−227	−68	231

[1] See Symbols, p. 4.

During the latter part of the day, from 1400 to 1730, much of the sensible heat is returned from the air to the surface. During the dark period both soil and air yield comparatively small amounts of energy to sustain radiative and evaporative losses, the latter being quite small, however. The wind data on April 29 demonstrate a perfect valley breeze pattern.

WIND DATA STUDIES

The wind data presented in this report are for periods when the wind was from the east, south, and west quadrants. It was noticed that the guy wires originally used to support the mast affected the data. Consequently, the data obtained when the guy wires and anemometers were in line with the wind were omitted.

Profiles, selected to represent various windspeeds for each experiment, are shown in figures 31, 32, 33, and 34. The windspeed at Z_5 does not appear to be related to the other windspeeds except under conditions of low windspeeds (figs. 33 and 34). This discrepancy was not due to the anemometers, since they were compared on a test bar before and after experiments. The 2.5-meter cyclone fence enclosing the lysimeter field appeared to have affected the wind, causing a datum-level displacement, d, of approximately 300 cm. Consequently, $\overline{U_5}$ was disregarded.

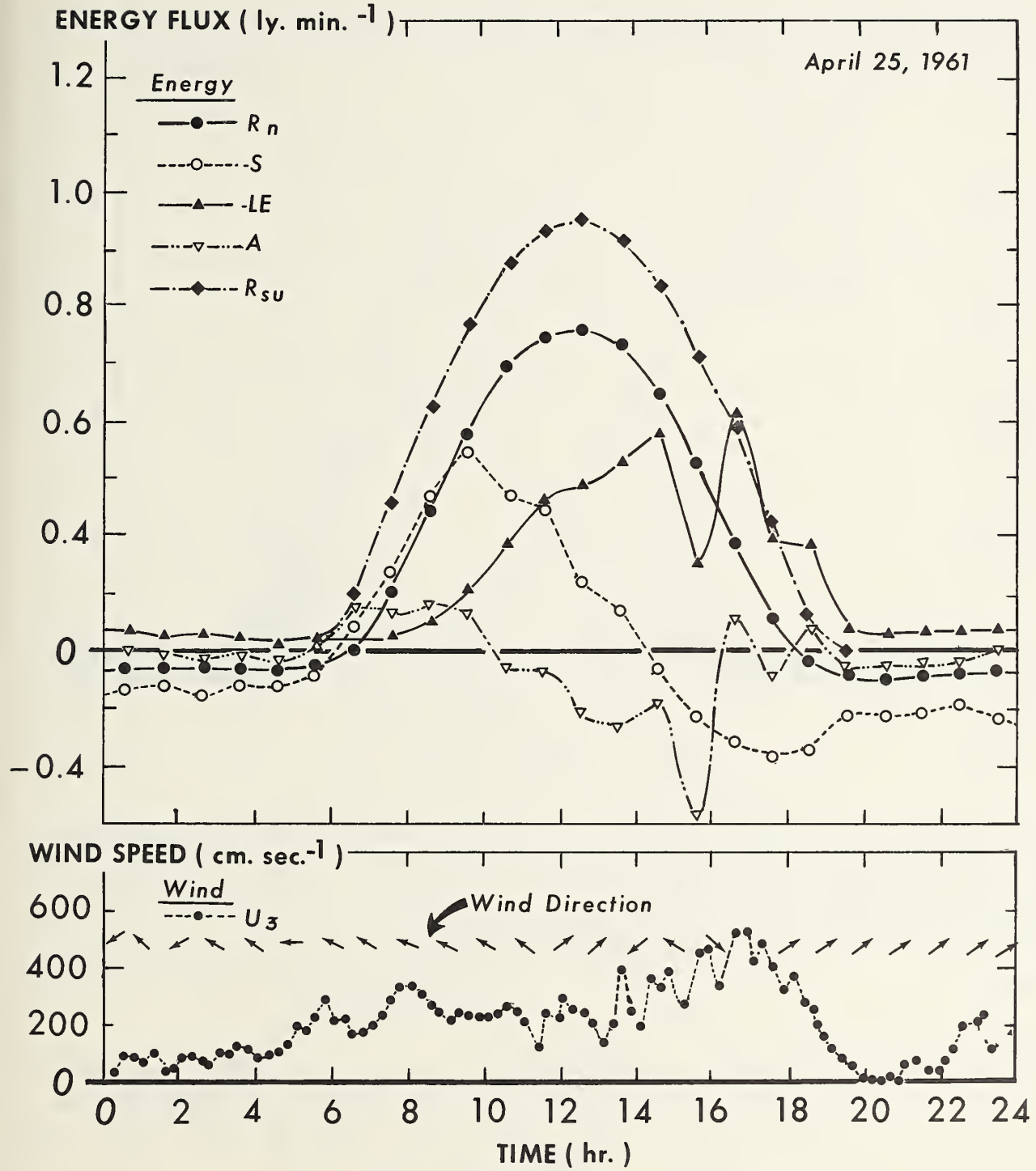

FIGURE 29.—Energy balance components for Big Splash 1, April 25, 1961.

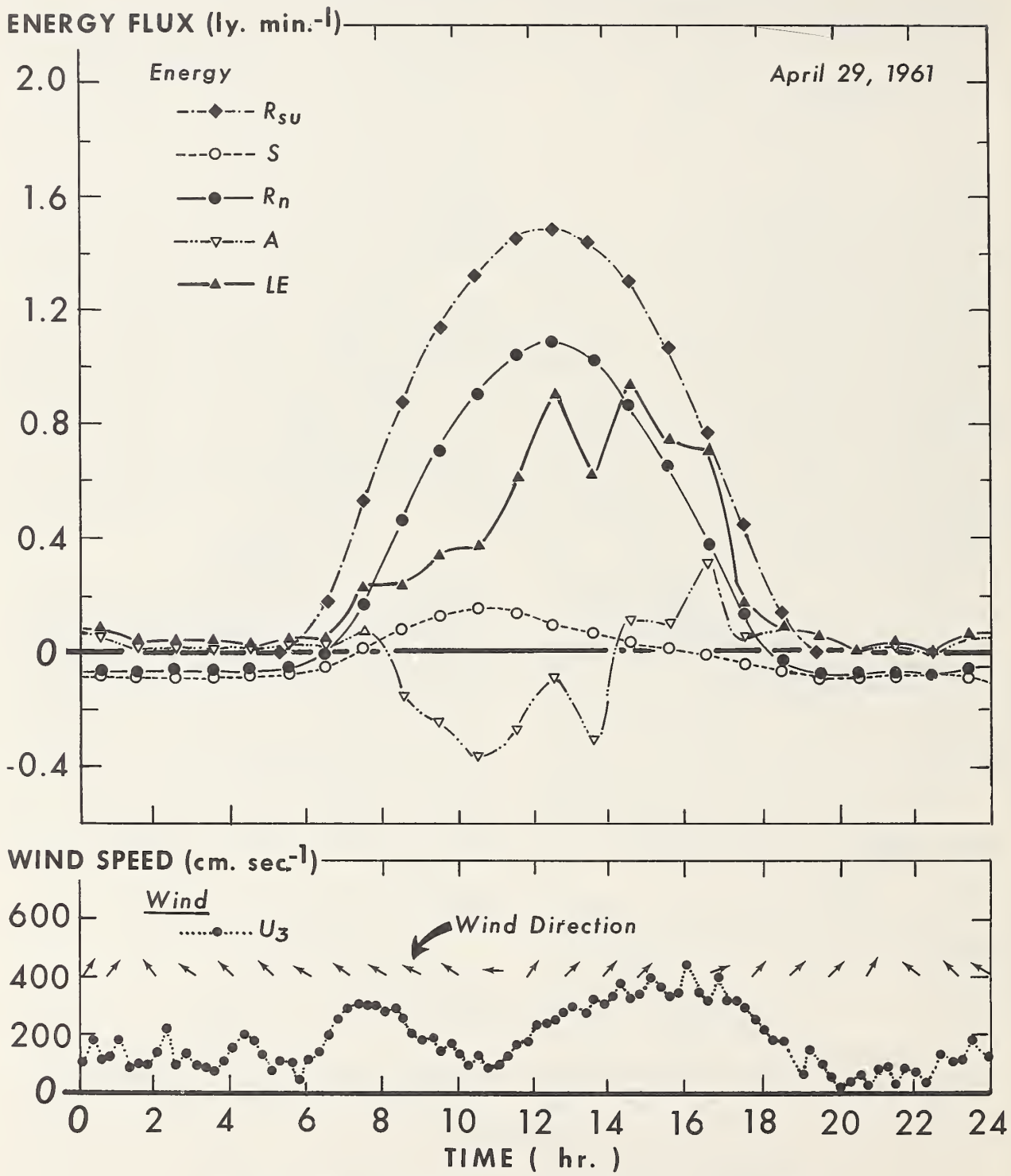

FIGURE 30.—Energy balance components for Big Mud 1, April 29, 1961.

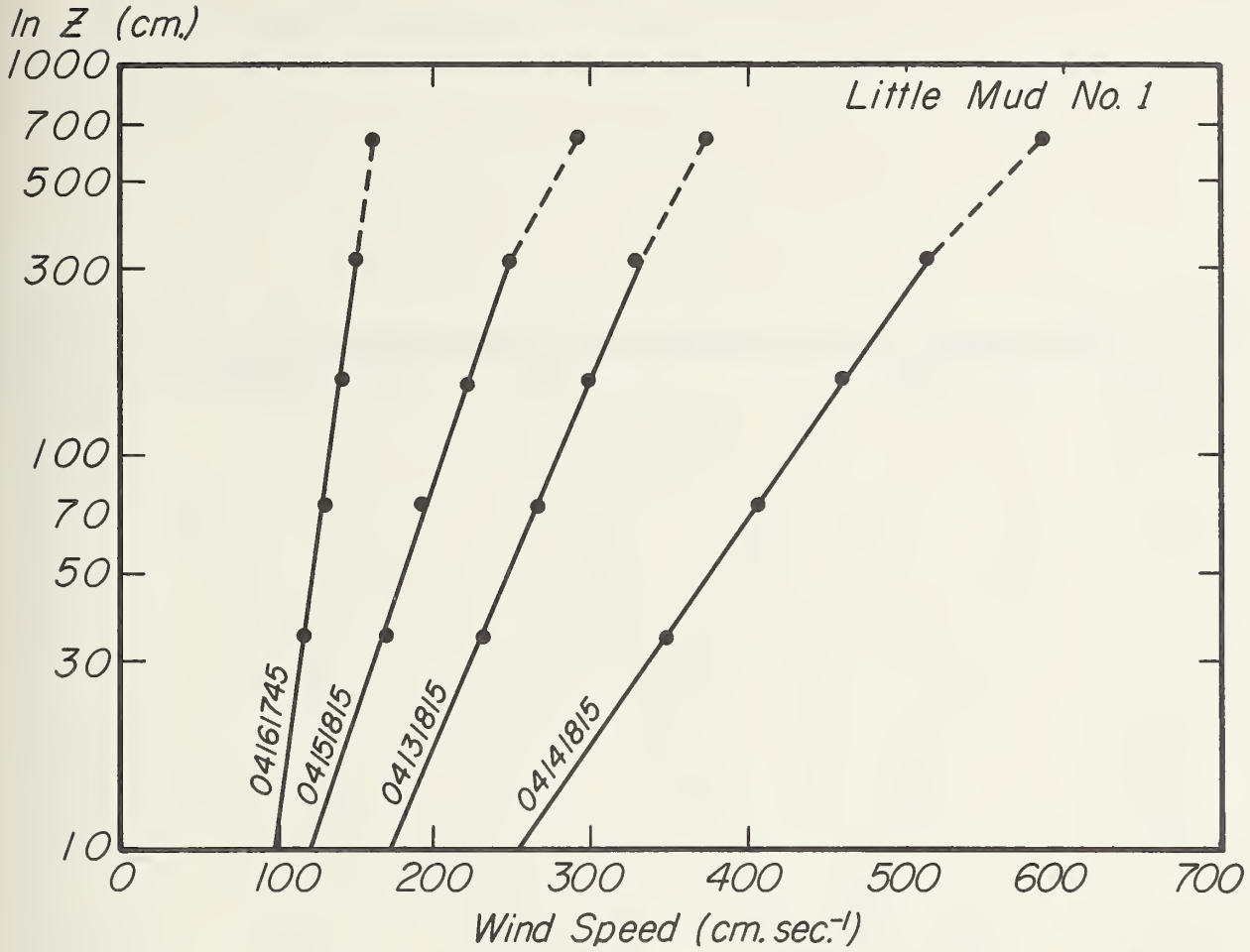

FIGURE 31.—Selected windspeed profiles for Little Mud 1.

Linear regressions of ln Z on $\overline{U}$ were computed for all periods of neutral stability. The equations, the standard deviations from regression (cm. sec.$^{-1}$), and the ln Z intercepts or Z_0, are listed in tables 9, 10, 11, and 12. The largest sample standard deviations from regression were obtained in Big Splash 1 and appear to be associated with the lower windspeeds, indicating that the starting and running speeds of the anemometers may have been interfering factors. On the average the sample standard deviations from regression were very low, about 5 cm. sec.$^{-1}$ or 45 contact closures for a 15-minute period.

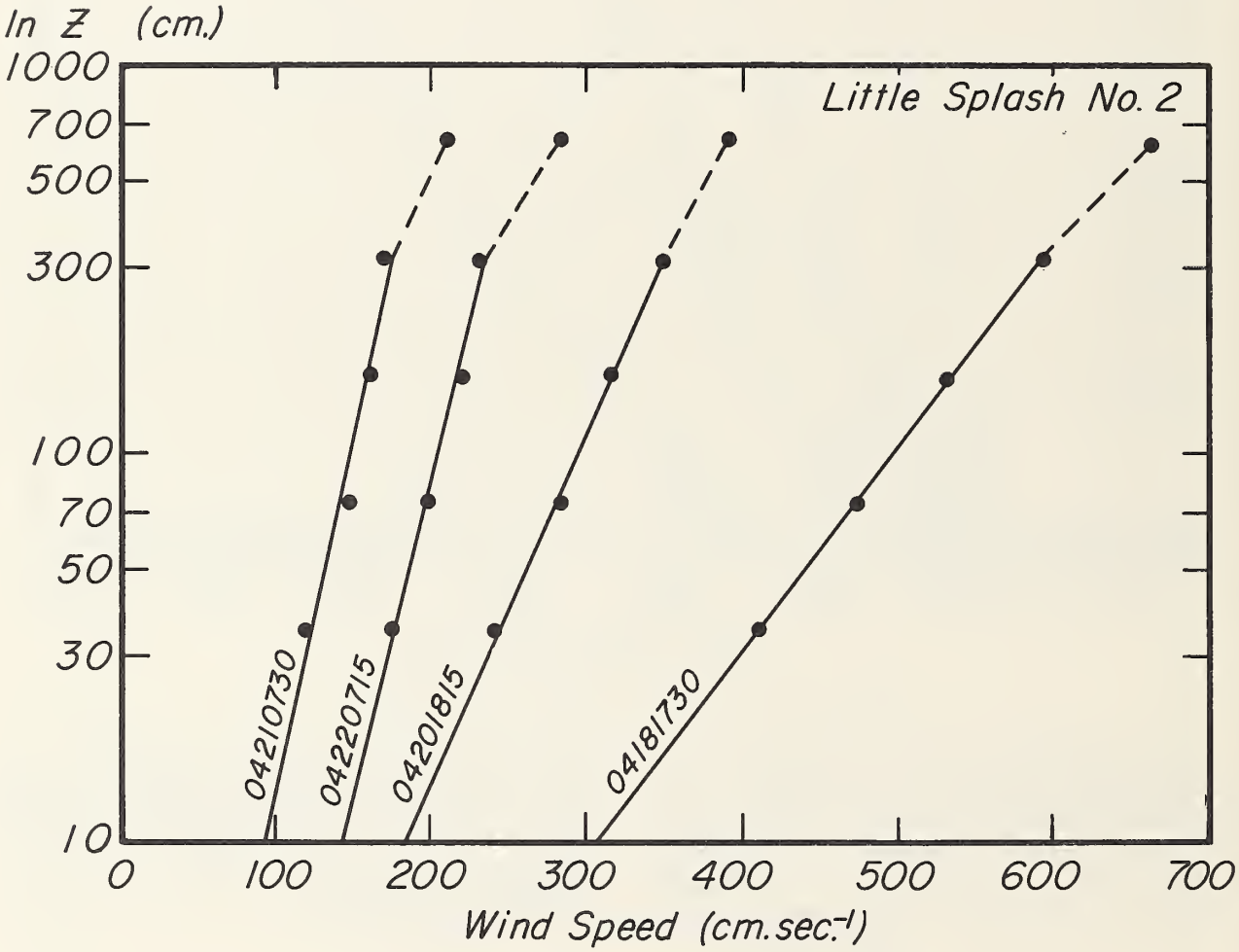

FIGURE 32.—Selected windspeed profiles for Little Splash 2.

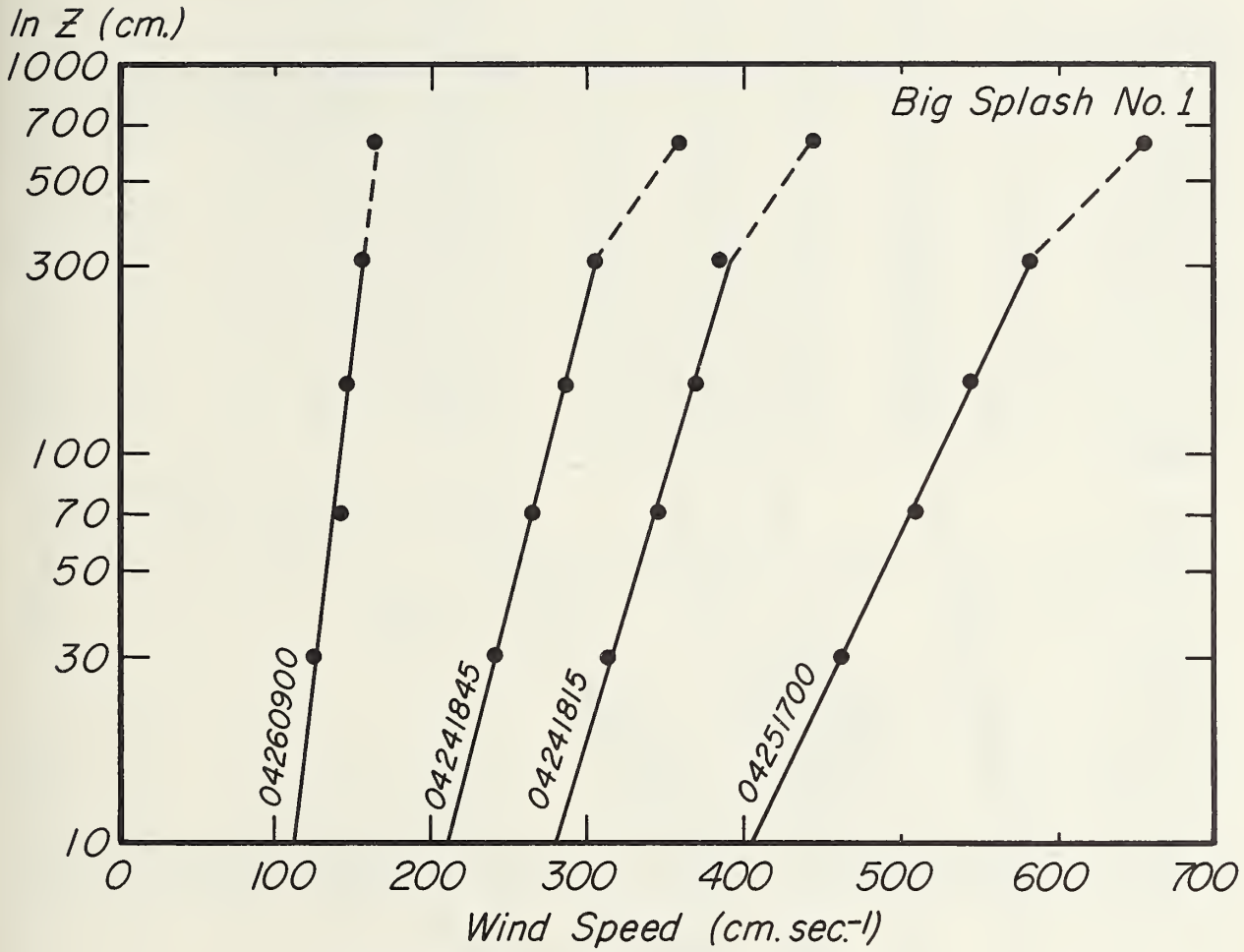

FIGURE 33.—Selected windspeed profiles for Big Splash 1.

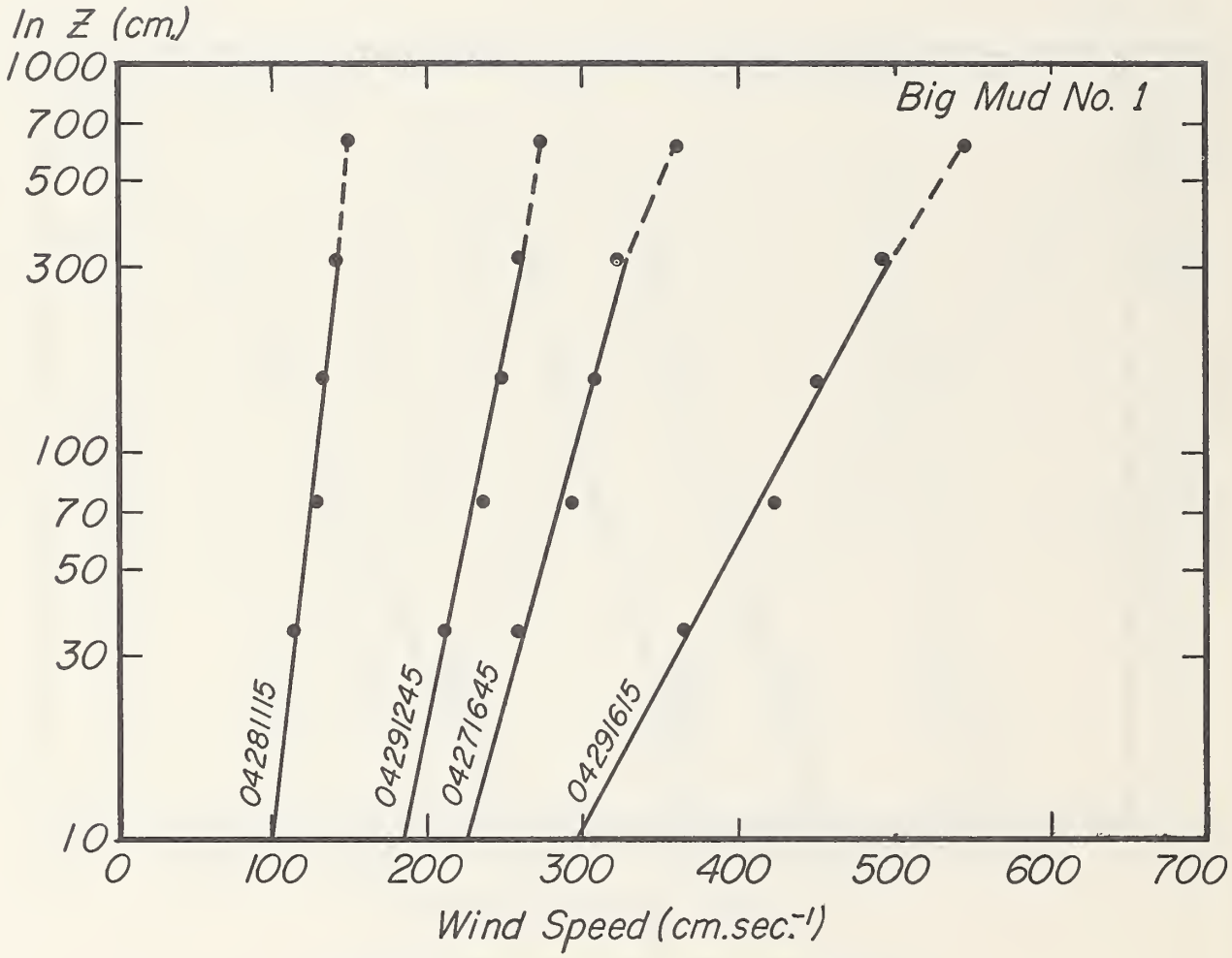

FIGURE 34.—Selected windspeed profiles for Big Mud 1.

TABLE 9.—*Wind data for all periods of neutral stability, Little Mud 1, Tempe, Ariz., 1961*

Time [1]	T_3	U_3	Regression equation	$sy.x$ [2]	U_*	Z_0	τ	C_D at 160 cm.	$\frac{U_* Z_0}{\nu}$	K_m
	°C.	Cm. sec.$^{-1}$	Y=	Cm. sec.$^{-1}$	Cm. sec.$^{-1}$	Cm.	Dynes cm.$^{-2}$			Cm.^{2} sec.$^{-1}$
04131815	20. 74	300	1n0. 217+0. 02197X	5. 64	18. 21	0. 217	0. 423	0. 007	256. 93	1092. 60
04140645	7. 54	133	1n1. 010+0. 03753X	3. 77	10. 60	1. 010	. 145	. 012	72. 11	636. 00
04140700	7. 73	171	1n0. 296+0. 03634X	4. 36	11. 01	. 296	. 155	. 008	229. 83	660. 60
04140715	8. 56	190	1n0. 188+0. 03484X	4. 73	11. 48	. 188	. 168	. 007	151. 24	688. 80
04140730	9. 91	189	1n0. 087+0. 03970X	1. 37	10. 08	. 087	. 130	. 006	6. 10	604. 80
04140745	10. 60	254	1n0. 150+0. 02680X	5. 41	14. 92	. 150	. 284	. 007	15. 48	895. 20
04141745	26. 11	577	1n0. 289+0. 01090X	5. 21	37. 70	. 289	1. 814	. 008	68. 35	2262. 00
04141800	25. 09	466	1n0. 241+0. 01387X	8. 02	28. 84	. 241	1. 061	. 008	7. 50	1730. 40
04141815	24. 30	459	1n0. 316+0. 01350X	5. 04	29. 63	. 316	1. 120	. 008	59. 79	1777. 80
04150715	12. 84	167	1n0. 778+0. 03055X	4. 63	13. 09	. 778	. 219	. 012	69. 56	785. 40
04150730	14. 05	225	1n0. 156+0. 03049X	1. 73	13. 12	. 156	. 220	. 007	13. 90	787. 20
04150745	14. 78	295	1n0. 133+0. 02379X	4. 86	16. 81	. 133	. 361	. 006	15. 08	1008. 60
04150800	15. 31	396	1n0. 087+0. 01890X	2. 41	21. 16	. 087	. 571	. 006	12. 41	1269. 60
04151800	23. 97	274	1n0. 124+0. 02619X	4. 10	15. 27	. 124	. 298	. 006	12. 09	916. 20
04151815	23. 11	221	1n0. 344+0. 02757X	6. 97	14. 51	. 344	. 269	. 009	32. 06	870. 60
04160715	12. 44	94	1n2. 100+0. 04364X	5. 84	9. 17	2. 100	. 107	. 019	14. 55	550. 20
04160730	13. 92	129	1n0. 037+0. 06422X	1. 49	6. 23	. 037	. 050	. 005	1. 56	373. 80
04160745	14. 49	180	1n0. 103+0. 04087X	2. 28	9. 79	. 103	. 122	. 006	0. 68	587. 40
04161715	28. 97	244	1n0. 021+0. 03702X	3. 78	10. 80	. 021	. 149	. 004	1. 31	648. 00
04161745	29. 23	142	1n0. 008+0. 07076X	1. 81	5. 65	. 008	. 041	. 003	. 28	339. 00
04170700	8. 20	158	1n3. 500+0. 02261X	8. 07	17. 69	3. 500	. 399	. 025	436. 64	1061. 40
04170715	8. 26	162	1n0. 699+0. 03329X	1. 45	12. 02	. 699	. 184	. 011	59. 25	721. 20
04170730	9. 45	193	1n0. 142+0. 03619X	1. 34	11. 05	. 142	. 156	. 007	11. 00	663. 00
04170745	11. 87	226	1n0. 055+0. 03533X	2. 71	11. 32	. 055	. 164	. 005	4. 28	679. 20
04170800	11. 66	271	1n0. 055+0. 03013X	4. 70	13. 54	. 055	. 234	. 005	5. 12	812. 40

[1] Month, day, hours, and minutes.
[2] Sample standard deviation from regression.

TABLE 10.—*Wind data for all periods of neutral stability, Little Splash 2, Tempe, Ariz., 1961*

Time [1]	T_3	U_3	Regression equation	$sy.x$ [2]	U_*	Z_0	τ	C_D at 160 cm.	$\frac{U_* Z_0}{\nu}$	K_m
	°C.	Cm. sec.$^{-1}$	Y=	Cm. sec.$^{-1}$	Cm. sec. ^{1}	Cm.	Dynes cm.$^{-2}$			Cm.^{2} sec.$^{-1}$
04181730	30. 35	531	1n0. 241+0. 01213X	2. 69	32. 98	0. 241	1. 388	0. 008	48. 97	1979. 00
04181745	29. 53	523	1n0. 202+0. 01259X	4. 19	31. 77	. 202	1. 288	. 007	39. 54	1906. 00
04190645	17. 91	338	1n0. 468+0. 01680X	8. 99	23. 81	. 468	. 723	. 009	73. 80	1429. 00
04190700	18. 34	368	1n0. 284+0. 01693X	4. 26	23. 62	. 284	. 712	. 008	44. 42	1417. 00
04190730	20. 08	321	1n0. 197+0. 02037X	8. 49	19. 64	. 197	. 492	. 008	25. 30	1178. 00
04190745	21. 17	338	1n0. 218+0. 01923X	4. 30	20. 80	. 218	. 514	. 008	29. 48	1248. 00
04191830	23. 60	423	1n0. 286+0. 01504X	2. 72	26. 60	. 286	. 903	. 008	48. 58	1596. 00
04191845	23. 31	392	1n0. 371+0. 01534X	1. 66	26. 08	. 371	. 868	. 009	62. 14	1565. 00
04201800	23. 11	340	1n0. 179+0. 01996X	4. 12	20. 04	. 179	. 512	. 007	23. 04	1202. 00
04201815	22. 91	315	1n0. 215+0. 02089X	2. 24	19. 15	. 215	. 468	. 007	26. 44	1149. 00
04201830	22. 29	282	1n0. 094+0. 02653X	3. 23	15. 08	. 094	. 290	. 006	9. 16	905. 00
04201845	21. 79	334	1n0. 255+0. 01941X	3. 40	20. 61	. 255	. 542	. 002	33. 97	1237. 00
04210700	9. 87	160	1n0. 117+0. 06547X	2. 38	6. 11	. 117	. 048	. 006	4. 98	367. 00
04211815	23. 87	304	1n0. 083+0. 02504X	3. 29	15. 97	. 083	. 325	. 006	8. 46	958. 00
04211830	23. 67	256	1n0. 146+0. 02724X	4. 14	14. 68	. 146	. 275	. 007	13. 69	881. 00
04211845	22. 75	233	1n0. 220+0. 02798X	1. 87	14. 30	. 220	. 261	. 008	20. 21	858. 00
04220645	9. 21	229	1n0. 615+0. 02332X	7. 12	17. 15	. 615	. 375	. 011	73. 91	1029. 00
04220700	10. 20	181	1n0. 162+0. 03868X	3. 53	10. 85	. 162	. 150	. 007	12. 23	651. 00
04220715	11. 55	219	1n0. 146+0. 03763X	3. 35	10. 63	. 046	. 144	. 005	3. 36	638. 00
04221715	24. 13	507	1n0. 228+0. 01291X	5. 07	30. 98	. 228	1. 225	. 008	45. 10	1859. 00
04221730	23. 70	573	1n0. 163+0. 01196X	1. 40	33. 44	. 163	1. 427	. 007	34. 81	2006. 00
04221800	22. 58	636	1n0. 305+0. 00976X	8. 30	40. 98	. 305	2. 143	. 008	80. 28	2459. 00
04230630	9. 09	141	1n0. 730+0. 03611X	5. 05	11. 08	. 730	. 157	. 012	56. 68	665. 00
04230645	10. 73	206	1n0. 053+0. 02883X	2. 99	10. 30	. 053	. 135	. 005	3. 78	618. 00
04230700	10. 82	202	1n0. 034+0. 04218X	3. 82	9. 48	. 034	. 115	. 004	2. 23	569. 00

[1] Month, day, hours, and minutes.
[2] Sample standard deviation from regression.

TABLE 11.—*Wind data for all periods of neutral stability, Big Splash 1, Tempe, Ariz., 1961*

Time [1]	T_3	U_3	Regression equation	$sy.x$ [2]	U_*	Z_0	τ	C_D at 160 cm.	$\frac{U_* Z_0}{\nu}$	K_m
	°C	Cm. sec.$^{-1}$	Y=	Cm. sec.$^{-1}$	Cm. sec.$^{-1}$	Cm.	Dynes cm.$^{-2}$			Cm.^{2} sec.$^{-1}$
04241645	18. 80	473	ln0. 001+0. 02510X	9. 21	15. 93	0. 001	0. 324	0. 002	0. 10	956. 00
04241700	19. 00	496	ln0. 004+0. 02149X	9. 12	18. 61	. 004	. 442	. 003	. 49	1117. 00
04241730	19. 53	389	ln0. 001+0. 03010X	8. 38	13. 28	. 001	. 225	. 002	. 09	797. 00
04241800	19. 46	301	ln0. 017+0. 04292X	8. 72	9. 32	. 017	. 111	. 002	1. 04	559. 00
04241815	19. 03	368	ln0. 001+0. 03193X	8. 35	12. 52	. 001	. 200	. 002	. 08	751. 00
04241830	18. 28	332	ln0. 001+0. 03641X	8. 04	10. 98	. 001	. 154	. 002	. 07	659. 00
04241845	18. 31	285	ln0. 004+0. 03721X	5. 41	10. 75	. 004	. 147	. 002	. 28	645. 00
04250700	9. 48	181	ln0. 005+0. 05635X	4. 72	7. 09	. 005	. 064	. 003	. 25	425. 00
04250930	14. 12	240	ln0. 000+0. 07378X	2. 27	5. 42	0	. 038	. 001	0	325. 00
04251100	17. 18	248	ln0. 000+0. 06593X	5. 17	6. 07	0	. 047	. 001	0	364. 00
04251230	18. 30	269	ln0. 000+0. 05986X	7. 23	6. 68	0	. 057	. 001	0	401. 00
04251300	19. 19	224	ln0. 000+0. 06955X	6. 29	5. 75	0	. 042	. 001	0	345. 00
04251500	21. 33	401	ln0. 002+0. 03107X	10. 43	12. 87	. 002	. 211	. 002	. 17	772. 00
04251630	21. 96	437	ln0. 002+0. 02607X	7. 45	15. 34	. 002	. 300	. 002	. 20	920. 00
04251645	21. 46	530	ln0. 002+0. 02152X	9. 99	18. 59	. 002	. 441	. 002	. 24	1115. 00
04251700	21. 46	542	ln0. 004+0. 01939X	8. 56	20. 63	. 004	. 543	. 003	. 53	1238. 00
04251730	21. 33	491	ln0. 004+0. 02156X	8. 55	18. 55	. 004	. 439	. 003	. 48	1113. 00
04251745	20. 57	400	ln0. 002+0. 02898X	8. 46	13. 03	. 002	. 217	. 002	. 17	782. 00
04251800	20. 64	325	ln0. 000+0. 05701X	8. 70	7. 02	0	. 063	. 001	0	421. 00
04251830	19. 82	306	ln0. 010+0. 03164X	9. 88	12. 64	. 010	. 204	. 003	. 83	758. 00
04260700	7. 77	137	ln0. 000+0. 13669X	3. 13	2. 93	0	. 020	. 001	0	176. 00
04260745	11. 39	179	ln0. 001+0. 06461X	4. 50	6. 19	. 001	. 049	. 002	. 04	371. 00
04260900	14. 29	146	ln0. 002+0. 07795X	4. 68	5. 13	. 002	. 034	. 003	. 07	308. 00
04261245	22. 09	211	ln0. 000+0. 08153X	4. 16	4. 91	0	. 031	. 001	0	295. 00
04261330	23. 11	134	ln0. 000+0. 13592X	4. 37	2. 94	0	. 011	. 001	0	176. 00
04261430	23. 74	215	ln0. 000+0. 07156X	4. 58	5. 59	0	. 040	. 001	0	335. 00
04261515	22. 19	378	ln0. 000+0. 03757X	9. 49	10. 65	0	. 145	. 002	0	639. 00
04261545	23. 51	275	ln0. 000+0. 05385X	6. 58	7. 43	0	. 070	. 002	0	446. 00
04261630	24. 30	267	ln0. 000+0. 05673X	4. 39	7. 05	0	. 063	. 001	0	423. 00
04261645	23. 47	173	ln0. 000+0. 10072X	3. 05	3. 97	0	. 025	. 001	0	238. 00
04261700	23. 77	250	ln0. 000+0. 05686X	4. 28	7. 04	0	. 063	. 002	0	422. 00
04261715	24. 13	211	ln0. 002+0. 06104X	4. 43	6. 55	. 002	. 055	. 002	. 08	393. 00
04261730	23. 41	272	ln0. 001+0. 04412X	5. 25	9. 07	. 001	. 105	. 002	. 06	544. 00
04270745	13. 90	251	ln0. 036+0. 05725X	6. 15	6. 99	. 036	. 062	. 001	1. 71	419. 00
04270800	14. 55	224	ln0. 000+0. 06502X	5. 59	6. 15	0	. 048	0	0	369. 00
04271015	19. 78	218	ln0. 000+0. 06487X	6. 16	6. 17	0	. 049	. 002	0	370. 00

[1] Month, day, hours, and minutes.
[2] Sample standard deviation from regression.

TABLE 12.—*Wind data for all periods of neutral stability, Big Mud 1, Tempe, Ariz., 1961*

Time [1]	T_3	U_3	Regression equation	$sy.x$ [2]	U_*	Z_0	τ	C_D at 160 cm.	$\frac{U_* Z_0}{\nu}$	K_m
	°C.	Cm. sec.$^{-1}$	Y=	Cm. sec.$^{-1}$	Cm. sec.$^{-1}$	Cm.	Dynes cm.$^{-2}$			Cm.^{2} sec.$^{-1}$
04271630	25. 98	185	ln0. 009+0. 05296X	4. 87	7. 59	0. 009	0. 074	0. 003	0. 43	471. 00
04271645	26. 44	307	ln0. 004+0. 03435X	7. 99	11. 64	. 004	. 173	. 003	. 29	722. 00
04271700	26. 04	293	ln0. 006+0. 03511X	6. 39	11. 39	. 006	. 166	. 003	. 43	706. 00
04271745	25. 72	259	ln0. 023+0. 03404X	6. 92	11. 75	. 023	. 176	. 004	1. 70	728. 00
04280700	11. 22	220	ln0. 076+0. 03402X	2. 49	11. 76	. 076	. 176	. 006	6. 18	729. 00
04280915	17. 74	383	ln0. 002+0. 03032X	15. 37	13. 19	. 002	. 222	. 002	. 18	818. 00
04281630	30. 45	235	ln0. 006+0. 04361X	4. 91	9. 18	. 006	. 094	. 003	. 34	569. 00
04291145	27. 98	172	ln0. 001+0. 06847X	2. 62	5. 84	. 001	. 044	. 002	. 04	362. 00
04291245	28. 74	247	ln0. 002+0. 04530X	6. 33	8. 83	. 002	. 100	. 003	. 11	548. 00
04291345	30. 39	331	ln0. 014+0. 02787X	3. 63	14. 35	. 014	. 263	. 004	1. 23	890. 00
04291400	29. 89	313	ln0. 005+0. 03279X	5. 91	12. 20	. 005	. 190	. 003	. 38	756. 00
04291430	30. 19	382	ln0. 014+0. 02417X	7. 94	16. 55	. 014	. 350	. 004	1. 43	1026. 00
04291515	30. 68	405	ln0. 047+0. 01974X	8. 78	20. 26	. 047	. 524	. 005	5. 83	1256. 00
04291615	30. 26	450	ln0. 058+0. 01738X	10. 19	23. 02	. 058	. 676	. 005	8. 23	1427. 00
04301345	30. 19	260	ln0. 002+0. 04684X	4. 58	8. 54	. 002	. 093	. 002	. 10	530. 00
04301415	29. 70	296	ln0. 007+0. 03368X	7. 70	11. 88	. 007	. 180	. 003	. 51	737. 00
04301445	29. 70	303	ln0. 005+0. 03444X	5. 90	11. 61	. 005	. 172	. 003	. 36	720. 00
04301530	30. 78	232	ln0. 006+0. 04433X	5. 84	9. 02	. 006	. 104	. 003	. 33	559. 00
04301630	31. 05	398	ln0. 016+0. 02295X	2. 40	17. 43	. 016	. 388	. 004	1. 71	1080. 00
05020915	24. 59	263	ln0. 012+0. 03570X	4. 88	11. 20	. 012	. 160	. 007	. 84	694. 00
05020930	25. 61	230	ln0. 005+0. 04472X	4. 25	8. 94	. 005	. 102	. 003	. 28	554. 00
05021615	31. 64	470	ln0. 088+0. 01583X	4. 20	25. 27	. 008	. 815	. 006	1. 23	1567. 00
05021630	31. 37	534	ln0. 063+0. 01458X	3. 68	27. 44	. 063	. 961	. 005	10. 59	1701. 00
05021700	30. 39	595	ln0. 079+0. 01269X	2. 81	31. 52	. 179	1. 268	. 006	15. 34	1954. 00
05021715	30. 91	577	ln0. 070+0. 01328X	3. 66	30. 12	. 070	1. 157	. 005	12. 92	1867. 00

[1] Month, day, hours, and minutes.
[2] Sample standard deviation from regression.

The surface roughness for these four experiments are quite different. The field was leveled before the experiments; however, some small clods still remained on the surface. The average roughness appeared to be approximately 1 cm. for LM1 and LS1. For BS1, a water surface existed that was quite smooth. In BM1, the surface ranged from a mud flat to a dry surface, with a roughness of 0.25 cm.

The values of the roughness parameter, Z_0, computed from the regression equations, appear to be related to the physical surface but not constant for a given surface. A great amount of variability was noticed.

The computed values of the drag coefficient, C_D, agree in magnitude with those presented by Deacon (*2*) and Sutton (*11*). As the surface in Big Splash was smoother, it had smaller drag coefficients than the surfaces in Little Splash 2, Little Mud 1, and Big Mud 1. The largest values of C_D were obtained in Little Splash 2 and Little Mud 1.

According to Nikuradse's criteria, the flow over surfaces in Little Mud 1 and Little Splash 2 was fully rough (tables 9 and 10), whereas aerodynamically smooth flow existed over the water in Big Splash 1 (table 11). The flow in Big Mud 1 ranged from transitional flow to fully rough flow.

The values computed for the coefficient of eddy viscosity, K_m, (tables 9, 10, 11, and 12) are of the same order of magnitude as those indicated by Sutton. K_m is not constant and appears to be consistently larger over the dry and rough surfaces than over the wet and smooth surfaces.

DISCUSSION

Since there is no final data analysis and summary of the four studies of net radiation and energy balance, all conclusions and comparisons can be few and tentative only.

In all instances net radiation shows a regular pattern, indicating that albedo rather than surface temperatures determine its magnitude. Data presented here, however, do not reveal short-time variations. Plots of 15-minute net radiation data show definite variation in net radiative flux that cannot be explained by changes in albedo.

Considering the daily totals of net radiation, we find that over shallow water R_n equals about 0.63 R_{su}, whereas over drying land R_n varies from 0.55 R_{su} to 0.40 R_{su}, depending upon the dryness of the surface.

Another outstanding difference between the water-covered and the drying soil surface is the storage of heat in the water itself. A comparison of figures 29 and 30 shows clearly the difference and its effect on the sensible heat flux into the air. Over shallow water the air yields energy early in the day and takes up energy during the rest of the day. Over bare, wet soil the air is heated first from morning until midafternoon, to yield some of this energy later in the day. Evaporation, both in amount and distribution, is very similar over open water and bare, wet soil in the BS1 and BM2 experiments.

If all available daily balances are considered, sensible heat flux in the air is mostly negative, with the exception of LS2 for obvious reasons. This fact may be surprising in the light of local climatic conditions and of the nature of the site that is, in essence, an oasis of a few square miles in an immense desert. The LS2 situation and the first day of LM1 represents a "micro oasis" and even then the sensible heat flux contributes a maximum of 0.25 of the total energy for evaporative flux. It is a pertinent fact that no observation period was characterized by strong winds, as 600 cm. sec.$^{-1}$ was about the highest 15-minute average.

It would be erroneous to conclude from the daily data that net radiation minus soil (or water) heat flux is always identically partitioned over evaporation and heating of the air. To the contrary, we observed the magnitude and sign of the air heat flux to vary considerably and unpredictably except during the night. This could imply that the concept of a constant or typical Bowen ratio simply does not apply to the energy balance of a terrestrial surface.

Despite the smooth and predictable course of net radiation and soil or water heat flux, evaporative flux shows many irregularities that are real; that is, the irregularities are not attributable to random error of measurement. It is tempting to ascribe these variations to changes in the fetch, speed, and gustiness of the wind, and there are several indications that this may be true. Actually, the phenomena of horizontal windspeed at one height close to the surface, turbulent transfer, sensible heat flux, and evaporative flux are so mutually connected that cause and effect are difficult to separate. Hopefully, a further analysis of the data will bring about more understanding of this important issue.

LITERATURE CITED

(1) Brown, A. I., and Marco, S. M.
1951. INTRODUCTION TO HEAT TRANSFER. Pp. 44–79. McGraw-Hill Book Co., Inc., New York.

(2) Deacon, E. L.
1953. VERTICAL PROFILES OF MEAN WIND IN THE SURFACE LAYERS OF THE ATMOSPHERE. Gr. Brit. Met. Off. Geophys. Mem. 11 (91), 68 pp.

(3) Fritschen, L. J.
1960. CONSTRUCTION AND CALIBRATION DETAILS OF THE THERMAL-TRANSDUCER-TYPE NET RADIOMETER. Amer. Met. Soc. Bul. 41: 180–183.

(4) ——— and Van Wijk, W. R.
1959. USE OF AN ECONOMICAL THERMAL TRANSDUCER AS A NET RADIOMETER. Amer. Met. Soc. Bul. 40: 291–294.

(5) Gier, J. T., and Dunkle, R. V.
1951. TOTAL HEMISPHERICAL RADIOMETERS. Amer. Inst. Elect. Engin. 70: 1–7.

(6) Hatfield, H. S., and Wilkins, F. J.
1950. A NEW HEAT-FLOW METER. Jour. Sci. Instruments 27: 1–3.

(7) Jakob, Max.
1957. HEAT TRANSFER II. Pp. 1–89. John Wiley & Sons, Inc., New York.

(8) Portman, D. J.
1954. the measurement of air temperature profiles. Johns Hopkins Univ. Lab.Climatol. 7: 250–260.

(9) Sheppard, P. A.
1958. transfer across the earth's surface and through the air above. Roy. Met. Soc. [London] Quart. Jour. 84, No. 361. 205–224.

(10) Suomi, V. E., Franssila, M., and Islitzer, N. F.
1954. an improved net-radiation instrument. Jour. Met. 11: 276–282.

(11) Sutton, O.G.
1953. micrometeorology. 333 pp. McGraw-Hill Book Co., Inc., New York.

(12) Sverdrup, H. V.
1937. on the evaporation from oceans. Jour. Marine Res. 1: 3–14.

(13) United States Geological Survey.
1954. water-loss investigations: lake hefner studies, technical report. U.S. Geol. Survey Prof. Paper 269, 158 pp.

(14) Zemansky, M. W.
1957. heat and thermodynamics. 106 pp. McGraw-Hill Book Co., Inc., New York.

APPENDIX [13]

MEASUREMENT OF NET RADIATION BY THERMAL TRANSDUCER

If one uses a thermal transducer in place of the blackened plate, net radiation is measured as follows:

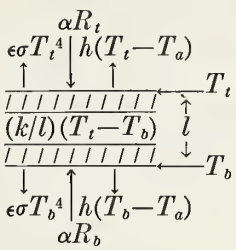

On surface t, the energy balance is

$$\alpha R_t=\epsilon\sigma T_t^4+h(T_t-T_a)+\frac{k}{l}(T_t-T_b). \quad (12)$$

Similarly, the energy balance on surface b is

$$\alpha R_b=\epsilon\sigma T_b^4+h(T_b-T_a)-\frac{k}{l}(T_t-T_b). \quad (13)$$

Subtracting equation 13 from equation 12, we have

$$R_n=\alpha(R_t-R_b)$$
$$=\epsilon\sigma(T_t^4-T_b^4)+h(T_t-T_b)+\frac{2k}{l}(T_t-T_b). \quad (14)$$

If the term involving thermal convection was eliminated, equation 14 would become

$$R_n=\epsilon\sigma(T_t^4-T_b^4)+\frac{2k}{l}(T_t-T_b). \quad (15)$$

The heat-flow through the sensing element may be expressed as

$$H=k(T_t-T_b)/1. \quad (16)$$

Since a thermocouple assembly is located within the thermal transducer, a temperature difference is set up between the hot and cold junctions. This temperature difference is related to the overall temperature difference (T_t-T_b) by a proportionality constant C.

A thermoelectric potential G is set up which is related to the heat flow by

$$G=BC(T_t-T_b). \quad (17)$$

By using the approximations that

$$T_t+T_b\approx 2T_t \text{ and } T_t^2+T_b^2\approx 2T_t^2 \quad (18)$$

in equation 15 and substituting in equation 19, we have

$$R_n=\left(4\epsilon\sigma T_t^3+\frac{2k}{l}\right)(T_t-T_b). \quad (19)$$

$$R_n=\left(4\epsilon\sigma T_t^3+\frac{2k}{l}\right)\frac{G}{BC}=gG \quad (20)$$

where g is the calibration constant that depends upon the temperature, emissivity, conductivity, and thickness of the thermal transducer. The magnitude of $4\epsilon\sigma T_t^3$ (8.38×10^{-4} if $T=300A$) is very small when compared with $\frac{2k}{l}$ (7.26) and can safely be disregarded.

[13] See Symbols listed for net radiation studies, p. 5.

NONEQUILIBRIUM METHOD FOR EMISSIVITY OF CALIBRATION CHAMBER

The emissivity of the calibration chamber was obtained by the *nonequilibrium method* (*14*). With this method a blackened silver disk is placed in the center of the chamber after the whole chamber has reached a constant temperature. The temperature of the silver disk was recorded as a function of time. From the resulting heating curve, the slope dT/dt is obtained. Assuming the silver disk to be a blackbody and putting $dQ=C_p dT$, we have

$$\frac{C_p dT}{dt}=A\sigma(\epsilon_w T_w^4-T^4) \tag{21}$$

or

$$\frac{C_p dT}{dt A\sigma T^4}=\frac{\epsilon_w T_w^4}{T^4}-1 \tag{22}$$

where T_w is the temperature of the wall, T is the temperature of the silver disk, dQ is the heat transferred in time dt to the whole body whose area is A, and C_p is the heat capacity at constant pressure. If $\frac{T_w^4}{T^4}$ is plotted against $\frac{dT}{dt\sigma T^4}$, the slope of the line is equal to ϵ_w.

DERIVATION OF HEAT TRANSFER BY RADIATION

Heat transfer by radiation between the two halves of the calibration box, separated by a nonabsorbing medium, is illustrated by the following equations adapted from Brown and Marco (*1*). Let

A=Areas of the radiating surface
ϵ=Emissivity of the surface
E=Total emissive power where $E=\sigma T^4$ for a blackbody
f=The fraction of energy leaving one surface and falling on the other surface
r=Reflectivity where $r=1-\epsilon$

Subscripts 1 and 2 refer to the surfaces 1 and 2, respectively.

The emission of surface A_1 may be written as $\epsilon_1\sigma A_1 T_1^4$ and if Kirchoff's Law is used, surface A_1 absorbs $\epsilon_2\epsilon_1\sigma A_1 T_1^4$ and reflects $r_2\epsilon_1\sigma A_1 T_1^4$. The energy that originates at A_1 and falls on A_2 is then $\epsilon_1\sigma A_1 T_1^4 f_2$. The surface A_2 absorbs part of this energy and reflects the amount $r_2\epsilon_1 A_1\sigma T_1^4 f_1 f_2$. The fraction of this reflected energy that falls on A_1 is then $r_2\epsilon_1 A_1\sigma T_1^4 f_2$. Surface A_1 will reflect a part of the reflected energy equal to $r_1 r_2\epsilon_1 A_1\sigma T_1^4 f_1 f_2$ and the fraction of this energy that falls on A_2 is $r_1 r_2\epsilon_1 A_1\sigma T_1^4 f_1 f_2^2$. This process goes on indefinitely.

The amount of energy originating at A_1 and falling on A_2 may be written as

$$q_a=\epsilon_1 A_1\sigma T_1^4 f_2+r_1 r_2\epsilon_1 A_1\sigma T_1^4 f_1 f_2^2 +r_1^2 r_2^2\epsilon_1 A_1\sigma T_1^4 f_1^2 f_2^3+\ \ldots \tag{23}$$

This is only a part of the energy that falls on surface A_2. A part of the energy originating at A_2 that is reflected from surface A_1 also falls on A_2. This can be written as

$$q_b=r_1\epsilon_2 A_2\sigma T_2^4 f_1 f_2+r_1^2 r_2\epsilon_2 A_2\sigma T_2^4 f_1^2 f_2^2+\ \ldots \tag{24}$$

The total energy that falls on A_2 from A_1 is then $q_{1-2}=q_a+q_b$ or,

$$q_{1-2}=\epsilon A_1 f_2\sigma T_1^4(1+r_1 r_2 f_1 f_2+r_1^2 r_2^2 f_1^2 f_2^2+\ \ldots) +\epsilon_2 A_2 r_1\sigma T_2^4 f_1 f_2(1+r_1 r_2 f_1 f_2+r_1^2 r_2^2 f_1^2 f_2^2+\ \ldots) \tag{25}$$

or,

$$q_{1-2}=(\epsilon_1 A_1\sigma T_1^4 f_2+\epsilon_2 r_1 A_2\sigma T_2^4 f_1 f_2) (1+r_1 r_2 f_1 f_2+r_1^2 r_2^2 f_1^2 f_2^2+\ \ldots) \tag{26}$$

The second expression is a geometric expression having a common multiplier $r_1 r_2 f_1 f_2$; consequently, equation 26 may be written as

$$q_{1-2}=\frac{\epsilon_1 A_1\sigma T_1^4 f_2+\epsilon_2 r_1 A_2\sigma T_2^4 f_1 f_2}{1-r_1 r_2 f_1 f_2}. \tag{27}$$

A similar expression may be written for the energy that originates at, or is reflected from, surface A_2 and falls on A_1. The net energy exchange between the two surfaces is then $q=q_{1-2}-q_{2-1}$ or,

$$q=\frac{\left[\begin{array}{l}\epsilon_1 A_1\sigma T_1^4 f_2-\epsilon_2 A_2\sigma T_2^4 f_1\\ +\epsilon_2 r_1 A_2\sigma T_2^4 f_1 f_2-\epsilon_1 r_2\sigma T_1^4 f_1 f_2\end{array}\right]}{1-r_1 r_2 f_1 f_2}. \tag{28}$$

It can be shown from "Heat Transfer" (*7*) that f_1 and f_2 are approximately equal to one for the calibration box and, furthermore, $A_1=A_2$. If $\epsilon_1=\epsilon_2$, then $r_1=r_2$ and equation 28 becomes

$$q=\frac{\epsilon A\sigma(T_1^4-T_2^4+rT_2^4-rT_1^4}{1-r^2}. \tag{29}$$

If ϵ is very nearly one, r then is nearly equal to zero and can be neglected. Equation 29 becomes

$$q=\epsilon A\sigma(T_1^4-T_2^4). \tag{30}$$

By dividing equation 30 by A, we obtain an equation for flux per unit area.

The above derivation is only correct when one is considering a nonabsorbing medium; however, the absorption of radiation by water vapor and carbon dioxide is included in the determination of the emissivity, as described previously.

U.S. GOVERNMENT PRINTING OFFICE: 1963 O—687-198

AD---------- Accession Nr----------
United States Department of Agriculture, Agricultural Research Service, United States Water Conservation Laboratory, Tempe, Arizona.
SURFACE ENERGY BALANCE IN ARID LANDS AGRICULTURE: 1960-61, by C. H. M. van Bavel and others.
Pub. 1963, U.S. Dept. Agr. Prod. Res. Rpt. 76 (DA Project 3A99-27-005-08). 46 pp.—33 illustrations. Unclassified Report.

Tbis report discusses methods and preliminary results of a study of tbe disposition of radiant energy over bare land that is wetted or ponded in an arid, hot climate. Evaporative flux at the surface is evaluated from a triplicate precision weigbing lysimeter installation. Other metbods are conventional.

(1) Comparison of small with large evaporating surfaces show relatively small advective effects at tbe surface.

(2) Over large, wet areas, daily balances show, as a rule, no net extraction of beat from tbe air.

(3) Heat flow into the air is extremely variable during tbe day, depending on tbe nature of surface and wind conditions.

More detailed analysis of the data are planned as well as continued studies involving surfaces with a vegetative cover.

UNCLASSIFIED

1. Evaporation—Bare land
2. Evaporation—Lysimeter method
3. Net Radiation—Measurement
4. Energy Balance—Arid climate
5. Energy Balance—Advective effects

Contract 3A99-27-005-08

AD---------- Accession Nr----------
United States Department of Agriculture, Agricultural Research Service, United States Water Conservation Laboratory, Tempe, Arizona.
SURFACE ENERGY BALANCE IN ARID LANDS AGRICULTURE: 1960-61, by C. H. M. van Bavel and others.
Pub. 1963, U.S. Dept. Agr. Prod. Res. Rpt. 76 (DA Project 3A99-27-005-08). 46 pp.—33 illustrations. Unclassified Report.

This report discusses methods and preliminary results of a study of the disposition of radiant energy over bare land that is wetted or ponded in an arid, hot climate. Evaporative flux at the surface is evaluated from a triplicate precision weighing lysimeter installation. Other methods are conventional.

(1) Comparison of small with large evaporating surfaces show relatively small advective effects at the surface.

(2) Over large, wet areas, daily balances show, as a rule, no net extraction of heat from the air.

(3) Heat flow into the air is extremely variable during the day, depending on the nature of surface and wind conditions.

More detailed analysis of the data are planned as well as continued studies involving surfaces with a vegetative cover.

UNCLASSIFIED

1. Evaporation—Bare land
2. Evaporation—Lysimeter method
3. Net Radiation—Measurement
4. Energy Balance—Arid climate
5. Energy Balance—Advective effects

Contract 3A99-27-005-08

AD---------- Accession Nr----------
United States Department of Agriculture, Agricultural Research Service, United States Water Conservation Laboratory, Tempe, Arizona.
SURFACE ENERGY BALANCE IN ARID LANDS AGRICULTURE: 1960-61, by C. H. M. van Bavel and others.
Pub. 1963, U.S. Dept. Agr. Prod. Res. Rpt. 76 (DA Project 3A99-27-005-08). 46 pp.—33 illustrations. Unclassified Report.

This report discusses methods and preliminary results of a study of the disposition of radiant energy over bare land that is wetted or ponded in an arid, hot climate. Evaporativc flux at the surface is evaluated from a triplicate precision weighing lysimeter installation. Other metbods are conventional.

(1) Comparison of small witb large evaporating surfaces show relatively small advective effects at the surface.

(2) Over large, wet areas, daily balances show, as a rule, no net extraction of beat from the air.

(3) Heat flow into the air is extremely variable during tbe day, depending on the nature of surface and wind conditions.

More detailed analysis of the data are planned as well as continued studies involving surfaces with a vegetative cover.

UNCLASSIFIED

1. Evaporation—Bare land
2. Evaporation—Lysimeter method
3. Net Radiation—Measurement
4. Energy Balance—Arid climate
5. Energy Balance—Advective effects

Contract 3A99-27-005-08

AD---------- Accession Nr----------
United States Department of Agriculture, Agricultural Research Service, United States Water Conservation Laboratory, Tempe, Arizona.
SURFACE ENERGY BALANCE IN ARID LANDS AGRICULTURE: 1960-61, by C. H. M. van Bavel and others.
Pub. 1963, U.S. Dept. Agr. Prod. Res. Rpt. 76 (DA Project 3A99-27-005-08). 46 pp.—33 illustrations. Unclassified Report.

Tbis report discusses methods and preliminary results of a study of the disposition of radiant energy over bare land that is wetted or ponded in an arid, bot climate. Evaporative flux at the surface is evaluated from a triplicate precision weighing lysimeter installation. Other methods are conventional.

(1) Comparison of small witb large evaporating surfaces sbow relatively small advective effects at the surface.

(2) Over large, wet areas, daily balances show, as a rule, no net extraction of heat from tbe air.

(3) Heat flow into the air is extremely variable during the day, depending on tbe nature of surface and wind conditions.

More detailed analysis of the data are planned as well as continued studies involving surfaces with a vegetative cover.

UNCLASSIFIED

1. Evaporation—Bare land
2. Evaporation—Lysimeter method
3. Net Radiation—Measurement
4. Energy Balance—Arid climate
5. Energy Balance—Advective effects

Contract 3A99-27-005-08